Dottorato di Ricerca in Ingegneria Civile ed Edile/Architettura
Graduate School in Civil and Architectural Engineering

XXIX Cycle (XV New Series)

Shifting from a standard protocol of communication to an emergency protocol in the monitoring of large infrastructural systems

PhD Thesis
Michele Vece

Advisor
Prof. Sara Casciati

Reviser
Prof. Lucia Faravelli

December 2016

Dottorato di Ricerca in Ingegneria Civile ed Edile/Architettura
Graduate School in Civil and Architectural Engineering

XXIX Ciclo/*Cycle* (XV Nuova Serie/*New Series*)

Settore: *Field:*	Ingegneria *Engineering*
Sede Amministrativa non consortile: *Administrative location:*	Università degli Studi di Pavia *University of Pavia*
Durata: *Duration:*	3 anni *3 years*
Periodo formativo estero: *Period in foreign organizations:*	come previsto dal regolamento del dottorato di ricerca *as required by the School rules*
Numero minimo di corsi: *Minimum number of courses:*	6 corsi *6 courses*

Recapiti/*Contact numbers and address*

via Ferrata 3 - 27100 Pavia - Italy
Tel. 0382/985450-51

Coordinatore/*Coordinator*

CASCIATI Fabio Professore Ordinario (ICAR/08)

Dipartimento di Ingegneria Civile e Architettura
via Ferrata 3 - 27100 Pavia - Italia Tel. 0382/985787
e-mail: fabio.casciati@unipv.it

Collegio dei docenti/*Scientific Board*

BERIZZI Carlo	Ricercatore (ICAR/14)
CASCIATI Fabio	Professore Ordinario (ICAR/08)
CASELLA Vittorio	Professore Associato (ICAR/06)
CINQUINI Carlo	Professore Ordinario (ICAR/08)
CIAPONI Carlo	Professore Ordinario (ICAR/02)
COLLIVIGNARELLI Maria Cristina	Ricercatore (ICAR/03)
DE LOTTO Roberto	Professore Associato (ICAR/20)

DEL GROSSO Andrea Enrico	Professore (ICAR/09) in quiescenza dal 01/11/2015
FARAVELLI Lucia	Professore Ordinario (ICAR/08)
GALLATI Mario	Professore (ICAR/01) in quiescenza dal 01/11/2015
GHILARDI Paolo	Professore Associato (ICAR/01)
GOBETTI Armando	Professore Associato (ICAR/08)
GRECO Alessandro	Professore Associato (ICAR/10)
MAGRINI Anna	Professore Ordinario (ING-IND/11)
MARCELLINI Alberto	Dirigente CNR Milano in quiescenza dal 01/11/2014
MOISELLO Ugo	Professore (ICAR/02) in quiescenza dal 01/11/2015
MORANDOTTI Marco	Professore Associato (ICAR/10)
PAPIRI Sergio	Professore Associato (ICAR/02)
SALA Roberto	Professore (ING-IND/08) in quiescenza dal 01/11/2014

Organizzazione del corso

Il dottorato di ricerca in *Ingegneria Civile ed Edile/Architettura* presso la Facoltà di Ingegneria dell'Università degli Studi di Pavia è stato istituito nell'anno accademico 2010/11 (XXVI ciclo; XII ciclo Nuova Serie).

L'obiettivo formativo peculiare del dottorato è addestrare giovani laureati allo svolgimento di attività di ricerca e viene perseguito nell'ambito dei settori disciplinari di Ingegneria Civile ed Architettura (ICAR), senza tralasciare alcune interdisciplinarietà, in via di consolidamento, con discipline strumentali o complementari. Il corso consente al dottorando di scegliere tra sei distinti curricula: compositivo, idraulico, sanitario, sismico, strutturale e tecnologico.

In particolare, le tematiche di ricerca sono quelle che caratterizzano i raggruppamenti disciplinari ICAR/01, ICAR/02, ICAR/03, ICAR/06, ICAR/08, ICAR/09, ICAR/10, ICAR/14, ICAR/18, ICAR/20, tutte di pertinenza dell'ingegneria civile e architettura. A questi si aggiungono ING-IND/11 (fisica tecnica ambientale) e ING-IND/08 (macchine a fluido).

L'attività di ricerca si svolge soprattutto presso il Dipartimento di Ingegneria Civile e Architettura (DICAr) dell'Università degli Studi di Pavia.

Durante i primi due anni sono previsti almeno sei corsi, seguiti da prove finali che il dottorando è tenuto a sostenere.

Il Collegio dei Docenti organizza i corsi con lo scopo di fornire allo studente di dottorato opportunità di approfondimento su alcune delle discipline di base per i settori componenti, ingegneria idraulica, strutturale ed edile/architettura. Corsi e seminari vengono tenuti da docenti di università nazionali ed estere.

Alla fine di ogni anno i dottorandi devono presentare una relazione sull'attività svolta. Al termine del primo anno viene richiesta una presentazione orale, al contrario al termine del secondo anno il dottorando è tenuto a scrivere una tesina su un argomento pertinente alla propria ricerca di dottorato.

Sulla base di tali relazioni il Collegio dei Docenti, previa valutazione dell'assiduità e dell'operosità dimostrata dall'iscritto, può proporre al Rettore l'esclusione del candidato dal corso o non approvarne il passaggio all'anno successivo.

Il dottorando può svolgere attività di ricerca di tipo teorico, numerico e sperimentale, grazie ai laboratori di cui il Dipartimento dispone.

Course Organization

The Graduate School in Civil and Architectural Engineering at the School of Engineering of the University of Pavia, was established in the academic year 2010/2011 (XXVI cycle, XII new series cycle).

Its peculiar educational aim is to train young graduates to conduct research activities and it is pursued by the disciplinary fields of Civil Engineering and Architecture (ICAR), without omitting some interdisciplinary, which are consolidating, with supporting or complementary disciplines. The course allows the PhD student to choose between six different curricula: composition, hydraulic, sanitary, seismic, structural and technological.

The research themes are chosen from the disciplinary areas ICAR/01, ICAR/02, ICAR/03, ICAR/06, ICAR/08, ICAR/09, ICAR/10, ICAR/14, ICAR/18, ICAR/20 belonging to civil engineering and architecture. In addition, there are ING-IND/11 (environmental technical physics) and ING-IND/08 (fluid machines).

The research activity takes place mainly at the Department of Civil Engineering and Architecture (DICAr) of the University of Pavia. During the first two years, at least 6 courses are required, followed by final examination that the PhD student has to take. The Teaching Staff organizes courses with the aim of providing the PhD student the opportunity to deepen some basic disciplines in the components fields, such as hydraulic engineering, structural, and building engineering and architecture. Courses and seminars are held by professor of national and foreign universities.

At the end of each year, the PhD students have to present an activity report. At the end of the first year, an oral presentation is requested, at the end of the second year the PhD student is required to write a term paper about a topic connected to the doctoral research. On the basis of these reports, the Teaching Staff, after the evaluation of the demonstrated regularity and hard work of the PhD student, may propose to the Rector the exclusion of the candidate from the course or not to approve to the next year. The PhD student can carry out research activities both theoretical and experimental, thanks to the laboratories owned by the Department.

Elenco delle tesi/*Theses List*

1. Valentina Giacometti (XXVI Ciclo, XII Ciclo Nuova Serie), Cultura dell'accessibilità e Accessibilità della Cultura: uno strumento di valutazione per l'edilizia universitaria storica, relatore: Prof. A. Greco, ottobre 2013.
2. Enrico Murari (XXVI Ciclo, XII Ciclo Nuova Serie), Adattamento dei sistemi idropotabili a scenari di carenza idrica, relatore: Prof. C. Ciaponi, ottobre 2013.
3. Emanuele Zamperini (XXVI Ciclo, XII Ciclo Nuova Serie), Evoluzione tecnologica e tipologica delle coperture lignee in Italia nel periodo 1800-1950, relatore: Prof. M. Morandotti, ottobre 2013.
4. Cecilia Morelli di Popolo (XXVI Ciclo, XII Ciclo Nuova Serie), La città flessibile. Le dimensioni della flessibilità nella città contemporanea e futura, relatore: Prof. R. De Lotto, aprile 2014.
5. Umut Yıldrım (XXVI Ciclo, XII Ciclo Nuova Serie), System identification towards diagnosis to prognosis, relatore: Prof. F. Casciati, aprile 2014.
6. Daniele Bortoluzzi (XXVII Ciclo, XIII Ciclo Nuova Serie), Control systems for the mitigation of footbridge vibrations, relatore: Prof. L. Faravelli, ottobre 2014.
7. Federico Castagnola (XXVII Ciclo, XIII Ciclo Nuova Serie), Applicazione di una tecnologia MBR termofila funzionante in condizioni aerate/non aerate per la minimizzazione di fanghi di depurazione civili ed industriali, relatore: Prof. M.C. Collivignarelli, ottobre 2014.
8. Valentina Cinieri (XXVII Ciclo, XIII Ciclo Nuova Serie), Patrimonio edificato diffuso. Un approccio sostenibile alla conservazione e alla gestione, relatori: Proff. M. Morandotti, D. Besana, ottobre 2014.
9. Kan Liu (XXVII Ciclo, XIII Ciclo Nuova Serie), Cultural transfer and architecture. Foreign architectural practice in Shanghai after 1949, relatore: Prof. Z. Shiling, ottobre 2014.

10. Edoardo Gino Macchi (XXVII Ciclo, XIII Ciclo Nuova Serie), Experimental and numerical studies on RF ablation: advances on physical understanding and efficiency, relatore: Prof. M. Gallati, ottobre 2014
11. Daniele Molognoni (XXVII Ciclo, XIII Ciclo Nuova Serie), Microbial Fuel Cells Application to Wastewater Treatment: laboratory experience and controlling strategies, relatore: Prof. A. Capodaglio, ottobre 2014.
12. Marco Sordi (XXVII Ciclo, XIII Ciclo Nuova Serie), Applicazione di un sistema MBR termofilo aerobico per il trattamento di rifiuti liquidi ad elevata concentrazione di COD, tensioattivi, solventi e cloruri, relatore: Prof. M.C. Collivignarelli, ottobre 2014.
13. Andrea Fenocchi (XXVII Ciclo, XIII Ciclo Nuova Serie), Circulation dynamics in a shallow fluvial lake - The case of the Superior Lake of Mantua, relatore: Prof. S. Sibilla, giugno 2015.
14. Nawal Benabdelkader (XXVII Ciclo, XIII Ciclo Nuova Serie), The restoration and enhancement. The historical site of Mansourah - Tlemcen, relatore: Prof. M. Morandotti, ottobre 2015.
15. Giovanni Anselmo (XXVIII Ciclo, XIV Ciclo Nuova Serie), Effetti idrologici e idraulici dell'urbanizzazione e possibili interventi di mitigazione, relatori: Proff. S. Papiri e G. Barbero, ottobre 2015.
16. Lorenzo Elia (XXVIII Ciclo, XIV Ciclo Nuova Serie), Metaheuristic optimization tools for structural monitoring, relatore: Prof. L. Faravelli, ottobre 2015.
17. Emanuele Giorgi (XXVIII Ciclo, XIV Ciclo Nuova Serie), Man and environment: looking for the future, relatori: Proff. Z. Shiling e F. Casciati, ottobre 2015.
18. Elena Romano (XXVIII Ciclo, XIV Ciclo Nuova Serie), Uno strumento per il miglioramento prestazionale dell'edilizia esistente: il caso delle residenze universitarie, relatore: Prof. A. Greco, ottobre 2015.

19. Babak Jafarzad Eslami (XXVIII Ciclo, XIV Ciclo Nuova Serie), Impiego di smorzatori sismici nella protezione dei beni architettonici, relatore: Prof. E.A. Del Grosso, aprile 2016.
20. Michele Vece (XXIX Ciclo, XV Ciclo Nuova Serie), Shifting from a standard protocol of communication to an emergency protocol in the monitoring of large infrastructural systems, relatore: Prof. S. Casciati, dicembre 2016.
21. Giammaria Gabbianelli (XXIX Ciclo, XV Ciclo Nuova Serie), Numerical model for framed structures with thin-walled cross-section members, relatore: Prof. A. Gobetti, dicembre 2016.
22. Matteo Locatelli (XXIX Ciclo, XV Ciclo Nuova Serie), Strumento per la valutazione e definizione di strategie per il miglioramento dell'edilizia scolastica esistente. Il tema della scuola primaria e secondaria, relatore: Prof. A. Greco, dicembre 2016.
23. Rosamaria Olivadese (XXIX Ciclo, XV Ciclo Nuova Serie), Il riuso degli edifici esistenti a scopo residenziale in Italia: nuovi standard per l'innovazione dei modelli abitativi, relatore: Prof. C. Berizzi, dicembre 2016.
24. Elisabetta Maria Venco (XXIX Ciclo, XV Ciclo Nuova Serie), La pianificazione preventiva per la riduzione del rischio: definizione di scenari preventivi nel contesto della città flessibile e resiliente, relatore: Prof. R. De Lotto, dicembre 2016.
25. Francesca Maria Torchia (XXIX Ciclo, XV Ciclo Nuova Serie), Materiali da riciclo e da scarto innovativi per l'edilizia: caratterizzazione acustica, termica ed analisi del ciclo di vita, relatore: Prof. P. Ricciardi, dicembre 2016.
26. Laura Menoni (XXIX Ciclo, XV Ciclo Nuova Serie), Sviluppo di "smart control strategies" per l'automazione di processo negli impianti a fanghi attivi, relatore: Prof. G. Bertanza, dicembre 2016.

Table of Contents

List of Figures

List of Tables

Introduction

Recent catastrophic failures of civil engineering infrastructure systems, such as the I-35 Bridge collapse (Minneapolis, 2007), the PG&E gas pipeline explosion (San Bruno, 2010) and the freight train derailment (Viareggio, 2009), have drawn attention on the need to better manage these complex engineered systems to ensure their safe use by the society.

Structural health monitoring (SHM) has emerged over the past decade as an active, interdisciplinary research field dealing with the development of sensing technologies and data processing methods aimed to perform condition assessment and damage detection of structural systems.

Though many advances have been made over the decade, some technological hurdles remain. For instance, high costs and laborious installations of monitoring systems hinder their widespread. In addition, a lack of user-friendly data processing algorithms that extract information from sensors data exists.

Measuring displacements from civil structures is often challenging and costly with the conventional structural health monitoring applications. To overcome the drawbacks due to the wired solutions and the use of expensive equipment, alternative methods were recently developed. Many kinds of wireless sensors or indirect measurements have been prototyped, but most of them suffers of large time delays and accuracy issues.

This thesis addresses some of these bottlenecks. The advancement of wireless sensors for cost-effective structural monitoring is at the core of the dissertation. Wireless sensors have the potential to reduce the cost of monitoring systems while offering onboard data processing capabilities for sensor-based data interrogation.

Moreover, a Kalman filter-based data fusion is adopted to make a precise measurement of the displacements induced on civil structures. The needed accuracy in GPS measurements can be reached exploiting the real-time satellite corrections provided by a single reference station. For this reason, an approach based on the wireless communication and supported by GNSS receivers with three-axial accelerometers is introduced.

The proposed system is validated, showing control mechanism and laboratory tests, in order to provide a reliable way that may be adopted in the real-time structural health monitoring and managed by remote control.

The thesis comes with two main innovative aspects. First, it is focused on the adopted wireless sensing technology including its field validation. The author activity addresses then the need to transmit the information, mainly in emergency situations, by satellites to the location where the collected data are supposed to be processed.

The organization of the thesis is planned in six chapters and two appendices. A brief description of them is given below:

Chapter 1 – Real-time structural health monitoring introduces the state of the art of the current systems used for measuring the structural response in civil engineering applications. SHM methods involving wired and wireless sensor are presented. A comparison between them follows. Benefits and challenges of a wireless sensing unit are investigated as well.

Chapter 2 – A brief overview on compressive sensing provides an overview on the recent compression approaches adopted by several authors to reduce the amount of data traffic in Wireless sensor Networks (WSNs). In addition, the problem formulation and the protocols description of each method are presented.

Chapter 3 – System architecture for the data collection is explored as one of the major topics of the thesis. The strategy for the local collection of the message through a WSN is discussed. The possibility to transmit the basic information to the "outside world" by a Wide Area Network (WAN) is faced, and a Kalman filtering based on a combination of accelerations and displacements is proposed to identify the critical issues of a civil infrastructure.

Chapter 4 – Hardware and software integration presents the main components of the entire system. In particular, attention is focused on the wireless sensor platform, which is used as its data collection tool. A detailed description of implementation environment and communication protocol is provided, including details about its extended-range radio as well as the software design.

Chapter 5 – Performance assessment summarizes the laboratory experimentations of the first prototype. A specialty test-bed was used, and field validations of the proposed system are carried out in order to show the reliability of a low-cost, low-power protocol of communication between the sending side and the receiving one.

Chapter 6 is reserved to the conclusions, highlighting achievements and key contributions of the thesis with a discussion on future extensions of the research.

Chapter 1 Real-time structural health monitoring

Real-time structural health monitoring (SHM) is considered a crucial procedure in the field of the civil engineering. It is based on the acquisition of structural responses and environmental factors in order to assess the structural conditions for potential maintenance actions.

The first step is to identify the types of physical quantities to be monitored, which are generally affected by accuracy, user-friendliness, and cost of the measurement.

Acceleration and displacement are the most widely measured responses for SHM to determine the dynamic characteristics, the stability and the soundness of large structures.

The currently available techniques for measuring the displacements are divided into: (i) direct measurement, and (ii) indirect estimation approaches. The direct methods include linear variable differential transformers (LVDT), LASER-based transducers [1-2], and vision based system [3-9]. Their main drawbacks are the high costs and the synchronization issues when multiple points are required. Furthermore, the data acquisition systems have to be placed between a measurement point and a stationary reference, with challenging issues resulting from the need of wired connections.

The indirect estimation approach converts other structural responses (i.e., acceleration and strain) to displacements on the basis of their physical relationships. However, it suffers from low accuracy by numerical errors and imperfect physical relationships.

The conversion from acceleration to displacement also involves large low-frequency drift errors caused by the numerical integration in the discrete time domain [10]. For these reasons, this type of approach is not welcome for SHM applications.

Accuracy enhancements are achieved by employing multiple responses, based on a data fusion model, to reduce the drawbacks of each single acquisition [11-13]. Indeed, the conversion of the acceleration can be improved by referencing displacement measured by a high precision GNSS (Global Navigation Satellite System) device in the Kalman filtering. This method has been actively studied in the GPS (Global Positioning System) navigation field, but it needs to make a post-data fusion between accelerations and displacements as well [14-21].

The GPS has provided new opportunities for direct measurement of infrastructure deflections, which so far relied on different solutions such as liquid levels, plumb lines, laser interferometry, digital image processing for real-time tracking and variations on the motion detection of the reflected light sources. A differential GPS depends on the accurate measurement of transit times for radio waves from the satellite to the receiver, and promises direct and absolute measurement of deflection without the issues associated with the optical system [22].

A base station GPS antenna is set up on a stable reference location as close as possible to the monitored structure, with the line of sight at least for five GPS satellites. A rover antenna is installed on the structure, also with the satellite visibility. The locations of rover and base station are achieved through the appropriate geodetic coordinates. However, they have an own measure of inaccuracy that depends on factors affecting radio transmission times between the satellites and the receivers. Since the base station and the receiver are close each to the other, the factors should affect the signals in the same way. Moreover, the differences between the known position of the reference system and that one computed by the GPS can be transmitted as errors in real time to the rover, whose location is corrected to determine a more accurate fix. This Real Time Kinematic (RTK) form of GPS measurement [23] should be capable to provide positional accuracy better than 1cm at rates of 10Hz. Positional errors increase with the separation of the two devices, but it has been claimed [24] that accuracy of 1mm can be obtained using GPS, although not necessarily with real-time systems.

The alternative to the real-time mode is the data processing after their acquisition by separate receivers. These data provide full information about signal transit times and satellite parameters, enabling the adoption of processing algorithms and the derivation of positional quality indicators. A recent development by the greater GPS equipment suppliers is the “virtual reference system” where location corrections are available from a national network of supplier-managed receivers. In this way, a dedicated base station is not needed.

An extension of the Republic Plaza system [25] shows that real-time solutions can defect displacements of 2-3mm. The accuracy is difficult to evaluate due to the absence of reliable alternate measures, although having two rovers installed (separated by 11m) indicates the probable errors. Experience in this trial shows that variance errors can be as large as the normal movement of a building, which is in the range of a few centimeters.

Other recent projects demonstrate the GPS potential for the monitoring performance for the Chicago project [26], where a fast offline processing is applied to the GPS data from three skyscrapers and radio mast measurements in Japan [27]. That is remarkable about the latter study is the identification of the mast response in the second vibration mode at 2.16Hz, from 10Hz GPS data recorded during an earthquake signal.

In case that slower sample rates are required, an adaptive filtering can be implemented to remove the noise and to obtain more accurate static solutions. This technique is often used by the operators of dams and other structures, where slow movements are of particular concern as indicators of the structural health [28].

For further reading, proceedings of symposia and conferences organized by the International Federation of Surveyors (FIG) present a growing number of GPS applications to civil SHM on many classes of structure. The most successful applications are carried out where the base station can be located close to the structure and where the structural movements can be measured in centimeters with very slow dynamic or static movements. This makes GPS ideal for tracking performance of long-span suspension bridges, such as Akashi-Kaikyō and Tsing Ma [29], due to the very slow movements arising from the environmental loads.

1.1 Tracking of civil infrastructure systems

Modern cable-supported bridges carry enormous loads across great distances due to their designed capability to slightly move under varied conditions [30-34]. In Hong Kong, a Real Time Kinematic GPS monitoring system provides the centimeter-level accuracy (at any weather conditions) to detect the movements of some bridges beyond the normal ranges. Indeed, many of them can move from several centimeters to several meters under different types of loading conditions.

Although these displacements may not create hazardous conditions for the traffic on the bridge, they increase in size, affecting the structural integrity and the maintenance needs of the bridge. The real-time GPS accuracy has recently improved to the centimeter-level precision, making it well suited to monitor the three-dimensional motion variations of the bridge in response to wind, temperature, and traffic loads. The next sections describe the layout and technical performance requirements of such a system.

The Highways Department of Hong Kong Special Administrative Region designed the Wind and Structural Health Monitoring System (WASHMS) for three large cable-supported bridges: Tsing Ma Bridge, Kap Shui Mun Bridge, and Ting Kau Bridge (TKB), in the Tsing Ma Control Area (TMCA) of western Hong Kong.

1.2 The Ting Kau Bridge

The Ting Kau Bridge (TKB) is a three-tower cable-stayed bridge with two main spans of 448m and 475m, and two side spans of 127m [35-39]. The bridge deck is separated into

two carriageways with a width of 18.8m. Between them, three slender single-leg towers with heights of 170m, 194m, and 158m, respectively. Each carriageway consists of two longitudinal steel girders along the deck edges with steel cross girders at 4.5m intervals, and a concrete slab on top. They are linked with a 5.2m gap at 13.5m intervals by connecting cross girders. The deck is supported by 384 stay cables in four cable planes.

The unique feature of the bridge is its arrangement of the three single-leg towers, which are strengthened by longitudinal and transverse stabilizing cables. Eight longitudinal stabilizing cables with lengths up to 465m are used to diagonally connect the top of the central tower to the side towers, while 64 transverse stabilizing cables are used to strengthen the three towers in the lateral direction.

Since it is part of a long-term SHM system devised by the Hong Kong SAR Government Highways Department, more than 230 sensors have been permanently installed on the TKB after completing the bridge construction in 1999 [40, 41]. The sensors deployed on the bridge include accelerometers, strain gauges, displacement transducers, anemometers, temperature sensors, GPS, and weigh-in-motion sensors [42, 43]. The layout of the accelerometers at the eight deck sections on the TKB is shown in Figure 1.1.

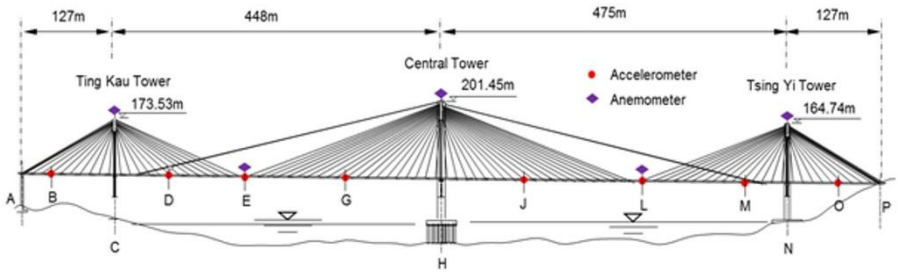

Figure 1.1 TKB and layout of accelerometers on bridge deck

Overall, 24 uniaxial accelerometers, 20 bi-axial accelerometers and 1 three-axial accelerometer (totally 67 accelerometer channels) are permanently installed at the deck of the two main spans and two side spans, the longitudinal stabilizing cables, the top of the three towers, and the base of the central tower to monitor the dynamic response of the bridge. Figure 1.2 illustrates the deployment of the accelerometers on the four deck sections of the TKB with a sampling frequency of 25.6Hz.

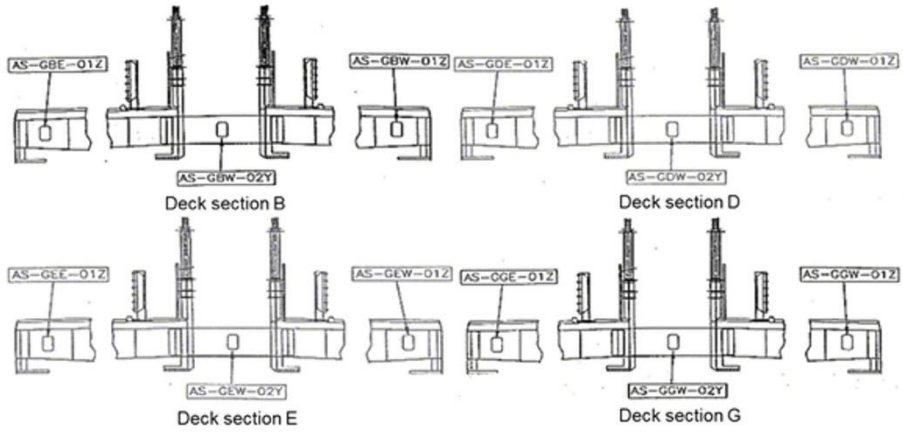

Figure 1.2 Deployment of accelerometers on four deck sections

The modular concept used for the structural health monitoring of the Ting Kau Bridge had a significant influence on the design of the new SHM systems in Hong Kong and China [44]. There are six integrated modules, which include: (i) the sensory system, (ii) the data acquisition and transmission system, (iii) the data processing and control system, (iv) the structural health evaluation system, (v) the structural-health data management system, and (vi) the inspection and maintenance system.

The first one is the sensory system. It is referred to the sensors and their corresponding interfacing units for input signals gathered from various monitoring equipment. These sensors are categorized into four groups. The first group consists of the sensors for monitoring of environmental status and effects. They include anemometers, temperature sensors, corrosion cells, hygrometers, barometers, and rainfall gauges. The second group is made of the sensors for monitoring traffic loads, which include dynamic weight-in-motion stations, digital video cameras and dynamic strain gauges. The third group includes the sensors for monitoring the bridge characteristics that include fixed and removable or portable servo-type accelerometers, global positioning systems, level sensing stations, and dynamic strain gauges. The fourth group collects the sensors for monitoring bridge responses. They include dynamic strain gauges, static strain gauges, displacement transducers, global positioning systems, tilt meters, fixed servo-type accelerometers, buffer sensors, bearing sensors and tension magnetic gauges.

The second module is the Data Acquisition and Transmission System (DATS). The DATS is composed of four sub-system, which are Data Acquisition System (DAS), Local Cabling Network System (LCNS), Global Cabling Network System (GCNS), and

Commercial Cabling Network System (CCNS). The DAS is composed of several fixed and portable PC-based Data Acquisition Units (DAUs). The fixed DAUs are permanently installed in the bridge deck/towers for the collection and the processing of signals received from the sensory system. The portable DAUs are used to collect signals from portable servo-type accelerometers and corrosion cells. The LCNS is composed of two local cabling networks. The first is the copper cabling network for the transmission of the signals from the sensory system to the DAUs. The second is the fiber optic cabling network for the transmission of the signals from the Global Positioning System to the DAUs. The GCNS is composed of two backbone cabling networks. The first is the electro-magnetic signal transmission cabling network for the transmission of the digitized signals. The second one is the digital video signal transmission cabling network for the transmission of digital video signals. The CCNS is the leased high speed line with a data transmission rate of no less than 40Mbps for data communication.

The third module is the Data Processing and Control System (DPCS). It is located in the Bridge Monitoring Room, and is made of two high performance computers (DPCS-1 and DPCS-2). They are equipped with customized software and standard software packages.

The fourth module is the Structural Health Evaluation System (SHES). It carries out the off-time structural health evaluation process. It is made of two sets of multi-processor Itanium-2 servers, each equipped with a control console, and two Itanium-2 workstations. The servers are devised to act as a solver for all numerical and statistical analytical work.

The fifth module is the Structural Health Data Management System (SHDMS). It is a data warehouse, and the source of data is mainly supplied from the severs DPCS-1 and DPCS-2. These severs are the operational data stores for data processing and analysis.

The sixth module is the Inspection and Maintenance System (I&MS). It is made of two notebook computers (I&MS-1 and I&MS-2) and a tool-box. Its function is devised to carry out inspection and maintenance works on the sensory system, the Data Acquisition Units, the Local Cabling Network Systems and the Global Cabling Network Systems. All information regarding system design, system installation, system operation and system maintenance is stored and operated in I&MS-1. All manuals regarding system operation and maintenance are stored and operated in I&MS-2. The toolbox is for carrying out inspection and mirror remedial works.

1.2.1 The GPS-OSIS

The structural design of the cable-supported bridges is based on displacements. Displacements or movements of cables, decks, and towers that deviate from the designed geometrical configurations will redistribute stresses and strains among the bridge components, affecting the load-carrying capacity of the whole bridge.

Until recently, the WASHMS for Tsing Ma Bridge (TMB), Kap Shui Mun Bridge (KSMB) and Ting Kau Bridge (TKB) consisted of 774 sensors in seven main types: anemometers, temperature sensors, dynamic weigh-in-motion sensors, accelerometers, displacement transducers, level sensing stations, and strain gauges.

The commissioning of the real-time GPS On-Structure Instrumentation System (GPS-OSIS) in January 2001 brought an additional 29 sensors into the overall system. Now operational, the GPS-OSIS operates as an additional integral system to the existing WASHMS for improving efficiency and accuracy of the bridge health monitoring works.

Although the geometrical configurations of the three bridges are measured by the annual TMCA geodetic survey, they are used for monitoring geometrical variations due to permanent and long-term structural actions such as dead loads and super-imposed dead loads. Geodetic surveying cannot detect the instant responses of the bridges to transient and variable structural actions such as primary live loads. Before the GPS deployment, the accelerometers monitored the geometrical variations, but this method is due to uncertainties or unknown integration constants. Therefore, it only provides relative local displacements at measurement locations, and does not give overall absolute displacements.

This difference becomes very important in the case, for instance, of: (i) strong wind swaying the bridge deck alignment steadily to one side, (ii) daily temperature variation raising, or (iii) lowering bridge deck level. In addition, it is needed to sustain these changes over a specific period before returning to normal position. The accelerometers can not detect such continuous or steady displacement of the massive deck, but only instant local vibration, and they do not give an overall true or absolute displacement. Their limitation in detecting the slow global displacement would introduce an error in the mathematical derivations.

In the past, level sensing stations and servo-type accelerometers monitored the bridge responses in TMCA. The level sensing stations, at a sampling rate of 2.56Hz, provide real-time monitoring of displacements, with a measurement accuracy of 2mm at the typical deck sections and at the vertical planes only. These level sensing stations are used only on the TMB and KSMB, but not on TKB, because the installation cost of the pipeline systems along the bridge would be high.

However, they can not measure the lateral and longitudinal displacements of the deck sections in the horizontal plane. High precision servo-type accelerometers monitor the local vertical, lateral and rotational accelerations of the decks, cables and bridge-towers of TMB, KSMB and TKB. A displacement monitoring requires double-integration of the measured acceleration data to determine the three-dimensional motions of the three cable-

supported bridges. Because the natural frequencies of the decks are of very low values, double-integration of their accelerations may not reflect the actual displacement values.

After trial tests carried out on TMB in 1999 and 2000 that demonstrated GPS applicability and the required accuracy level, the HyD decided to employ GPS with the RTK function to monitor the displacements of the three cable-supported bridges. The GPS-OSIS monitors real-time motions of the main suspension cables, decks, and bridge towers of TMB, KSMB, and TKB. It derives the relevant stress status acting on the major bridge components. At last, it works with other WASHMS instrumentation systems to monitor the overall bridge health and the schedule inspections/maintenance activities.

1.2.1.1 System Description

The real-time GPS On-Structure Instrumentation System (GPS-OSIS) consists of five sub-systems: the GPS receivers, a local data acquisition system, a global data acquisition system, a computer system, and a fiber optic network (Figure 1.3).

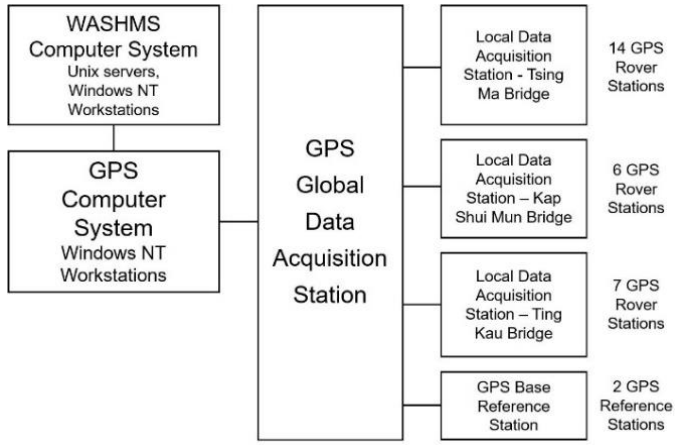

Figure 1.3 GPS-OSIS structure

The GPS-OSIS improves the efficiency and the accuracy of the WASHMS monitoring and evaluation activities by:

- reporting displacements, reflecting loading and stress conditions,
- providing more information to estimate distribution of stresses and strains in the major bridge components,

- documenting abnormal loading incidents such as typhoons, earthquakes, traffic overloads, and ship collisions with bridge piers,
- detecting damage or accumulated damage in the main bridge components,
- estimating bridge load-carrying capacities and validating design assumptions and parameters,
- providing information for planning and scheduling bridge inspection and maintenance activities.

The GPS sensory system is made of two base reference stations and 27 dual-frequency, 24-channel, carrier-phase rover stations, which collect data at a 10Hz sampling rate with a position latency less than 0.03s.

The local data acquisition system consists of three junction cabinets with fiber optic multiplexers, one on each bridge. One cabinet with fiber optic multiplexers in the bridge monitoring room constitutes the global data acquisition system. The GPS computer system is composed by two workstations and a custom software system. The fiber optic network includes 6.5km of single mode fiber and 18km of multimode one.

The real-time bridge monitoring with a centimeter level precision has a time delay of approximately two seconds to show the bridge motions in the monitoring room due to data transmission, processing, and graphical conversion times. Since it is an integrity monitoring system, two base reference stations monitor the quality of the RTK correction broadcast and its performance, including GPS availability and geometry. The GPS-OSIS operates 24 hours a day with an automatic control for data acquisition, processing, archiving, display, and storage. The GPS data post-processing with the relevant data from other WASHMS sensors provides the structural evaluation needed by HyD engineers.

1.2.1.2 Receivers location

The rover receivers has been installed on bridge locations where one expects to see maximum displacements: at the edges of deck sections, at mid span and quarter spans, where applicable, and at tower tops. Figure 1.4 shows TKB rover locations for the displacement measurements.

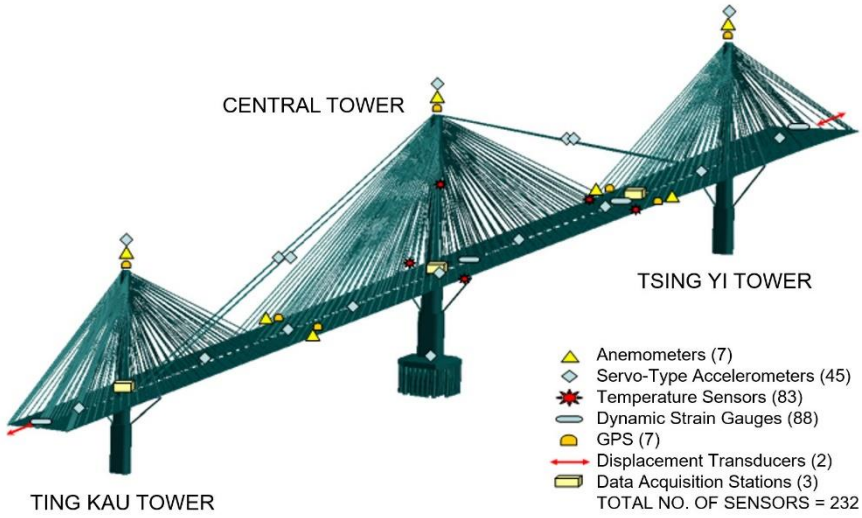

Figure 1.4 Location of GPS rover receivers on the Ting Kau Bridge

Most GPS receivers are adjacent to the level sensing stations or to the accelerometers. In this way, it is possible to compare the GPS results with data from other sensors.

The reference stations are carried out by choke-ring antennas (with domes) to reduce interferences, RF jamming, and vibration. Due to size and weight considerations, rover positions used micro-band antennas. In order to reduce signal interference from physical obstruction, all rovers are mounted with view angles greater than 15 degrees, taking care to avoid obstructions caused by double-decker buses and high-body vehicles running in the slow vehicle lane closest to the bridge edges.

The GPS-OSIS provides real-time motions of bridge decks at 10Hz. It also derives the variation in geometrical configuration at centerlines of deck sections and records the time-history motions of the bridges at measuring locations. At last, it performs similar monitoring procedures for the towers.

The position latency in the GPS sensory system is less than 0.03 seconds, significantly better than evaluated by the GPS systems in 1992. The RTK technique measures bridge displacement even when the bridge components move at irregular speed (i.e., the aerodynamic effects under varying the wind conditions). To fully monitor the bridge structural health, one needs to see its structural response to such conditions (whose time of occurrence is acquired by other sensors) within this 30 millisecond timeframe. Therefore, it is well note that the raw GPS data achieved through the RTK method meets the basic requirements for the real-time displacement monitoring.

1.3 The Akashi Kaikyō Bridge

The health monitoring of long-span bridges has been also one of particular concerns of the engineering community in Japan [45]. Effective monitoring, reliable data analysis, rational data interpretation and correct decision-making are challenging problems for the engineers specialized in this field. A current practice is represented by the Akashi Kaikyō Bridge monitoring system (Figure 1.5).

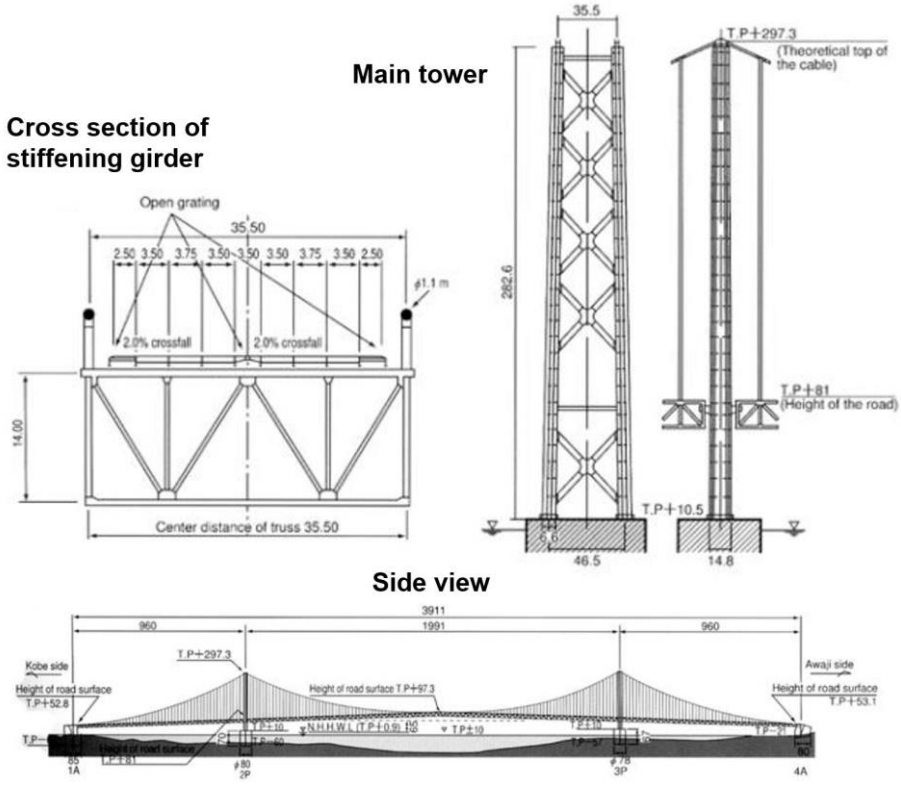

Figure 1.5 General view of Akashi Kaikyō Bridge

Figure 1.5 shows a general view of the Akashi Kaikyō Bridge. It is a three-span suspension bridge, with a center span of 1991m and two side spans of 960m. Two anchorages, 1A and 4A, were constructed on the reclaimed land on both shores. Two tower foundations, 2P and 3P, were constructed in the deep sea. Towers, cables and

stiffening girders are of steel. The top of the tower is 297m above the sea. The stiffening girder is a truss girder [46].

Due to the type of long span bridge, the design adopted some newly developed design codes for aerodynamic, seismic stability and design constants. Some newly developed challenging technologies that have been applied in Akashi Kaikyō Bridge are: wind resistant design, seismic design, run ability of train on suspension bridge, large-scale underwater foundation, working platform on the sea and seabed excavation method [47].

The dynamic response against strong wind and earthquake are subjected to unknown factors those are uneasy to predict. Therefore, it is necessary to establish a monitoring system that can collect data on dynamic response of the bridge in order to verify the assumptions and constant used for the design due to strong wind and earthquake. The wind load for long-span bridges has great importance in their structural design. It usually consists of time averaged wind force and some contribution of the dynamic response due to the wind fluctuation, but there still remain uncertainties in expression of wind characteristics to define the accurate and reliable wind load.

To overcome this it will be important to compile information of the wind at many bridge site [48]. As the example of monitoring results, the deformation characteristics of the bridge response due to typhoon are elucidated. By comparing the analyzed simulation results through wind tunnel test and field-measured results [49], the reliability of the current monitoring system is confirmed.

Furthermore, by applying newly developed technology in intelligent material (TRIP steels) and intelligent measurement systems [50], together with recent development of information and telecommunication infrastructure technology [51], a better constructive monitoring system has been managed [52]. Particularly, this new bridge management can include remote monitoring to obtain key information concerning bridge structural health, such as, relative motion, fatigue, and true stress occurred in structure member that in an accumulated and combined way contribute to the damage profile of the structure. This proposed system is easily accessible, economically feasible and durable to provide information for structural health maintenance. Specifically, the newly developed technology to monitor peak displacements at bridge pedestal dampers and true-stresses in main cables and anchorages of bridges is discussed.

The current long span bridge monitoring system was developed to be a reliable device to observe the bridge in earthquake and/or typhoon accurately, besides have a self-check function to sense the disorder of the system itself.

1.3.1 Monitoring purposes

Generally, the objectives of long bridge monitoring are the design verification, the structural maintenance, and the traffic management. The scope of monitoring includes two main types of parameters: the load effects, and the responses. The load effects refer to those due to wind, earthquake, temperature and live loads (movements, highways or railways). The responses refer to displacements, accelerations, stresses, strains and forces of the members of bridge structure, and displacements and stresses of main cables.

Japan as a country in which natural hazards occurs frequently, such as, typhoon and earthquake, monitoring of the peak displacements and real stresses of the main cables and their anchorages are the important subjects to be considered. The primary monitoring items due to design verification of Akashi Kaikyō Bridge is shown in Table 1.1.

Table 1.1 Design verification monitoring items [53]

Item	Main focus	Measured parameter
Earthquake characteristics	Seismic motion and magnitude	Acceleration
	Earthquake frequency characteristics	
	Ground characteristics	
	Phase difference	
Earthquake dynamic response	Acting seismic force	Response acceleration
	Displacement	Displacement
	Natural frequency	
	Superstructure seismic motion	Response acceleration
Wind characteristics	Basic wind speed	Wind direction, and wind speed
	Design wind speed	
	Variable wind speed characteristics	
Wind dynamic response	Superstructure natural frequency	Response acceleration
	Vibration mode configuration	Displacement
	Displacement	Predominant frequency
	Structural damping	Wind speed, and response acc.
	Gust response Action of main tower	Response displacement

1.3.2 Sensor configuration

In this chapter, the dynamical monitoring of Akashi Kaikyō Bridge is highlighted. In particular, Figure 1.6 shows the sensor configuration of the world longest suspension bridge.

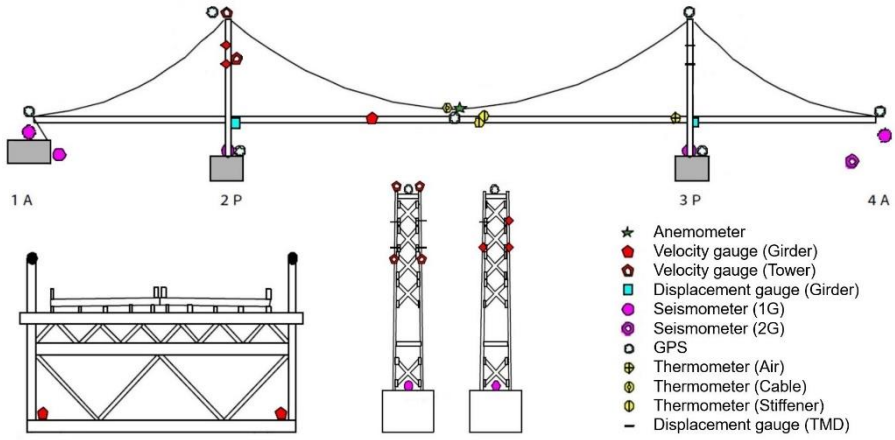

Figure 1.6 Sensor configuration of Akashi Kaikyō Bridge

As shown in Figure 1.6 following devices were installed:

- two seismometers were installed in 1A and 4A. To avoid response vibration influence of the 1A foundation to the original seismic motion, the seismometer at this point was installed at a place that has a distance about 100 meters from bridge axis. Another seismometer at 4A was installed at approximately T.P. –20 meters in the granite rock near the 4A concrete block.
- in order to determine the wind characteristics of the bridge structure, the distribution of directional wind speed is measured in the longitudinal and transversal directions. To monitor spatial correlation in the horizontal direction, the anemometer is installed in the middle of center span.
- to verify the real dynamic structural behavior due to earthquake of each foundation with design values, a three-component accelerometer was installed in at least one location on each foundation.
- velocity gauges were installed to monitor the vibration response due to wind and earthquake of the girders and main tower.

- GPS units were installed on the tops of the 1A and 2P tower and in the middle of the center span [54]. The coordinate of 1A was fixed as original point (OPT = Original Point Terminal), and other measure point displacements (MPT = Measure Point Terminal) were calculated in longitudinal, vertical and transversal components.
- displacement gauges were installed on the west and east edges of the 2P center-span side, and on the west side of the 3P side-span.
- since the main tower has a height approximate to 300m, it was confirmed through wind tunnel test that vortex oscillation would occur following a wind speed even lower than design wind speed. For stabilization purpose, Tuned mass damper (TMDs) were installed inside the tower and its displacement were measured by displacement gauges.
- three cable thermometers were installed in order to compensate with the displacement measured by GPS, and one atmospheric thermometer was installed in the middle of the center span.

1.3.3 System network

The monitoring system network of Akashi Kaikyō Bridge is shown in Figure 1.7 and consists of four parts: terminal, workstation, data processor, and data control device.

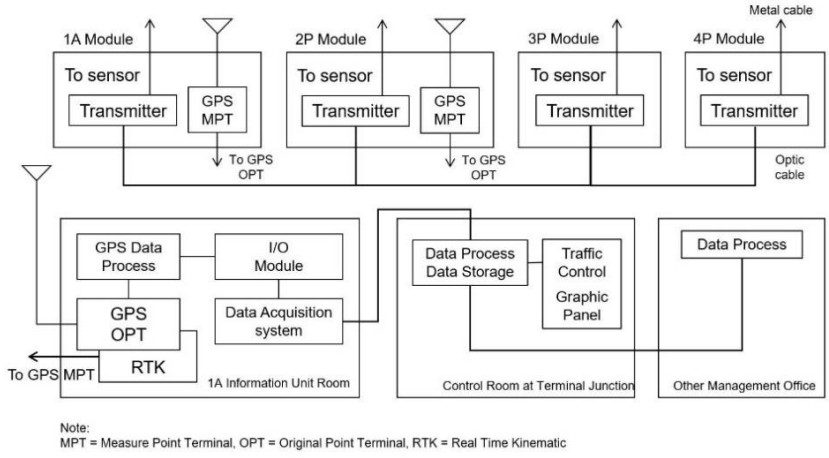

Figure 1.7 Monitoring system network of Akashi Kaikyō Bridge

Monitoring sensors were divided into blocks based on their location of installation, and adding with data converters and transmitters, terminals were established for each block. Collected data at each terminal is transmitted digitally by optic fibers, and those are concentrated by a network workstation located in the 1A information unit room.

The data processor located in the 1A information unit room was divided into a data collection portion (mainly for trigger detection and data storage) and a processing portion (to display the monitoring data).

Data control device was used for analyzing recorded data, such as, time history data graphing, statistical and analytical processing. The data was formed into a database by a data processor located in control room at Tarumi junction.

1.4 Limitation and opportunities

The sensors have became quickly popular for their relatively low cost as well as higher reliability compared to the traditional inspection methods. The most common sensor types include accelerometer, strain gauge, and inclinometer. Due to the inexpensive cost of wired sensors, large amount of them can be installed to generate detailed information on the stress of the different bridge locations and to understand the stress level of embedded reinforcement or concrete deck. However, one of the main drawbacks in the usage of wired-sensors is the wiring system that connects the sensors with the central server, which required labor-intensive cabling [55].

Indeed, each sensor installed has to be connected to a data acquisition system in order to transmit the collected data and to be power supplied. Using a large number of sensors, the amount of cables involved will increase accordingly. Intensive cabling will result in great amount of labor cost along with the cost of the cable itself. Since the sensors are directly connected to the central system, the communication among the sensors has to be restrained.

In recent years, the wireless feature has been introduced to the sensors used in civil structural health monitoring. With already reliable and accurate sensor devices, the wireless feature brought the SHM into a brand new level. Portability and reusability of the wireless sensors are the great benefits over the wired devices. After the vibration monitoring experiment performed on Dongying Huanghe River Bridge [56], it was concluded that the wireless sensors provide flexibility and reduce the number of sensors required, since they can be easily installed and removed in a short duration of time. With the easiness in reinstallation of wireless sensors, multiple tests can be conducted at different sets of locations on the same bridge. Therefore, a wireless sensor provides a more economical and effective way to perform the health monitoring of a bridge.

Due to the wireless feature, the sensors require batteries as the power sources. As a result, the power supply is limited and the batteries need to be replaced periodically. However, several adjustments have been suggested by other authors [57-64] to reduce the power consumption by the sensors in different aspects. First, operating the wireless sensors at low duty cycle can extend the monitoring period. It is important to select ultra-low power hardware (i.e., sensors, microprocessor, and antenna) to minimize the power consumption of the sensor nodes. In addition, programming the sensor nodes to send valuable information instead of raw data can significantly extend battery life as well. At last, using data communication method such as multi-hop networks can help in reducing power consumption. With advantages such as portability, reusability and convenience over wired sensors, the wireless sensors are clearly an outstanding, reliable and cost effective option to use for SHM purposes.

1.4.1 Features of a WSN

A Wireless Sensor Network (WSN) consists of spatially distributed autonomous wireless sensors to monitor physical or environmental conditions such as temperature, sound, vibration, pressure, motion or pollutants. Moreover, it has to cooperatively pass their data through the wireless network to a main location [65].

The WSN is made of some nodes, from a few to several hundreds or even thousands, where each node is connected to one or several sensors. Each sensor network node is typically composed by several parts:

- a radio transceiver with an internal antenna or connection to an external one,
- a microcontroller with a memory,
- an Analog to Digital Converter (ADC),
- a signal conditioner for interfacing with the sensors,
- a power management, and
- an energy source (i.e., batteries or other forms of energy harvesting).

The typology of the WSN can vary from a simple “star” network to an advanced “multi-hop wireless mesh” network. The propagation technique between the hops of the network can be carried out by routing or flooding.

There are many broadly used standard wireless technologies, which can be used for a wireless sensor, like Cellular network, Wi-Fi and Bluetooth. Although they are mature and popular, these technologies do not feature low-cost and low-power. These two features are addressed only by IEEE802.15.4, and ZigBee.

The emerging ZigBee™ protocol is a specification for a suite of high-level communication protocols using small, low-power digital radio based on the IEEE 802.15.4 standard for wireless personal area networks (WPANs). ZigBee™ is poised to become the global control/sensor network standard. It can be simply implemented and contains features like low power consumption and low data rate. The focus of ZigBee™ technique is to define a general-purpose, low-cost, low-power, self-organizing mesh network that can be used for various applications where low data transfer rate is sufficient.

Low cost allows the technology to be widely deployed in wireless control and monitoring applications. Low power allows longer life with smaller batteries. Mesh networking provides high reliability and a more extensive range.

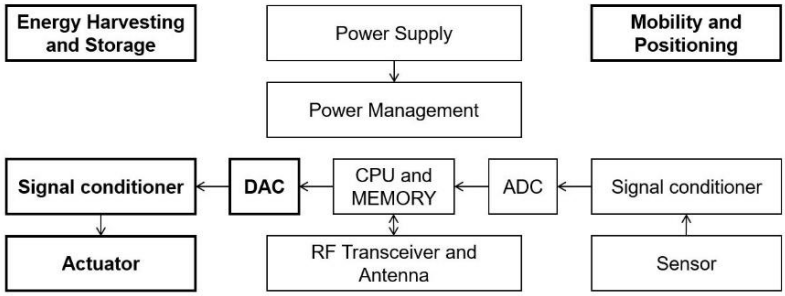

Figure 1.8 The block diagram of an ideal autonomous wireless sensor

In recent years, some new concepts marked in bold in the Figure 1.8 for a WSN are emerged: actuator management, energy harvesting and storage for self-powered perpetual wireless sensor, self-positioning and mobility.
Conventional wireless sensor network can only offer monitoring function. However, its functionality can be extended to include actuation capabilities by integrating an actuation signal generation module for controlling an actuator. For instance, in [66] the authors proposed a wireless sensor prototype capable of data acquisition, computational analysis and actuation to use in a structure control system with a semi-active magnetorheological (MR) damper as the actuator.

Besides integration of actuator in a wireless sensor network, mobility is another attractive function for structural health monitoring. Compared with static sensors, mobile sensor networks offer flexible system architectures with adaptive spatial resolutions. The authors in [67] propose a mobile sensing node that is capable of maneuvering on structures built with ferromagnetic materials. The mobile sensing node can also attach/detach an accelerometer into/from the structural surface.

There are also many other bio-inspired robot techniques which have the potential to provide mobility for wireless sensor. The authors in [68] propose proposes two small-scale agile wall climbing robots, *Geckobot* and *Waalbot*, able to navigate on smooth vertical surfaces, which use adhesive materials for attachment. *Geckobot* is a lizard-inspired climbing robot with similar kinematics to a gecko-climbing gait. *Waalbot* uses two actuated legs with rotary motion and two passive revolute joints at each foot. The authors in [69] propose a *RiSE* robot, which is a biologically inspired to a six-legged climbing robot and designed for general mobility in scansorial environments (i.e., vertical walls, horizontal ledges, ground level). The authors in [70] propose a new bio-inspired climbing robot designed to scale smooth vertical surfaces using directional adhesive materials. The robot, called *Stickybot*, draws its inspiration from geckos and other climbing lizards. It employs similar compliance and force control strategies to climb smooth vertical surfaces including glass, tile and plastic panels.

Self-positioning is another desirable feature for a wireless sensor. Position itself is an importance physical variable for a wireless sensor. In structural monitoring, the positioning sensor can be used to monitor the deformation or displacement of a structure [71]. Combining the feature of mobility and self-positioning, it is possible for the wireless sensor to autonomously move to a designated location.

There are many positioning technologies available with different accuracy. Besides the well known and broadly used out-door GPS technique, there are many other methods appropriate for in-door positioning, including received signal strength (RSS), angle of arrival (AOA), time of arrival (TOA), round trip time of flight (RTOF) and time difference of arrival (TDOA) [72]. Especially, the IEEE802.15.4 physical layers standard is updated to IEEE802.15.4a, which is capable of TOA distance measurement through two additional physical layers using ultra-wideband (UWB) and chirp spread spectrum (CSS) [73].

1.4.2 Challenges for WSNs

For structural health monitoring purposes, one needs to read acceleration signals down to 500μG (1G is the gravity) [74], at a frequency higher than 100Hz synchronously at all nodes. In addition to these real-time, high fidelity performance requirements, there are other ones. Monitoring needs be economical. The cost includes the system itself, installation, and maintenance. We do not want to disturb the structure being monitored, and introduce no hazards. The requirements of a Structural Health Monitoring can be challenging to WSN for the following reasons:

- *High accuracy of sample*, it means the final reading needs to detect signals down to 500μG without significant distortion. Sources of distortion include the noise floor of the system, installation error, and temperature variation.
- *High-frequency sampling*, it implies a low variation in sampling intervals (jitter).
- *Time synchronization*, sampling needs to start at the same time on all nodes. Furthermore, this needs be done in spite of differences in drift of each clock.
- *Large-scale multi-hop network*, in case the structure spans a long distance (i.e., 1km), it is impossible to cover the entire structure with single hop communication, and a multi-hop network is necessary to provide connectivity.
- *Reliable command dissemination*, if one fails to start some nodes the data for those points will be missed, making analysis very difficult or impossible.
- *Reliable data collection*, data needs to be transferred reliably as well.

As in many other WSN applications, synchronization of the network is highly desirable in SHM applications. However, because of the specific features in SHM (i.e., high sampling frequency and extended sensing duration) synchronization of data is not automatically guaranteed even with accurately synchronized clocks. For this reason, it is important to face the specific features and the imposed challenges in the time synchronization of a WSN [75-83].

1.4.2.1 Synchronized clocks and sensing

One of the distinct features of SHM is that data are typically collected at high frequency. Civil engineering structures vibrate at high frequency, and a sampling rate that is at least twice of the frequency of interest is needed to capture the meaningful dynamic responses. In addition, responses at high frequency are more sensitive to local damage and the accuracy of time synchronization at high frequency is of great importance for damage detection. For instance, a 1ms synchronization error between two measured acceleration responses will result in 3.6° error in phase angle at 10Hz and 36° error at 100Hz [84].

Some authors performed experimental modal analysis on a simply supported beam and illustrated that a small time shift (30μs) at one sensor location resulted in a noticeable error in mode shapes, especially for higher-order modes [85]. For damage detection methods that rely on mode shape information, such as Modal Strain Energy-based Methods [86, 87] and Modal curvature-based methods [88], the mode shape error due to such a small inaccuracy in time synchronization, depending on applications, can lead to false results in damage detection.

For the Jindo Bridge WSNs, the deck and cable vibrations were measured at 25Hz and 50Hz, respectively. The cable network uses a higher sampling frequency because the maximum cable modal frequency required for calculating cable tension is around 20Hz [89]. For the Government Bridge, acceleration responses were measured at 50Hz in order to capture damage-sensitive modal information [90]. Other civil engineering structures such as low-rise buildings can have even higher natural frequencies and higher sampling rates are required when monitoring these structures.

Because of the stringent requirement of synchronization accuracy in the measured data, accurate synchronization of the clocks in a WSN is not always adequate in SHM. Synchronized clocks do not guarantee synchronized data because of three main factors related to both software and hardware issues as summarized in [84]. First, due to the random variation of the processing time in the sensor board driver, the sensors do not start sensing at exactly the same time. Moreover, the low-cost wireless smart sensors are often equipped with low-quality crystals. Therefore, the actual sampling frequencies among the sensor nodes are different and the sampling frequency for each individual sensor node can also fluctuate over time because of jitter. It is well note also that because of software timing issues, compared with real-time Operating Systems, the randomness in sensing start time is more prominent in sensors implemented on event-driven operating system platforms such as TinyOS.

1.4.2.2 Extended sensing duration

Compared with other monitoring applications such as environmental monitoring, in which a single or a few data points are collected during a sensing event, sensing for SHM is characterized by much more sampled data points and therefore requires longer sensing duration (minutes or even hours). One reason is that a large number of data points are needed to extract meaningful information of structural characteristics. For instance, under a given frequency bandwidth, more data points provide higher resolution once the data is converted into the frequency domain. Therefore, higher accuracy of estimated modal frequencies can be achieved. In addition, extended sensing duration is required to fully capture a transient event such as the swinging process of the Government Bridge and the forced vibration due to a train crossing the bridge.

In the case of Jindo Bridge network, for each sensing task, 10000 data points were collected at 25Hz, resulting in 400s of sensing duration. For the Government Bridge, to capture the entire vibration response during a swing event, 10 minutes of data was collected at 50Hz because the swinging takes about 7 minutes. Also to capture the complete record of the forced vibration caused by a train crossing the bridge, which takes about 10 minutes, longer sensing duration is required.

A direct impact of extended sensing duration is that the effect of clock skew becomes significant. Clock skew is a phenomenon that two clocks drift away from each other because of differential clock speed. Even though the clocks were accurately synchronized when sensing started, they can drift away from each other during sensing and cause errors in timestamps, which in turn leads to synchronization error in the sampled data. The authors in [84] tested Imote2 nodes and estimated the maximum clock drift rate among the tested set of nodes to be around 50μs per second, which can lead to 20ms synchronization error after a 400-s measurement. Appropriate clock skew compensation is necessary to eliminate or reduce such an impact.

1.4.2.3 Temperature variation during sensing

Structural Health Monitoring systems are typically deployed in outdoor environment where temperature can change drastically during a short period of time. For example, sensors that are in the shade at the beginning of sensing can soon come under direct sunlight, which can heat up the sensor quickly and introduce large temperature variation during sensing period.

In addition, sensing for SHM occurs at high frequency and lasts for long period of time and therefore can generate a lot of heat, resulting in temperature change on the sensor board. Some authors performed 10-min sensing using Imote2s and SHM-A sensor boards [91]. Temperature readings were collected during the process. The onboard temperatures of Imote2s increased by almost 6°C because of the heat generated by the Imote2 CPU and the analog-to-digital converter (ADC) chip on the SHM-A board.

Nonlinear clock drift is a direct consequence of temperature change during sensing. The clock of a wireless smart sensor is typically driven by a quartz crystal, whose resonant frequency is temperature dependent. Other authors showed clear correlation between temperature and different pairs of clocks exhibit different clock skew change patterns with respect to temperature [92]. In the aforementioned experiments, i.e., [91], significant nonlinearity in clock drift was observed induced by temperature change during sensing.

1.4.2.4 Rapid response to transient events

To conserve energy, smart sensors are often designed to spend most of their time in deep sleep mode and wake up periodically to listen for external commands. After waking up, if the network receives a command to collect data, it has to be synchronized again before starting sensing. Therefore, a delay is introduced between the reception of the command and the start of sensing because of the need for resynchronization. Such a delay may cause the entire transient event such as earthquakes to be missed.

For instance, in the case of the Jindo Bridge network, the resynchronization takes 30s to collect beacon packets to estimate the linear clock drift rate, which is used later to perform drift compensation for the data timestamps.

In the Government Bridge case, when the sentry sensor detects the movement of the swing span, it has to wake up the entire network first and perform resynchronization before the collection of data; therefore, a significant portion of the swing event is missed. Although the time needed for waking up the network also contributes to the delay, minimizing the delay due to time synchronization is critical towards capturing the entire transient structural response.

1.5 References

[1] Nassif, H.H., Gindy, M. & Davis, J. 2005. Comparison of laser Doppler vibrometer with contact sensors for monitoring bridge deflection and vibration. NDT&E International, 38(3), 213-218.

[2] Bai, R., Ostachowics, W., Radzienski, M. & Cao M. 2014. Vibrational damage detection using fractal surface singularities with noncontact laser measurement. Journal of Vibration and Control, 22(11), 1-13.

[3] Olaszek, P. 1999. Investigation of the dynamic characteristic of bridge structures using a computer vision method. Measurement, 25(3), 227-236.

[4] Wahbeh, A.M., Caffrey, J.P. & Masri, S.F. 2003. A vision-based approach for the direct measurement of displacements in vibrating systems. Smart Materials and Structures, 12(5), 785-794.

[5] Lee, J.J. & Shinozuka, M. 2006. A vision-based system for remote sensing of bridge displacement. NDT&E International, 39(5), 425-431.

[6] Casciati, F., Casciati, S. & Wu, L-J. 2013. Vision-based sensing in dynamic tests. Key Engineering Materials, 569-570, 767-774.

[7] Wu, L-J. & Casciati, F. 2014. Local positioning systems versus structural monitoring: a review. Structural Control Health Monitoring, 21(9), 1209-1221.

[8] Wu, L-J., Casciati, F. & Casciati, S. 2014. Dynamic testing of a laboratory model via vision-based sensing. Engineering Structures, 60, 113-125.

[9] Casciati, F. & Wu, L-J. 2014. Structural monitoring through acquisition of images (Book Chapter). Mechanics and Model-Based Control of Advanced Engineering Systems, 67-74.

[10] Park, K.T., Kim, S.H., Park, H.S. & Lee, K.W. 2005. The determination of bridge displacement using measured acceleration. Engineering Structures, 27(3), 371-378.

[11] Sim, S.H., Spencer Jr., B.F., Nagayama, T. 2011. Multimetric sensing for structural damage detection. Journal of Engineering Mechanics, 137(1), 22-30.

[12] Kim, J., Kim, K. & Sohn, H. 2014. Autonomous dynamic displacement estimation from data fusion of acceleration and intermittent displacement measurements. Mechanical Systems and Signal Processing, 42(1-2), 194-205.

[13] Sung, S.H., Park, J.W., Nagayama, T. & Jung H.J. 2014. A multi-scale sensing and diagnosis system combining accelerometers and gyroscopes for bridge health monitoring. Smart Materials and Structures, 23(1), 1-14.

[14] Roberts, G.W., Meng, X. & Dodson, A.H. 2004. Integrating a global positioning system and accelerometers to monitor the deflection of bridges. Journal of Surveying Engineering, 130(2), 65-72.

[15] Casciati, F. & Fuggini, C. 2011. Monitoring a steel building using GPS sensors. Smart Structures and Systems, 7(5), 349-363.

[16] Casciati, F. & Fuggini, C. 2009. Engineering vibration monitoring by GPS: Long duration records. Earthquake Engineering and Engineering Vibration, 8(3), 459-467.

[17] Park, J.W., Sim, S.H. & Jung, H.J. 2013. Displacement estimation using multimetric data fusion. IEEE/ASME Transactions on Mechatronics, 18(6), 1675-1682.

[18] Park, J.W., Sim, S.H. & Jung, H.J. 2014. Wireless displacement sensing system for bridges using multi-sensor fusion. Smart Materials and Structures, 23(4), 1-12.

[19] Cho, S., Sim, S.H., Park, J.W. & Lee, J. 2014. Extension of indirect displacement estimation method using acceleration and strain to various types of beam structures. Smart Structures and Systems, 14(4), 699-718.

[20] Cho, S., Yun, C.B. & Sim, S.H. 2015. Displacement Estimation of Bridge Structures using Data Fusion of Acceleration and Strain Measurement Incorporating Finite Element Model. Smart Structures and Systems, 15(3-4), 645-663.

[21] Sim, S. 2016. Estimation of Flexibility Matrix of Beam Structures Using Multisensor Fusion. Journal of Structural Integrity and Maintenance, 1(2), 60-64.

[22] Brownjohn, J.M.W. 2007. Structural health monitoring of civil infrastructure. Philosophical Transactions of the Royal Society A: Mathematical, Physical and Engineering Sciences, 365 (1851), 589–622.

[23] Rizos, C. 2002. Making sense of the GPS techniques. Manual of Geospatial Science and Technology, 2, 146-161.

[24] Ashkenazi, V. & Roberts, G.W. 1997. Experimental monitoring of the Humber Bridge using GPS. Proceedings of Institution of Civil Engineering, 120(4), 177-182.

[25] Brownjohn, J.M.W., Rizos, C., Tan, G.H. & Pan, T.C. 2004. Real-time long-term monitoring of static and dynamic displacements of an office tower, combining RTK GPS and accelerometer data. Proceedings of 1st FIG Int. symposium on engineering surveys for construction works and structural engineering, 1-15.

[26] Kijewski-Correa, T.L. & Kareem, A. 2003. The Chicago monitoring project: a fusion of information technologies and advanced sensing for civil infrastructure. In Proceedings of SHMII-1, Structural Health Monitoring and Intelligent Infrastructures, 2, 1003-1010.

[27] Li, X., Ge, L., Peng, G.D., Rizos, C., Tamura, Y. & Yoshida, A. 2004. Seismic response of a tower as measured by an integrated RTK-GPS system. Proceedings of 1st FIG Int. symposium on engineering surveys for construction works and structural engineering, Nottingham, UK.

[28] Hillman, B.A., Baldwin, C. & Meyerholtz, S. 2003. Real-time GPS monitoring. Proceedings of 23rd USSD Annual Meetings and Conference Libby Dam, Libby, Montana.

[29] Wong, K.Y., Man, K.L. & Chan, W.Y. 2001. Monitoring Hong Kong's Bridges Real-Time Kinematic Spans the Gap. Reprinted from GPS World. USA, Advanstar Publication.

[30] Caetano, E., Cunha, A., Gattulli, V. & Lepidi, M. 2008. Cable-deck dynamic interactions at the International Guadiana Bridge: On-site measurements and finite element modelling. Structural Control and Health Monitoring, 15(3), 237-264.

[31] Cunha, A., Caetano, E., Magalhães, F. & Moutinho, C. 2013. Recent perspectives in dynamic testing and monitoring of bridges. Structural Control and Health Monitoring, 20(6), 853-877.

[32] Speranzini, E. & Agnetti, S. 2014. The technique of digital image correlation to identify defects in glass structures. Structural Control and Health Monitoring, 21(6), 1015-1029.

[33] Arangio, S. & Bontempi, F. 2015. Structural health monitoring of a cable-stayed bridge with Bayesian neural networks. Structure and Infrastructure Engineering, 11(4), 575-587.

[34] Buongiorno Nardelli, B., Pisano, A., Tronconi, C. & Santoleri, R. 2015. Evaluation of different covariance models for the operational interpolation of

high-resolution satellite Sea Surface Temperature data over the Mediterranean Sea. Remote Sensing of Environment, 164, 334-343.

[35] Ni, Y.Q., Wang, Y.W. & Xia, Y.X. 2015. Investigation of mode identifiability of a cable-stayed bridge: comparison from ambient vibration responses and from typhoon-induced dynamic responses. Smart Structures and Systems, 15(2), 447-468.

[36] Casciati, F., Casciati, S., Elia, L. & Faravelli, L. 2015. Tension Estimates in Cable-Stayed Bridge. Proceedings of International Conference on Performance-based Lifecycle Structural Engineering (PLSE 2015), Brisbane, Australia.

[37] Casciati, F., Casciati, S., Elia, L. & Faravelli, L. 2016. Optimal reduction from an initial sensor deployment along the deck of a cable-stayed bridge. Smart Structures and Systems, 17(3), 523-539.

[38] Casciati, S. & Elia, L. 2016. Estimating cable forces in a large cable-stayed bridge. Proceedings of 5th International Conference Smart and Multifunctional Materials, Structures and Systems (CIMTEC 2016), Perugia, Italy.

[39] Casciati, S. & Elia, L. 2016. Elaborations from the TKB monitoring database. Dynamics and Control of Advanced Structures and Machines, Springer.

[40] Wong, K.Y. 2004. Instrumentation and health monitoring of cable-supported bridges. Structural Control Health Monitoring, 11(2), 91-124.

[41] Ko, J.M. & Ni, Y.Q. 2005. Technology developments in structural health monitoring of large-scale bridges. Engineering Structures, 27(12), 1715-1725.

[42] Wong, K.Y. 2007. Design of a structural health monitoring system for long-span bridges. Structure and Infrastructure Engineering, 3(2), 169-185.

[43] Ni, Y.Q., Wong, K.Y. & Xia, Y. 2011. Health checks through landmark bridges to sky-high structures. Advances in Structural Engineering, 14(1), 103-119.

[44] Yuen K.C. 2007. Study on Ting Kau Bridge. Proceedings of Bridge Engineering, 2, University of Bath, Bath, UK.

[45] Sumitro S. 2001. Current and Future Trends in Long Span Bridge Health Monitoring System in Japan. A Workshop Sponsored by the National Science Foundation on Health Monitoring of Long Span Bridges, University of California, USA.

[46] Kitagawa, M. 2004. Technology of the Akashi Kaikyō Bridge. Structural Control Health Monitoring, 11(2), 75-90.

[47] Honshu-Shikoku Bridge Authority & JSCE. 1998. The Akashi-Kaikyō Bridge Design and Construction of the World's longest Bridge. Honshu-Shikoku Bridge Authority.

[48] Yamada, H., Katsuchi, H. & Kitagawa, M. 2000. Field Measurement of Wind Property at Ohnaruto Bridge and the Akashi Kaikyō Bridge. Proceedings of Workshop on Research and Monitoring of Long Span Bridges, 196-203.

[49] Abe K. & Amano, K. 1998. Monitoring system of the Akashi Kaikyō Bridge. Honshi Technical Report, 22(86), 29-34.

[50] Adachi, Y. & Unjoh, S. 1999. Development of shape memory alloy damper for intelligent bridge system. Proceedings of SPIE - The International Society for Optical Engineering, 3671, 31-42.

[51] Aktan, A.E., Catbas, F.N., Pervizpour, M., Kulcu, E., Grimmelsman, K., Barrish, R. & Qin, X. 2000. Real-time bridge health monitoring for management. Proceedings of 2nd Workshop on Advanced Technologies in Urban Earthquake Disaster Mitigation, Kyoto.

[52] Thompson, L. & Westermo, B. 1993. A new strain measurement technology for material damage assessment", Proceeding of SPIE, The International Society for Optical Engineering, 2191, 380-391.

[53] Kashima, S., Okano, S., Takeguchi M. & Mori K. 2000. Monitoring system of the Akashi Kaikyō Bridge. Proceedings of Workshop on Research and Monitoring of Long Span Bridges, 119-126.

[54] Fujino, Y., Murata, M., Okano, S. & Takeguchi, M. 2000. Monitoring system of the Akashi Kaikyō Bridge and displacement measurement using GPS", Proc. SPIE, 3995, 229-236.

[55] Teng, C-K. 2012. Structural Health Monitoring of a Bridge Structure Using Wireless Sensor Network, Master's Theses, Western Michigan University.

[56] Yu, Y., Xie, H., Ou, J. 2010. Vibration Monitoring Using Wireless Sensor Networks on Dongying Huanghe River Bridge. Earth and Space 2010: Engineering, Science, Construction, and Operations in Challenging Environments, ASCE, 2568-2576.

[57] Feltrin, G., Bischoff, R., Meyer, J., Saukh, O. 2010. Structural monitoring with wireless sensor networks: lessons learned from field deployments. Bridge Maintenance, Safety, Management and Life-Cycle Optimization. Dubendorf, Empa - Swiss Federal Laboratories of Materials Testing and Research.

[58] Casciati, S. & Chen, Z-C. 2011. A multi-channel wireless connection system for structural health monitoring applications. Structural Control and Health Monitoring, 18(5), 588-600.

[59] Casciati, S. & Chen, Z-C. 2012. An active mass damper system for structural control using real-time wireless sensors. Structural Control and Health Monitoring, 19(8), 758-767.

[60] Casciati, S., Faravelli, L. & Chen, Z-C. 2012. Energy harvesting and power management of wireless sensors for structural control applications in civil engineering. Smart Structures and Systems, 10(3), 299-312.

[61] Chen, Z-C. & Casciati, F. 2014. A low-noise, real-time, wireless data acquisition system for structural monitoring applications. Structural Control and Health Monitoring, 21(7), 1118-1136.

[62] Chen, Z-C., Casciati, S. & Faravelli, L. 2015. In-Situ validation of a wireless data acquisition system by monitoring a pedestrian bridge. Advances in Structural Engineering, 18(1), 97-106.

[63] Casciati, F., Casciati, S., Chen, Z-C., Faravelli, L. & Vece, M. 2015. Collecting data from a sensor network in a single-board computer. Journal of Physics: Conference Series, 628(1), 012113.

[64] Casciati, S., Chen, Z-C., Faravelli, L. & Vece, M. 2016. Synergy of monitoring and security. Smart Structures and Systems, 17 (5), pp. 743-751.

[65] Chen Z-C. 2011. Structural Monitoring and System Control Using a Wireless Sensor Network, PhD Thesis, University of Pavia, Italy.

[66] Lynch, J.P., Wang, Y., Swartz, R.A., Lu, K.C. & Loh, C.H. 2008. Implementation of a closed-loop structural control system using wireless sensor networks. Structural Control and Health Monitoring, 15(4), 518-539.

[67] Zhu, D., Yi, X., Wang, Y., Lee, K.M. & Guo, J. 2010. A Mobile Sensing System for Structural Health Monitoring: Design and Validation. Smart Materials and Structures, 19(5), 1-11.

[68] Unver, O., Murphy, M.P. & Sitti, M. 2005. Geckobot and Waalbot: Small-Scale Wall Climbing Robots. Proceedings of AIAA 5th Aviation, Technology, Integration, and Operations Conference.

[69] Saunders, A., Goldman, D., Full R. & Buehler, M. 2006. The RiSE Climbing Robot: Body and Leg Design. Proceeding of SPIE Defense & Security Symposium, Unmanned Systems Technology, Orlando, FL.

[70] Kim, S., Spenko, M., Trujillo, S., Heyneman, B., Mattoli, V. & Cutkosky, M.R. 2007. Whole body adhesion: hierarchical, directional and distributed control of adhesive forces for a climbing robot. Proceedings of IEEE International Conference on Robotics and Automation, Roma, Italy.

[71] Casciati, F. & Chen, Z-C. 2009. Using GPS Sensors in Structural Mechanics. Proceedings of 1st Japan-Austria Joint Workshop on Mechanics and Model Based Control of Smart Materials and Structures. H. Irschik, M. Krommer, K. Watanabe and T. Furukawa, Springer Wien New York.

[72] Liu, H., Darabi, H., Banerjee, P. & Liu, J. 2007. Survey of Wireless Indoor Positioning Techniques and Systems. IEEE Transactions on Systems, Man, and Cybernetics-Part C: Applications and Reviews, 37(6), 1067-1080.

[73] IEEE Computer Society. 2006. Wireless Medium Access Control (MAC) and Physical Layer (PHY) - Specifications for Low-Rate Wireless Personal Area Networks (WPANs). New York, Institute of Electrical and Electronics Engineers, Inc.

[74] Kim, S. 2005. Wireless Sensor Networks for Structural Health Monitoring. Master of Science in Computer Science. University of California at Berkeley, USA.

[75] Lynch, J.P. 2006. A summary review of wireless sensors and sensor networks for structural health monitoring. Shock and Vibration Digest, 38(2), 91-128.

[76] Lynch, J.P. 2007. An overview of wireless structural health monitoring for civil structures. Philosophical Transactions of the Royal Society A: Mathematical, Physical and Engineering Sciences, 365(1851), 345-372.

[77] Cho, S., Jo, H., Jang, S., Park, J., Jung, H-J., Yun, C-B., Spencer Jr., B.F. & Seo, J-W. 2010. Structural health monitoring of a cable-stayed bridge using wireless smart sensor technology: Data analyses. Smart Structures and Systems, 6(5-6), 461-480.

[78] Jang, S., Spencer Jr., B.F. & Sim, S-H. 2012. A decentralized receptance-based damage detection strategy for wireless smart sensors. Smart Materials and Structures, 21(5), 1-12.

[79] Linderman, L.E., Mechitov, K.A. & Spencer Jr., B.F. 2013. TinyOS-based real-time wireless data acquisition framework for structural health monitoring and control. Structural Control and Health Monitoring, 20(6), 1007-1020.

[80] Chen, Z-C. 2014. Energy efficiency strategy for a general real-time wireless sensor platform. Smart Structures and Systems, 14(4), 617-641.

[81] Sim, S-H., Li, J., Jo, H., Park, J-W., Cho, S., Spencer Jr., B.F., Jung, H-J. 2014. A wireless smart sensor network for automated monitoring of cable tension. Smart Materials and Structures, 23(2), 1-10.

[82] Cho, S., Giles, R.K., Spencer Jr., B.F. 2015. System identification of a historic swing truss bridge using a wireless sensor network employing orientation correction. Structural Control and Health Monitoring, 22(2), 255-272.

[83] Li, J., Mechitov, K.A., Kim, R.E., Spencer Jr., B.F. 2016. Efficient time synchronization for structural health monitoring using wireless smart sensor networks. Structural Control and Health Monitoring, 23(3), 470-486.

[84] Nagayama, T., Sim, S.H., Miyamori, Y. & Spencer Jr., B.F. 2007. Issues in structural health monitoring employing smart sensors. Smart Structures and Systems, 3(3), 299-320.

[85] Krishnamurthy, V., Fowler, K. & Sazonov, E. 2008. The effect of time synchronization of wireless sensors on the modal analysis of structures. Smart Materials and Structures, 17, 1-13.

[86] Cornwell, P., Doebling, S.W. & Farrar, C.R. 1999. Application of the strain energy damage detection method to plate-like structures. Journal of Sound and Vibration, 224(2), 359-374.

[87] Sazonov, E., Klinkhachorn, P., Halabe, U.B. & GangaRao, H. 2002. Non-baseline detection of small damages from changes in strain energy mode shapes. Nondestructive Testing and Evaluation, 18(3–4), 91-107.

[88] Pandey, A.K., Biswas, M. & Samman, M.M. 1991. Damage detection from changes in curvature mode shapes. Journal of Sound and Vibration, 145(2), 321-332.

[89] Sim, S., Li, J., Jo, H., Park, J., Cho, S., Spencer Jr., B.F. & Jung, H. 2014. Wireless smart sensor network for automated monitoring of cable tension. Smart Materials and Structures, 23(2), 1-10.

[90] Giles R. 2013. Development of a long-term, multimetric structural health monitoring system for a historic steel truss swing bridge. Ph.D. Thesis, University of Illinois at Urbana-Champaign.

[91] Li, J., Nagayama, T., Mechitov, K.A. & Spencer Jr., B.F. 2012. EC-tSHMUWS sensors, Proceedings of SPIE Smart Structures, San Diego, CA.

[92] Yang Z, Cai L, Liu Y, Pan J. Environmental-aware clock skew estimation and synchronization for wireless sensor networks. Proceedings IEEE INFOCOM, 2012.

Chapter 2 A brief overview on compressive sensing

Advanced studies have enabled the development of low-cost, low power devices that integrate sensing, processing and wireless communication capabilities [1-3]. These devices, named *sensor nodes*, implement a Wireless Sensor Network (WSN), which allows one to monitor the behavior of civil structures, during forced vibration testing or natural excitation.

When accomplishing the SHM (Structural Health Monitoring) tasks, one of the most fundamental issues is the so-called sensor reachback problem, which has recently received considerable attention [4]. In detail, it is related to the several difficulties appearing when the acquired sensor observations are transmitted to a data-collecting point (*sink node*), which has increased processing and power consumption capabilities.

The amount of data generated by the *sensor nodes* is immense, because structural monitoring applications need to transfer relatively large amounts of dynamic response measurement data with sampling frequencies as high as 1000Hz [5]. In literature, considerable research efforts have been made to reduce the amount of data traffic in WSNs. Since processing data usually consumes much less power than transmitting data in wireless medium, many works considered applying data compression techniques to reduce total power consumption by a *sensor node* [6]. Thus, some authors [7] have provided a comprehensive survey of practical data compression techniques based on compressed sensing, distributed transform coding, or differential pulse code modulation.

To handle the problem associated with the massive data generated at the *sensor nodes*, the correlation among measurements by neighboring sensors can be leveraged [8]. For instance, the data collected by the sensors on each span of a bridge are correlated since they are measuring the vibration of the same part of the physical structure. Moreover, in some cases of bridge design, two adjacent spans are connected to a common anchorage, resulting in the data across the two spans to be correlated.

Similarly, for large buildings, it is natural to group the sensors in their several distinct parts (i.e., the floors). Other authors [9] proposed a spatio-temporal protocol, based on the adaptive filtering technique, which tracks the time-varying prediction model at each sensor and consequently reduces the power consumption by reducing transmissions.

It is well know that all these approaches, as well as the Slepian-Wolf coding [10], offer the potential to greatly reduce the amount of information that needs to be transmitted. However, the Slepian-Wolf coding gives only information-theoretical bounds for data compression and it is quite difficult to be incorporated into a practical system.

On the other hand, many SHM research have led to the development of several strategies for damage detection and localization, which fulfill the requirements of effectiveness, simplicity, reliability and low amount of data storage [11-13]. Therefore, damage detection can be performed using time series analysis of vibration signals measured from a structure before and after damage. In particular, the authors in [14] used the autoregressive moving average (ARMA) time series model to develop features that discriminate between damage and non-damaged cases, and their efficacy was tested on an ASCE benchmark structure [15].

In this chapter, an overview on the recent compression solutions adopted by several authors to overcome the WSN issues above described is provided. In addition, the problem formulation is faced and a brief description of the developed protocols is presented to investigate the so far academic efforts carried out in the SHM field.

2.1 A prediction-error-based method

The aim of this method is to reduce the data transmission and storage from the *sensor nodes* to the *sink node* in a structural monitoring WSN, without harming its ability to detect damage [16]. The monitored structure is modelled as a time-invariant system and aim to predict its response to a given excitation at each sensor location. The prediction model is unique for each sensor and it is known by the *sink node*. In the studied strategy, only the excitation signal is transmitted continuously to the *sink node*. The transmission between any sensor and the *sink node* occurs only if the prediction error at the sensor exceeds a predefined limit. In that case, only the prediction error is transmitted. Therefore, a significant reduction can be achieved, i.e., up to *1/K* of the original transmission load, where *K* denotes the number of *sensor nodes*. Note that, using the prediction models and the excitation signal, the *sink node* can regenerate the measurements for any sensor at any time within some predefined accuracy. To model the structure, the prediction-error method (PEM) is employed, i.e., a common family of estimation methods in the system identification literature [17, 18].

Due to the fact that the transmission performance of this method is dependent on the time invariant prediction model, an increased number of transmissions from a certain sensor, i.e., an increase in the prediction error, indicates a change in that sensor's input-output relationship. Such a change may be induced as a result of damage. By exploiting its

sensitivity to the changes in the system, it can be argued that the prediction-error-based approach can be used to identify and localize newly occurring damages.

2.1.1 Prediction-error model

In order to alleviate the dense sensor reading transmission and storage problem, a prediction-error-based approach is studied. In this approach, each sensor reading is treated as the output of a random system, which is excited by some natural phenomenon.

Let us consider a subset consisting of K nodes, of a dense wireless sensor network deployed in a civil structure that we wish to monitor. Each sensor node k, at discrete time t, acquires the measurement $y_k(t)$, which is related to an event that takes place in the area where the wireless sensor network has been deployed. Due to the nature of the observed phenomenon the measurements' process $y_k(t)$ is commonly a predictable one, at least to some extent. Therefore, the subset sensors' measurements can be predicted with some accuracy by using prediction-error models and a common excitation signal. In brief, the input-output relation between the excitation and the sensor reading is modeled and using the excitation data in this model, the sensor's readings are predicted. This model is referred to as the Prediction-Error Model and it is of the following form:

$$A_k(q)y_k(t) = \frac{B_k(q)}{F_k(q)}u(t) + \frac{C_k(q)e_k(t)}{D_k(q)} \qquad (2.1)$$

where $u(t)$ is the common excitation data and can be provided by a *phenomenon dedicated* sensor, or extracted from the readings of a reliable set of similar sensors. The system output is the measurement $y_k(t)$, while $e_k(t)$ is white-noise disturbance. The sensor specific polynomials A_k, B_k, F_k, C_k, and D_k are specified by:

- the orders of polynomials na, nb, nf, nc and nd, respectively,
- the model parameter coefficients to be estimated, $a_{k,1} \ldots a_{k,na}$, $b_{k,0}$, $b_{k,1} \ldots b_{k,nb}$, $f_{k,1} \ldots f_{k,nf}$, $c_{k,1} \ldots c_{k,nc}$ *and* $d_{k,1} \ldots d_{k,nd}$, respectively, and
- the time-shift operator q.

For instance, for some discrete-time sequence $x(t)$, it holds $x(t) + k_1x(t-1) = K(q)x(t)$ *where* $K(q) = 1 + k_1q^{-1}$. It is well note that, from Eq. (2.1), the prediction model is employing not only the most recent excitation data $u(t)$ but also N previous history (i.e., $u(t-1), \ldots, u(t-N)$), where $N = nb + nd$.

The predicted value of the actual measurement $y_k(t)$, which is obtained by the prediction model, is denoted by $p_k(t)$. Thus, using its specific prediction model and the common excitation data, each sensor k performs some steps. Firstly, it predicts a value $p_k(t)$ for

given time instant *t*. Next, it subtracts the prediction from its actual reading $y_k(t)$ to generate an error signal $e_k(t)$,

$$e_k(t) = y_k(t) - p_k(t) \tag{2.2}$$

Finally, it compares the error with a selected threshold (transmission criterion), and decides whether to transmit the error or not. This approach is illustrated in Figure 2.1.

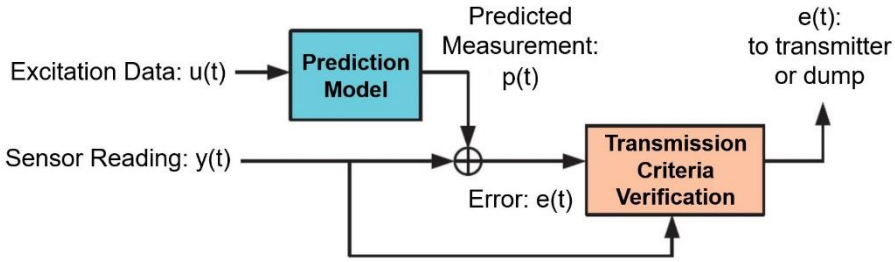

Figure 2.1 The protocol performed at each node

To decrease the noise effect, the data are filtered before estimating the model. Initially, a fast Fourier transform (FFT) analysis is conducted in order to transform the time domain data into the frequency domain. Afterwards, the peak frequency can be determined, i.e., the frequency with the highest magnitude conveying most of the information on the signal. Therefore, that frequency is selected to be the central frequency of a narrow band. To obtain a good model fit, it is crucial to choose the bandpass filter with the passband containing the peak frequency, which will be further discussed in the following section.

2.1.2 Protocol description

The prediction-based transmission approach reduces the amount of transmitted and hence stored data by the use of a sensor specific *prediction-error model* and *common excitation data*. Specifically, any sensor transmits its prediction error only if the error is greater than a predefined threshold. Consequently, the *sink* needs to store only the common excitation data and the error values for each sensor *k*, so it can reproduce the approximate measurement for sensor *k* whenever it needs to using the prediction function $P_k(\cdot)$:

$$\tilde{y}_k(t) = P_k\big(u(t), u(t-1), \dots, u(t-N)\big) + e_{k\,rec}(t) \tag{2.3}$$

Note that in Eq. (2.3) the prediction function $P_k(\cdot)$ stands for the prediction-error model described by Eq. (2.1), while $e_{k\,rec}(t)$ denotes the prediction-error sequence received by

the *sink*. Ideally, the *sink* is able to reconstruct the measurement $y_k(t)$ exactly, once it has all past excitation data up to time N, past measurements up to time $M = na + nf + nd$ as well as all past errors up to time $nf + nc$. However, in order to provide some energy savings in terms of the reduced number of transmissions, from the transmitter side only excitation data is used to approximate data in Eq. (2.3), after an initial training period.

The other terms are already incorporated in the past approximate measurements, which are known at the *sink*. Consequently, under the assumption that for K sensors a common excitation data source can be determined, this approach can reduce the requirements of data storage and transmission up to $1/K$ of the original requirements, in the limit case. Indeed, with relaxed error sensitivity (i.e., increased threshold), this limit can be approached. To enable the above defined WSN to operate properly, several critical points should be handled carefully such as:

- *Overall knowledge of the prediction model at both ends of the WSN*, in order to reduce the amount of both transmitted and stored data, the sensor k as well as the *sink* should have the prediction model $P_k(\cdot)$ by using a training period.
- *Selection of the sensor providing the excitation data*, in order to obtain an accurate prediction model, the excitation data source must be selected carefully. It may be difficult to select the best excitation source at the sensor and it may be needed to perform this selection centrally, at the *sink*, among many sensors.
- *Transmission threshold* (or error tolerance), it means a trade-off between the recorded data accuracy at the *sink* and the amount of transmission/storage. If the aim is to detect a change in trend, the threshold can be increased. Otherwise, if the aim is accuracy of data, the WSN becomes less error tolerant and more transmissions are needed. The threshold should be defined by the system operator based on the monitoring requirements of a specific structure. Furthermore, this threshold can be compared to either the absolute error criterion (i.e., the absolute value of the error defined in Eq. (2.2), or normalized error criterion). Here, the performance of the studied algorithm is analyzed for the latter criterion, defined as follows:

$$e_k = \frac{e_{k(t)}}{e_{k(t)}} \tag{2.4}$$

- *Storage requirements at each sensor*, each sensor should keep a history of the excitation data in order to perform prediction. Even though this history is rather small (only N values) it must be considered during the WSN setup.

In the light of the above discussions, the system operation can be divided into four phases as illustrated in Figure 2.2. These phases are labeled as: (i) Training, (ii) Model Coefficient Update, (iii) Normal Operation, and (iv) Alert Phase.

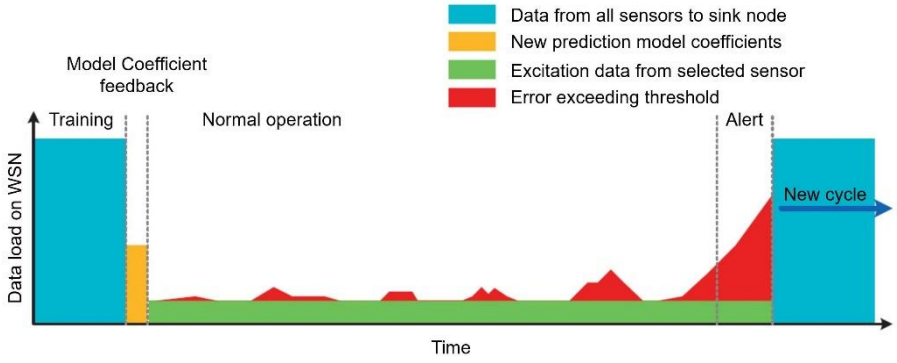

Figure 2.2 Transmission and storage load for different phases of the system.

Initially, during the Training and Model coefficient update phases all the sensor readings are transmitted to the *sink node* until it generates and feedbacks the model coefficients to each sensor. Then, the system enters the normal operation phase where the WSN acts as explained above. In particular, the transmission occurs only when the normalized error is greater than some predefined transmission threshold,

$$Transmit\big(e_k(t)\big) = \begin{cases} 0, & e_k \leq X \\ 1, & e_k \leq X \end{cases} \tag{2.5}$$

where X denotes the transmission threshold. Ideally, this phase should last a long time to prove beneficial. Finally, when the error transmissions increase in density from a given (or several) sensor(s), the *sink* enters the alert phase which induces a *Damage Detection* process and requires a model update for the considered sensors. In particular, the transition to the Alert Phase may be decided by performing a simple comparison test for each sensor k, i.e.,

$$n_{k\,trans} \leq \alpha_k \cdot n_{k\,expect} \tag{2.6}$$

where $n_{k\ trans}$ denotes the number of transmissions from the sensor k which actually happened, for a given period of time, while $n_{k\ expect}$ represents the expected number of transmissions, which can be previously calculated in the normal operation phase. The coefficient α_k should be defined by the system operator and it needs to be ≥ 1. Note that the increased and continuous error transmission from a *sensor node* implicitly means a

change in its input-output relation. Hence, its prediction model does not hold anymore. This may happen as a result of Eq. (2.1), a structural damage that occurred in the vicinity of the sensor, or Eq. (2.2) a change in the global response of the structure with reference to the excitation source. In order to determine which of these two cases occurred, the *sink node* should regenerate all the data (with certain distortion related to the transmission threshold), which is possible because it has knowledge of the prediction model as well as the prediction errors that were previously sent. After the signal reconstruction, more advanced damage detection methods can be performed. If there is no damage, the algorithm gets back to the Model Generation/Update phase.

2.2 A TDMA based cooperative protocol

The work of some authors [9] was extended to develop a communication protocol, which is based on a TDMA (Time Division Multiple Access) strategy and adaptive filtering techniques such as LMS (Least Mean Squares) and RLS (Recursive Least Squares) with the aim to overcome the difficulties associated with the sensor reachback problem [19].

To do so, the protocol allows the *sink node* to keep an exact replica of the adaptive filters that, at each node, exploit the spatial and temporal correlations among sensor measurements to predict the current measurement from their own past measurements as well as past measurements obtained by their neighbors.

Specifically, in the designed protocol each node is assigned a time slot that is divided into two sub-slots. During the first sub-slot, each sensor acquires a new measurement and computes the prediction error of its associated adaptive filter. If the prediction error is small enough (i.e., below a predefined threshold), then during the first sub-slot the considered *sensor node* sends the output of its filter to its neighbors, so that they can use this value as input for the prediction filters they operate. Otherwise, when the prediction error is not that small, the node updates its filter (i.e., using an LMS or RLS update step) and sends its actual measurement to its neighbors. Afterwards, if the prediction is not accurate, since a (MISO) Multiple Input Single Output channel is known to result in energy savings as compared to the SISO (Single Input Single Output) case [20], all the nodes that collaborated during the first sub-slot will form a MISO channel to simultaneously transmit the current measurement to the *sink node*. This way, with the aim of having an exact replica of all the filters implemented by the cooperating *sensor nodes*, the *sink node* is able to incorporate the transmitted measurement to the input of the aforementioned filters and update the filter associated with the considered *sensor node*.

2.2.1 Formulation of the problem

Let us consider a dense wireless sensor network consisting of N nodes, deployed on a civil structure that has to be monitored. Consider also that node n $(n = 1, 2 \ldots, N)$ has K neighbors, in the sense that they are close enough to node n so that wireless communication with low power can be accomplished. The neighbors of node n are denoted as $k_{n,1}, k_{n,2}, \ldots, k_{n,K}$. Each sensor node n, at some discrete time instant, acquires the measurement, which is related to an event that takes place in the area where the wireless sensor network has been deployed. For instance, $y_{n,t}$ may represent an acceleration measurement, that captures oscillations of the structure. Let us define the vectors of m past measurements of each sensor node n as:

$$y_{n,t} = \begin{bmatrix} y_{n,t-1} & y_{n,t-2} & \cdots & y_{n,t-m} \end{bmatrix}^T \qquad (2.7)$$
$$n = 1, 2, \ldots, N$$

Also, let us define the stacked vectors:

$$y_{n,t} = \begin{bmatrix} y^T{}_{n,t} & y^T{}_{k_{n,1},t} & y^T{}_{k_{n,2},t} & \cdots & y^T{}_{k_{n,K},t} \end{bmatrix}^T \qquad (2.8)$$
$$n = 1, 2, \ldots, N$$

which represent the past m measurements of all sensor nodes in the neighborhood of node n. Consider now the correlation matrices defined as:

$$\boldsymbol{R}_n = E\left[\boldsymbol{u}_{n,t} \quad \boldsymbol{u}^T{}_{n,t}\right] \qquad (2.9)$$
$$n = 1, 2, \ldots, N$$

Clearly, if matrices $\boldsymbol{R}_n$ are diagonal, the sensor measurements within all neighborhoods are correlated, neither in time nor in space. In contrast, if the matrices $\boldsymbol{R}_n$ are only block-diagonal with block size m, the measurements are correlated in time but spatially uncorrelated. In this work, we will focus on the general case where $\boldsymbol{R}_n$ are of a general form, implying that the sensor measurements are correlated both in time and in space.

2.2.2 Predictors and correlation of measurements

Thus, one is interested in deriving a network protocol able to transmit the sensor measurements to the data-collecting node in an energy-efficient way. To this end, if is possible to reduce the number of information bits that need to be transmitted, this would have a considerable effect on the energy spent by the data-gathering process. Such a reduction in the number of information bits that need to be transmitted can be accomplished taking advantage of the correlations among the measurements. In

particular, identifying and sending only the *new* information that lies in the measurements, significant energy savings would emerge. A way for identifying such *new information* employs the notion of signal predictors.

The nature of the observed phenomenon makes the measurements $y_{n,t}$ predictable, at least to some extent. In particular, if the data-collecting node had knowledge of previous measurements acquired by sensor n (and possibly previous measurements of other nodes in the vicinity of node n), then it could compute an estimate of $y_{n,t}$. This estimate, of course, corresponds to information already known to the data-collecting node. In principle, one can distinguish between two different types of prediction functions: (i) one that does not change with time, which implies that the correlation mechanism is constant or stationary, and (ii) a time-varying prediction function, implying that the statistics of the signals measured by the nodes of the network have a dynamic behavior. Assuming the process to be stationary, the prediction function can be realized as a linear filter with coefficients obtained by minimizing the mean-squared error between the measurements $y_{n,t}$ and their predicted values.

However, in most real world applications the observation processes are non-stationary since their statistical characteristics are changing in time. As a result, the optimal coefficients of the predictor are changing in time as well. In order to track these changes, a practical approach is to iteratively estimate them by updating previous filter coefficients as it is done in adaptive filters [21]. Such an approach offers the additional benefit that the data-collecting node does not need to know the statistics of the underlying process.

2.2.3 A simple cooperative TDMA protocol

As already mentioned in the introduction, another approach for reducing the energy required to transmit data relies on the concept of cooperative communications. In particular, in cooperative communications, a number of accurately synchronized nodes transmit data concurrently so that the system resembles a transmitter with multiple antennas. During the previous phase, the nodes have agreed upon the data that will be sent. In effect, benefits similar to (MIMO) Multiple Input Multiple Output systems can be achieved [20]. Hence, the terms virtual MIMO or distributed MIMO are often used alternatively to denote cooperative communication systems.

For illustration purposes, let us consider now a straightforward cooperative communication protocol for the problem at hand, in which correlation among the measurements acquired by the nodes of the network is not taken into account. According to this protocol, each sensor node is assigned its own time-slot in order to transmit information in a TDMA fashion. Cooperative communications can be incorporated into this protocol, by dividing each time-slot into two sub-slots as depicted in Figure 2.3.

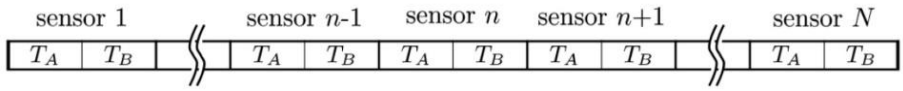

Figure 2.3 Each time-slots of the sensors is divided into two sub-slots

During the first sub-slot of duration T_A, each sensor n transmits its estimated (or observed) value to its K neighbors. During the second sub-slot of duration T_B, node n and its neighbors transmit to the *sink node* in a cooperative fashion. In such a scenario, both the AF (Amplify and Forward) as well as the DF (Decode and Forward) methods can be adopted [22].

2.2.4 Cooperative TDMA exploiting correlation

Consider now an extension of the aforementioned protocol, where the correlation of the measurements is taken into account. Since the measurements may be correlated both in time and in space, the idea of using past measurements acquired by node n as well as past measurements from nearby sensor nodes in order to predict new measurements of node n seems well justified. This fact can be used to save a noticeable percentage of the transmissions to the *sink node*, in the case where the *sink node* can itself predict the required measurements within some predefined accuracy. Thus, let each sensor node n keep a time varying prediction filter $\boldsymbol{f}_{n,t}$ as well as a data vector:

$$\tilde{\boldsymbol{u}}_{n,t} = \left[\tilde{\boldsymbol{y}}^T{}_{n,t} \;\; \tilde{\boldsymbol{y}}^T{}_{k_{n,1},t} \;\; \tilde{\boldsymbol{y}}^T{}_{k_{n,2},t} \;\; \dots \;\; \tilde{\boldsymbol{y}}^T{}_{k_{n,K},t}\right]^T \tag{2.10}$$

so that the output of the filter, defined as:

$$\hat{y}_{n,t} = \boldsymbol{f}_{n,t}^T \cdot \tilde{\boldsymbol{u}}_{n,t}^T \tag{2.11}$$

is an approximation of the actual measurement $y_{n,t}$ obtained by sensor n at time t. In particular, $\hat{y}_{n,t}$ is a prediction of the actual measurement $y_{n,t}$. In the above expressions, we have used the vectors:

$$\tilde{\boldsymbol{y}}_{n,t} = \left[\tilde{y}_{n,t-1} \;\; \tilde{y}_{n,t-2} \;\; \dots \;\; \tilde{y}_{n,t-m}\right]^T \tag{2.12}$$
$$n = 1, 2, \dots, N$$

to represent approximate versions of the past m measurements obtained by sensor n. Thus, vectors $\tilde{\boldsymbol{u}}_{n,t}$ and $\boldsymbol{f}_{n,t}$ have dimensions $m \cdot K \; x \; 1$. Let us now define a binary variable $b_{n,t}$ according to the prediction error, as:

$$\tilde{b}_{n,t} = \begin{cases} 0 & if \ \ |\hat{y}_{n,t} - y_{n,t}| \leq e \\ 0 & if \ \ |\hat{y}_{n,t} - y_{n,t}| > e \end{cases} \quad (2.13)$$

where e denotes a small positive constant. The approximate measurements $\tilde{y}_{n,t}$ are defined as:

$$\tilde{y}_{n,t} = \begin{cases} \hat{y}_{n,t} & if \ \ b_{n,t} = 0 \\ \hat{y}_{n,t} & if \ \ b_{n,t} = 1 \end{cases} \quad (2.14)$$

Based on the above definitions, the protocol of each sensor node n can be explained as follow. At a time instant t, each sensor acquires its new measurement $y_{n,t}$ and starts a synchronized loop to track the time-slots that will follow. Node n is active in two cases: (i) when the current slot index s is equal to n, and (ii) when the current slot index s is equal to the index of any of its neighbors.

In case (i), the node computes the output of its prediction filter and compares it to the actual measurement $y_{n,t}$. Thus, it computes the binary variable $b_{n,t}$ that determines whether the prediction was accurate or not. In the case where the prediction was not accurate, the prediction filter is updated using an adaptive algorithm. As a general rule, the LMS algorithm should be used when reduced computational complexity is required. On the other hand, one should opt for the RLS algorithm in the case where the statistics of the measurements change abruptly with time, given that the computational complexity requirements can be met. RLS also performs better when adaptation stalls and restarts very often during operations, as it is the case with the suggested technique. Regardless of the algorithm used for the update, $y_{n,t}$ is used as a desired response signal. Then, the sensor node n computes $\tilde{y}_{n,t}$, which is either the output of the prediction filter (accurate prediction) or the actual measurement (inaccurate prediction). Thus, sensor n updates its input vector $\tilde{\boldsymbol{u}}_{n,t+1}$ and sends $\tilde{y}_{n,t}$ and $b_{n,t}$ to its neighbors. Finally, $\tilde{y}_{n,t}$ is sent to the *sink node* only if the prediction was inaccurate, otherwise the *sink node* is able to compute $\tilde{y}_{n,t}$ using a prediction filter.

In case (ii), i.e., when a neighbor of is active, node listens for the transmitted values $\tilde{y}_{s,t}$ and $b_{s,t}$. It then updates its input vector $\tilde{\boldsymbol{u}}_{n,t+1}$ with the received value $\tilde{y}_{s,t}$ and, in the sequel, helps its neighbor transmit to the *sink* by relaying $\tilde{y}_{s,t}$ if $b_{s,t}$ was 1. The protocol followed by the *sink node* is carried out as follow: at each time instant, the *sink node* also executes a loop so as to track the N time-slots, in a synchronized fashion. For the first T_A seconds of each slot, the *sink node* is inactive because sensor-to-sensor communication takes place. At the following T_B seconds however, the *sink node* is receiving the measurement $\tilde{y}_{n,t}$ of the node assigned to the current slot. Of course, in the case where the prediction at node s was accurate, such a message will not be transmitted. Thus, the *sink node* must implement a procedure to detect such "empty" messages. The result of the detection process is a binary variable $\hat{b}_{s,t}$, which will be equal to $b_{s,t}$ in the case where the detection

is correct. In the sequel, the *sink node* is able to compute $\tilde{y}^{(S)}_{s,t}$, (that is, a copy of $\tilde{y}_{s,t}$ at the *sink*) either as the output of a local prediction filter:

$$\tilde{y}^{(S)}_{s,t} = \boldsymbol{f}^{(S)^T}_{s,t} \cdot \tilde{\boldsymbol{u}}^{(S)}_{s,t} \tag{2.15}$$

in the case where $\hat{b}_{s,t} = 0$ (accurate prediction) or by setting it equal to the received measurement $\tilde{y}_{s,t}$ (inaccurate prediction). In the case of inaccurate prediction, the *sink node* must use the same adaptive algorithm as the sensor *s* to update its local prediction filter for sensor *s*, so that the two filters are equal (of course, if all channels are error free). Finally, the *sink node* must update the input vectors of all the prediction filters affected by $\tilde{y}_{s,t}$, that is the prediction filter for node *s* and the local prediction filters of all its neighbors.

It can be verified by the above description of the proposed data collection protocol, that in the case where all channels are error-free, the reconstructed sequences $\tilde{y}^{(S)}_{s,t}$ at the *sink node* satisfy the distortion criterion

$$max_{\,n,t}\, |\tilde{y}^{(S)}_{n,t} - \, y_{n,t}| \leq e \tag{2.16}$$

Indeed, the maximum allowed distortion parameter *e* offers a trade-off between accurate reconstruction of the measurements by the *sink node*, and the number of transmissions required. Also, some other factors, such as the degree to which the measured signals can be predicted and the specific characteristics of the adaptive algorithm used to update the coefficients of the prediction filters, may influence the performance of the proposed protocol.

2.2.5 Cooperative neighborhood selection

Firstly, let us analyze the merits and drawbacks of having cooperation among the sensor nodes. For a given node *n*, cooperation with *K* neighbors actually requires *K* additional transmissions to these neighbors at each time instant. Although the energy cost of the additional inter-node transmissions can be low due to their proximity, one should also take into account the channel quality between the cooperating nodes which may introduce additional distortion to the data being sent.

On the other hand, the gains can overcome the cooperation costs in case that the number of transmissions toward the *sink* is reduced due to the exploitation of high spatial correlation among the measurements in the cooperating neighborhood. Certainly, the cooperation gains are not the same for all the nodes. In fact, the relation between the values of temporal correlation among the measurements of node *n* on one side, and the values of their spatial correlation with the measurements of the cooperating nodes should determine how beneficial the cooperation may be. Furthermore, an additional benefit can

be obtained once the transmissions toward the *sink* are required. As previously explained, the cooperating nodes may simultaneously transmit to the *sink node*; thus forming MISO channel and improving energy-efficiency.

Not surprisingly, in the simulation section it turns out that choosing the suitable cooperating neighborhood, in terms of its size and the actual nodes involved, plays a significant role in enhancing the performance of the protocol. Therefore, the optimization of the cooperating neighborhood requires: (i) the knowledge of all channels among the nodes (including the *sink*), and (ii) the knowledge of the auto- and cross- correlation functions of all nodes. Regarding the former issue, in a practical system, all the involved channels may be estimated during a training period in which all nodes participate. Initially, all the nodes would send the training sequence to the *sink* and all other nodes. Afterwards, the nodes would also transmit to the *sink* the sequences that are received from all other nodes. Consequently, the *sink* could estimate all the involved channels in a centralized manner.

2.3 A distributed diffusion-based LMS

Two major groups of energy aware and low-complex distributed strategies for estimation over networks have been studied in the literature, i.e., consensus strategies and the algorithms based on incremental or diffusion mode of cooperation.

In some initial works [23], the implementation of the consensus strategy is done in two stages. Unfortunately, this kind of implementation is not suitable for real time estimation as required in time-varying environments. Subsequently, motivated by the procedure obtained in [24], alternative implementations of the consensus strategy were presented in the literature [25, 26], which force agreement among the cooperating nodes in a single time-scale. The second group, which is in the focus of this paper, consists of a single time-scale distributed estimation algorithms that are based on distributing a specific stochastic gradient method under an incremental or a diffusion mode of cooperation. In the incremental mode [27, 28], each node communicates with only one neighbor, and consequently the data are processed in a cyclic manner throughout the network. A better reliability can be achieved at the expense of increased energy consumption in the so-called diffusion mode considered [29-31]. Under this strategy, each node can communicate with a subset of neighboring nodes.

Although there are many published techniques addressing different distributed estimation problems, only very few papers consider node-specific settings where the nodes have overlapped but different estimation interests. In the signal estimation case, for networks with a fully connected and tree topology, some authors proposed distributed algorithms

that allow to estimate node-specific desired signals sharing a common latent signal subspace [32, 33].

Regarding the parameter estimation case, there are also a few recent works addressing problems, which can be considered as NSPE (Node-Specific Parameter Estimation) problems. The approach presented in [34] is based on optimization techniques that force different nodes to reach an agreement when estimating parameters of common interest.

In the case of schemes based on a distributed implementation of adaptive filtering techniques, the literature is less extensive. In one of these works [35], the authors use diffusion adaption and scalarization techniques to solve the multi-objective cost function that appears in a NSPE problem and obtain a Pareto-optimal solution. A diffusion strategy with an adaptive combination rule proposed in [36] is suitable for clustering nodes in a network that are interested in different objectives. Consequently, it actually limits cooperation only to the nodes having exactly the same objectives.

In [37] the authors assume a NSPE setting, but the different parameters to be estimated using diffusion strategy are expressed through the same global parameter. In previous works [38, 39], a novel NSPE problem, where all nodes are interested in estimating simultaneously some parameters of local and global interest, was formulated. It was solved by employing incremental-based strategies for LMS (Least Mean Squares) and RLS (Recursive Least Squares) algorithms.

Motivated by the well-known robustness and learning abilities of the diffusion-based solutions, some authors present a LMS strategy to solve the aforementioned NSPE problem under two different versions of the diffusion mode of cooperation: Combine-then-Adapt (CTA) and Adapt-then-Combine (ATC) [40].

The following notation was used: (i) boldface letters for random variables, (ii) normal fonts for deterministic quantities, (iii) capital letters refer to matrices, (iv) small letters refer to both vectors and scalars. The notation $(\cdot)^H$ and $E\{\cdot\}$ stand for the Hermitian transposition and the expectation operator, respectively. Moreover, $R_A=E\{\boldsymbol{A}^H\boldsymbol{A}\}$, $R_{A,B}=E\{\boldsymbol{A}^H\boldsymbol{B}\}$ *and* $r_{A,b}=E\{\boldsymbol{A}^H\boldsymbol{b}\}$ for any random matrices $\boldsymbol{A}$, $\boldsymbol{B}$ and any random vector $\mathbf{b}$. Finally, $\|\cdot\|$ denotes the Euclidean norm and $0_{L\times M}$ represents an $L \times M$ zero matrix.

2.3.1 Problem statement

Let us consider a connected network consisting of N nodes (Figure 2.4). Hence, allowing each node to communicate with its neighbors, at each time instant there is always a path between any two pairs of nodes of the network.

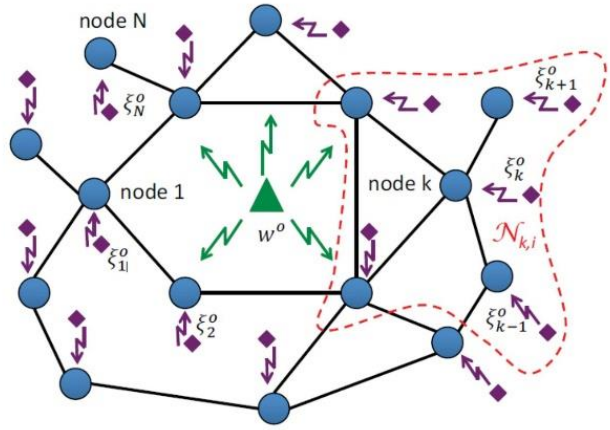

Figure 2.4 A network of *N* nodes with node-specific parameter estimation

As shown in Figure 2.4, the neighborhood of a node k at a specific time instant i, $N_{k,i}$, consists of the nodes linked to it, including node k itself.

At discrete time i, each node k has access to data $\{d_{k,i}, U_{k,i}\}$, corresponding to time realizations of zero-mean random processes $\{\boldsymbol{d}_{k,i}, \boldsymbol{U}_{k,i}\}$, with dimensions $L_k \times 1$ *and* $L_k \times M_k$, respectively. These data are related to events that take place in the network area through the subsequent model:

$$\boldsymbol{d}_{k,i} = \boldsymbol{U}_{k,i} w_k^o + \boldsymbol{v}_{k,i} \tag{2.17}$$

where, for each time instant i, wok equals the $M_k \times 1$ vector that gathers all parameters of interest for node k and $v_{k,i}$ denotes measurement and/or model noise with zero mean and covariance matrix $R_{vk,i}$ of dimensions $L_k \times L_k$.

Given the previous observation model and the data set $\{d_{k,i}, U_{k,i}\}$, the objective is to find the set of linear node-specific estimators $\{w_k\}_{k=1}^N$ that minimize the following global cost function:

$$J_{glob}(\{w_k\}_{k=1}^N) = \sum_{k=1}^{N} E\left\{\left\|\boldsymbol{d}_{k,i} - \boldsymbol{U}_{k,i} w_k\right\|^2\right\} \tag{2.18}$$

In most of the existing papers, i.e., [27-31], the derived adaptation strategies minimize in Eq. (2.18), when $w_k^o = w^o$ for all $k \in \{1, 2, \ldots, N\}$. In this work, we consider the novel node-specific parameter setting addressed in [38, 39], which goes one step further by considering a more general scenario where the parameters of interest can differ from one node to another. As shown in Figure 2.4, each vector $\{w_k^o\}_{k=1}^N$ might consist of parameters

of global interest to the whole network and parameters of local interest for node *k*. In particular, the global parameters might be related to a phenomenon making an impact on all the nodes, while the parameters of local interest may reflect an influence of some phenomena that are only present over the area monitored by one node of the network. Therefore, we can rewrite the observation model in Eq. (2.17), for each node *k*, as:

$$\boldsymbol{d}_{k,i} = \boldsymbol{U}_{k_g,i} w^o + \boldsymbol{U}_{k_l,i} \xi_k^o + \boldsymbol{v}_k^{(i)} \tag{2.19}$$

where sub-vectors wo $(M_g \times 1)$ and ξ_k^o $(M_{kl} \times 1)$ gather the parameters of global and local interest, respectively. Furthermore, $\boldsymbol{U}_{k_g,i}$ and $\boldsymbol{U}_{k_l,i}$ are matrices of dimensions $L_k \times M_g$ and $L_k \times M_{kl}$ that consist of the columns $\boldsymbol{U}_{k,i}$ associated with w^o and ξ_k^o, respectively. Thus, according to Eq. (2.18) and Eq. (2.19), the NSPE problem can be cast as minimizing:

$$\sum_{k=1}^{N} E\left\{\left\|\boldsymbol{d}_{k,i} - \boldsymbol{U}_{k_g,i}\, w - \boldsymbol{U}_{k_l,i} \xi_k\right\|^2\right\} \tag{2.20}$$

with respect to *w* and $\{\xi_k\}_{k=1}^N$. In the following section, the centralized solution to Eq. (2.20) is wrote and approximated in a distributed manner via diffusion-based approach.

2.3.2 Diffusion-based LMS for the NSPE problem

For simplicity and without losing generality, let us assume that $M_k = M$, $M_{kl} = M_l$ and $L_k = L$ for all $k \in \{1, 2 \ldots N\}$. From [38], the NSPE problem can be cast as:

$$\widehat{\widetilde{w}} = argmin_{\widetilde{w}} \left\{\sum_{k=1}^{N} E\left\{\left\|\boldsymbol{d}_{k,i} - \widetilde{\boldsymbol{U}}_{k,i}\, \widetilde{w}\right\|^2\right\}\right\} \tag{2.21}$$

where:

$$\widetilde{w} = [w^T \; \xi_1^T \;\; \xi_2^T \ldots \xi_N^T]^T \; (\widetilde{\mathrm{M}} \times 1) \tag{2.22}$$

$$\widetilde{\boldsymbol{U}}_{k,i} = \left[\boldsymbol{U}_{k_g,i} \;\; 0_{L \times M_a} \;\; \boldsymbol{U}_{k_l,i} \;\; 0_{L \times M_a}\right] \tag{2.23}$$

where $M_a = (k-1) \cdot M_l$, $M_b = (N-k) \cdot M_l$ and $M = M_g + N \cdot M_l$. Thus, the resulting solutions $\widehat{\widetilde{w}}$ are given by the normal equations [41]:

$$\left(\sum_{k=1}^{N} \boldsymbol{R}_{\widetilde{U}_{k,i}}\right) \cdot \widehat{\widetilde{w}} = \sum_{k=1}^{N} r_{\widetilde{U}_{k,i} d_{k,i}} \tag{2.24}$$

With the aim of improving energy efficiency, robustness and scalability of the centralized approach, it is highly desirable to design a distributed and adaptive scheme that allows each node to solve its NSPE problem. In case that $w_k^o = w^o$, diffusion strategies, i.e.,

CTA and ATC, are known to well approximate the corresponding centralized solution by relying solely on information available at each node from its neighborhood [29]. In this work, these strategies is extended to be applicable in the NSPE case.

To start with the derivation of the algorithm, let us define $\tilde{\psi}_k^{(i)}$ as the local estimate of $\widetilde{w}^o$ at time instant i and node *k*. Note that this local estimate is generally a noisy version of the optimal augmented vector $\widetilde{w}^o$. By employing a diffusion mode of cooperation, each node *k*, at each time instant *i−1*, has access to the set of local estimates from its neighborhood, i.e., $N_{k,i-1}$. Hence, node *k* can fuse its local estimate with the local estimates of its neighbors, at each time instant *i−1*, through a linear combiner as follows:

$$\tilde{\phi}_k^{(i-1)} = \sum_{j \in N_{k,i-1}} \tilde{C}_{k,j}\, \tilde{\psi}_j^{(i-1)} \tag{2.25}$$

where:

$$\tilde{C}_{k,j} = \mathrm{diag}\left\{c_{k,j}^{w} I_{M_g},\, c_{k,j}^{\xi_1} I_{M_l}, \ldots,\, c_{k,j}^{\xi_N} I_{M_l}\right\} \tag{2.26}$$

In Eq. (2.26), $c_{k,j}^{w}$ equals the weight coefficient used by node *k* when combining the local estimate of the global vector w^o from node *j*. Similarly, $c_{k,j}^{\xi_m}$ denotes the combination coefficients employed by node *k* when fusing the local estimates of ξ_m^o , where $m \in \{1, 2, \ldots, N\}$, from node *j* with its local estimates, respectively.

To determine the combination coefficients at each node *k*, we can interpret Eq. (2.25) as a weighted least squares estimate of the augmented vector of parameters $\widetilde{w}^o$ given its local estimate as well as the local estimates from the neighbor nodes [42]. This way, by collecting the local estimates of $\widetilde{w}^o$ in the neighborhood of node *k:*

$$\tilde{\psi}_{N_{k,i-1}} = col\left\{\left\{\tilde{\psi}_j^{(i-1)}\right\}_{j \in N_{k,i-1}}\right\} \tag{2.27}$$

and defining:

$$Q_{k,i-1} = col\{I_{\widetilde{M}}, I_{\widetilde{M}}, \ldots, I_{\widetilde{M}}\} \;\; \left(n_{k,i-1} \cdot \widetilde{M}\; x\; \widetilde{M}\right) \tag{2.28}$$

and $\tilde{C}_k = \mathrm{diag}\left\{\tilde{C}_{k,1}, \tilde{C}_{k,2}, \ldots, \tilde{C}_{k,n_{k,i-1}}\right\}$ with $n_{k,i-1}=|N_{k,i}-1|$, we can formulate the subsequent local weighted least-squares problem whose solution is given by:

$$argmin_{\tilde{\phi}_k}\left\{\left\|\tilde{\psi}_{N_{k,i-1}} - \tilde{Q}_{k,i-1}\, \tilde{\phi}_k\right\|_{\tilde{C}_k}^2\right\} \tag{2.29}$$

whose solution is given by:

$$\tilde{\phi}_k^{(i-1)} = \left[Q_{k,i-1}^T \, \tilde{C}_k \, Q_{k,i-1}\right]^{-1} Q_{k,i-1}^T \, \tilde{C}_k \, \tilde{\psi}_{N_{k,i-1}} \tag{2.30}$$

More precisely, focusing on the different sub-vectors that form $\tilde{\phi}_k^{(i-1)}$, the solution provided in Eq. (2.30) can be rewritten as:

$$\phi_{k,w}^{(i-1)} = \sum_{j \in N_{k,i-1}} \frac{c_{k,j}^{w}}{\sum_{l \in N_{k,i-1}} c_{k,l}^{w}} \, \tilde{\psi}_{j,w}^{(i-1)} \tag{2.31}$$

$$\phi_{k,\xi_m}^{(i-1)} = \sum_{j \in N_{k,i-1}} \frac{c_{k,j}^{\xi_m}}{\sum_{l \in N_{k,i-1}} c_{k,l}^{\xi_m}} \, \tilde{\psi}_{j,\xi_m}^{(i-1)} \tag{2.32}$$

where, for *k, j, m* $\in \{1, 2, \ldots, N\}$, $\phi_{k,w}^{(i-1)}$ and $\phi_{k,\xi_m}^{(i-1)}$ denote the sub-vectors of combiner $\tilde{\phi}_k^{(i-1)}$ associated with the local estimation of w^o and ξ_m at node *k* and time instant *i−1*, respectively. Analogously, $\tilde{\psi}_{j,w}^{(i-1)}$ and $\tilde{\psi}_{j,\xi_m}^{(i-1)}$ denote the sub-vectors of local estimate $\tilde{\psi}_j^{(i-1)}$ associated with the local estimation of w^o and ξ_m^o at node *j* and time instant *i−1*.

At this point, after a suitable re-writing of the combination coefficients that appear in Eq. (2.31) and Eq. (2.32), we can verify that the combination coefficients in Eq. (2.25) and Eq. (2.26) have to satisfy:

$$c_{k,j}^{w} = 0 \; if \; j \notin N_{k,i-1}; \sum_{j \in N_{k,i-1}} c_{k,j}^{w} = 1 \tag{2.33}$$

$$c_{k,j}^{\xi_m} = 0 \; if \; j \notin N_{k,i-1}; \sum_{j \in N_{k,i-1}} c_{k,j}^{\xi_m} = 1 \tag{2.34}$$

for *k, m* $\in \{1, 2, \ldots, N\}$. Next, in order to have an adaptive estimation of $\tilde{w}^o$ at each node *k*, we include the corresponding local aggregate estimate $\tilde{\phi}_k^{(i-1)}$ into the local LMS-type adaptive algorithm, at each node *k*. Therefore, the resulting diffusion-based strategy can be described as:

$$\begin{cases} Combination\ step: \\ \tilde{\phi}_k^{(i-1)} = \sum_{j \in N_{k,i-1}} \tilde{C}_{k,j} \, \tilde{\psi}_j^{(i-1)} \\ Adaptation\ step: \\ \tilde{\psi}_k^{(i)} = \tilde{\phi}_k^{(i-1)} - \mu_k \tilde{\boldsymbol{U}}_{k,i}^H \left[\boldsymbol{d}_{k,i} - \tilde{\boldsymbol{U}}_{k,i} \, \tilde{\phi}_k^{(i-1)}\right] \end{cases} \tag{2.35}$$

with $i \geq 1$, $\left\{\tilde{\psi}_k^{(i)}\right\}_{j \in N_{k,0}}$ equal to some initial guesses, $\tilde{C}_{k,j}$ defined in Eq. (2.26) and $\mu_k > 0$ is a suitably chosen positive step-size parameter.

Due to the structure of the augmented regressors $\widetilde{\boldsymbol{U}}_{k,i}$ defined in Eq. (2.23), a careful analysis of Eq. (2.35) reveals that, only 2 sub-vectors of $\tilde{\psi}_k^{(i)}$ are updated at each time instant i, when a specific node k performs the adaptation step of Eq. (2.35). In particular, according to Eq. (2.22) and Eq. (2.23), only the sub-vectors associated with the local estimates of w^o and ξ_k^o at node k and time i, denoted as $\tilde{\psi}_k^{(i)} = \tilde{\psi}_{k,w}^{(i)}$ and $\tilde{\xi}_k^{(i)} = \tilde{\psi}_{k,\xi_k}^{(i)}$, respectively, are updated based on the measurements $\{d_{k,i}, U_{k,i}\}$ and the corresponding aggregate estimates at time $i-1$ (i.e., $\phi_{k,w}^{(i-1)}$ and $\phi_{k,\xi_k}^{(i-1)}$). The previous fact allows setting the subsequent equalities in the combination coefficients:

$$c_{k,j}^{\xi_m} = 0 \; if \; k \neq j \; or \; k \neq m \tag{2.36}$$

These equalities together with Eq. (2.34) show that $c_{k,k}^{\xi_m} = 1$ for each node k. Hence, a node k does not essentially cooperate with any other node when estimating its vector of local parameters ξ_m^o. This is due to the fact that no other node j performs measurements where the vector ξ_k is involved.

2.4 References

[1] Casciati, S. & Chen, Z-C. 2012. An active mass damper system for structural control using real-time wireless sensors. Structural Control and Health Monitoring, 19, 758-767.

[2] Estrin, D., Girod, L., Pottie, G & Srivastavay, M. 2001. Instrumenting the world with wireless sensor networks. In Proceedings of IEEE International Conference on Acoustics, Speech, and Signal Processing (ICASSP 2001), 2034, 2033-2036.

[3] Lynch J.P. 2006. A summary review of wireless sensors and sensor networks for structural health monitoring. The Shock and Vibration Digest, 38, 91-128.

[4] Barros, J., Peraki, C. & Servetto, S. 2004. Efficient network architectures for sensor reachback. Proceedings of 13th International Zurich Seminar on Communications (IZS 2004), Zurich, Switzerland.

[5] Nagayama, T., Moinzadeh, P., Mechitov, K., Ushita, M., Makihata, N., Ieiri, M., Agha, G., Spencer Jr., B.F., Fujino, Y. & Seo, J. 2010. Reliable multi-hop communication for structural health monitoring. Smart Structure and Systems, 6(5), 481-503.

[6] Kimura, N. & Latifi, S. 2005. A survey on data compression in wireless sensor networks. Proceedings of International Conference on Information Technology, Coding and Computing (ITCC 2005), 12, 8-13.

[7] Srisooksai, T., Keamarungsi, K., Lamsrichan, P. & Araki, K. 2012. Practical data compression in wireless sensor networks: a survey. Journal of Network and Computer Applications, 35, 37-59.

[8] Barros, J. & Servetto, S. 2006. Network information flow with correlated sources. IEEE T. Inform. Theory, 52(1), 155-170.

[9] Ampeliotis, D., Bogdanovic, N., Berberidis, K., Casciati, F. & Al-Saleh, R. 2012. Power-efficient wireless sensor reachback for SHM. Proceedings of 6th International Conference on Bridge Maintenance, Safety and Management (IABMAS 2012), Stresa, Italy.

[10] Stankovic, V., Stankovic, L. and Cheng, S. (2010. Distributed source coding: Theory and applications. Proceedings of 18th European Signal Processing Conference (EUSIPCO 2010), Aalborg, Denmark.

[11] Masri, S., Smyth, A., Chassiakos, A., et al. 2000. Application of neural networks for detection of changes in nonlinear systems. Journal of Engineering Mechanics, 126, 666-676.

[12] Casciati, F. & Casciati, S. 2006. Structural health monitoring by Lyapunov exponents of non-linear time series. Structural Control and Health Monitoring, 13, 132-146.

[13] Casciati, S. 2008. Stiffness identification and damage localization via differential evolution algorithms. Structural Control and Health Monitoring, 15, 436-449.

[14] Nair, K.K., Kiremidjian, A.S. & Law, K.H. 2006. Time series-based damage detection and localization algorithm with application to the ASCE benchmark structure. Journal of Sound and Vibration, 291, 349-368.

[15] Johnson, E.A., Lam, H.F., Katafygiotis, L.S., et al. 2000. A benchmark problem for structural health monitoring and damage detection. Proceedings of 14th Engineering Mechanics Conference, Austin, USA.

[16] Yildirim, U., Oguz, O. & Bogdanovic N. 2013. A prediction-error-based method for data transmission and damage detection in wireless sensor networks for structural health monitoring. Journal of Vibration and Control, 19(15), 2244-2254.

[17] Soderstrom, T. & Stoica, P. 1989. System Identification. New York, Prentice Hall.

[18] Ljung, L. 2002. Prediction error estimation methods. Circuits, Systems and Signal Processing, 21, 11-21.

[19] Bogdanovic, N., Ampeliotis, D., Kostas Berberidis, K., Casciati, F. & Plata-Chaves, J. 2014. Spatio-temporal protocol for power-efficient acquisition wireless sensors based SHM. Smart Structures and Systems, 14(1), 1-16.

[20] Cui, S., Goldsmith, R. & Bahai, A. 2004. Energy efficiency of MIMO and cooperative MIMO techniques in sensor networks. IEEE Journal on Selected Areas in Communications, 22(6), 1089-1098.

[21] Sayed, A.H. 2008. Adaptive filters. John Wiley & Sons, Hoboken, NJ, USA.

[22] Hong, Y.W., Huang, W.J., Chiu, F.H. & Kuo, C.C. 2007. Cooperative communications in resource constrained wireless networks. IEEE Signal Processing Magazine.

[23] Olfati-Saber, R. & Murray, R.M. 2004. Consensus problems in networks of agents with switching topology and time-delays. IEEE Transactions on Automatic Control, 49(9), 1520-1533.

[24] Bertsekas, D.P. & Tsitsiklis, J.N. 1997. Parallel and distributed computation: numerical methods. Athena Scientific, Singapore.

[25] Schizas, I.D., Mateos, G. & Giannakis, G.B. 2009. Distributed LMS for consensus-based in-network adaptive processing. IEEE Transactions on Signal Processing, 57(6), 2365-2382.

[26] Dimakis, A.G., Kar, S., Moura, J.M.F., Rabbat, M.G. & Scaglione, A. 2010. Gossip algorithms for distributed signal processing. Proceedings of the IEEE, 98(11), 1847-1864.

[27] Lopes, C.G. & Sayed, A.H. 2007. Incremental adaptive strategies over distributed networks. IEEE Transactions on Signal Processing, 55(8), 4064-4077.

[28] Li, L., Chambers, J.A., Lopes, C.G. & Sayed, A.H. 2010. Distributed estimation over an adaptive incremental network based on the affine projection algorithm. IEEE Transactions on Signal Processing, 58(1), 151-164.

[29] Cattivelli, F.S. & Sayed, A.H. 2010. Diffusion LMS strategies for distributed estimation. IEEE Transactions on Signal Processing, 58(3), 1035-1048.

[30] Chouvardas, S., Slavakis, K. & Theodoridis, S. 2011. Adaptive robust distributed learning in diffusion sensor networks. IEEE Transactions on Signal Processing, 59(10), 4692-4707.

[31] Sayed, A.H., Tu, S-Y., Chen, J., Zhao, X. & Towfic, Z.J. 2013. Diffusion strategies for adaptation and learning over networks: an examination of distributed strategies and network behavior," IEEE Signal Processing Magazine, vol. 30, no. 3, pp. 155–171, 2013.

[32] Bertrand, A. & Moonen, M. 2010. Distributed adaptive node specific signal estimation in fully connected sensor networks - Part I: Sequential node updating. IEEE Transactions on Signal Processing, 58(10), 5277-5291.

[33] Bertrand, A. & Moonen, M. 2010. Distributed adaptive node specific signal estimation in fully connected sensor networks - Part II: Simultaneous and asynchronous node updating. IEEE Transactions on Signal Processing, 58(10), 5292-5306.

[34] Kekatos, V. & Giannakis, G.B. 2012. Distributed robust power system state estimation. IEEE Transactions on Power Systems, <http://arxiv.org/abs/1204.-0991>.

[35] Chen, J. & Sayed, A.H. 2012. Distributed Pareto-optimal solutions via diffusion adaptation. IEEE Statistical Signal Processing Workshop, 648-651.

[36] Zhao, X. & Sayed, A.H. 2012. Clustering via diffusion adaptation over networks. Proceedings of 3rd International Workshop on Cognitive Information Processing (CIP 2012), 1–6.

[37] Abdolee, R., Champagne, B. & Sayed, A.H. 2012. Diffusion LMS for source and process estimation in sensor networks. Proceedings of 17th Workshop on Statistical Signal Processing (IEEE/SP), 165-168.

[38] Bogdanovic, N., Plata-Chaves, J. & Berberidis, K. 2013. Distributed incremental-based LMS for node-specific parameter estimation over adaptive networks. Proceedings of 38th International Conference on Acoustics, Speech and Signal Processing (ICASSP 2013).

[39] Plata-Chaves, J., Bogdanovic, N. & Berberidis, K. 2013. Distributed incremental-based RLS for node-specific parameter estimation over adaptive networks. Proceedings of 21st European Signal Conference (EUSIPCO 2013).

[40] Plata-Chaves, J., Bogdanovic, N. & Berberidis, K. 2015. Distributed Diffusion-Based LMS for Node-Specific Adaptive Parameter Estimation. IEEE Transactions on signal processing, 63(13), 3448-3460.

[41] Sayed, A.H. 2011. Adaptive filters. Wiley-IEEE Press.

[42] Lopes, C.G. & Sayed, A.H. 2008. Diffusion least-mean squares over adaptive networks: Formulation and performance analysis. IEEE Transactions on Signal Processing, 56(7), 3122-3136.

Chapter 3 System architecture for the data collection

The data acquisition is a key component for successfully SHM (Structural Health Monitoring) and represents the main challenge of the author research activity. The need of wireless connections has emerged in recent years, since the wired monitoring systems suffer often of various problems due to the installation, the invasive effect, the vulnerability to mechanical damage, and the high costs for the maintenance of the cables as well. Though many wireless sensors have been proposed [1-6], wired solutions are still adopted in most practical applications of structural monitoring for their experienced availability, stability, and reliability.

In this chapter, a Kalman filter-based data fusion is adopted to make a precise measurement of the displacements induced on civil structures. The needed accuracy can be reached exploiting the real-time satellite corrections provided by a single reference station and making a combination between this type of data and accelerations coming from three axial accelerometers [7-9].

After that, recent wireless communication technology are used to develop an update solution that achieves the expected performance without additional cost and significant changes with respect to the existing analog cables. Based on the overall considerations, the ZigBee and the IEEE802.15.4 compliant transceiver CC2530 are the most suitable for applications in wireless SHM systems [10-14].

Once the message has been locally acquired, it is essential to send the information to a remote center. In this way, it can analyze the data and detect the operability of the structure under study.

The communication have not to be executed only by internet, since a crisis could interfere with the existing terrestrial network. Therefore, a VPN (Virtual Private Network) over satellite is also adopted to ensue the continuity of the monitoring operations. The features of the wireless transceivers and the tasks of a reliable satellite communication are discussed.

3.1 Overall structure

The European Union FP7 project named SPARTACUS (Satellite Based Asset Tracking for Supporting Emergency Management in Crisis Operations) funded the software development and the entire experimental campaign reported in this thesis.

A reliable and efficient sensor network needs low-cost and low power to become successful in the SHM field. For this reason, the expenses for local data collection are minimized using two affordable devices able to produce the same performance of more expensive systems.

3.1.1 Component specifications

The devices responsible for sending the acquired message are the ZigBee units. They are made of a CC2530 transceiver, equipped with a Wi-Fi antenna (dual band 2.4/5GHz), and ended with an USB connector. Further details are provided in Chapter 3.

The task of running them is assigned to a PCB (Printed Circuit Board), which has the size of a credit card and allows one to collect the information as an usual personal computer. The adopted electronic board is named Raspberry Pi and is prized in the range of US$20 to US$35. Secure Digital (SD) cards with different capacities may be used to store the operating system and program memory.

In the testing carried out, Ellipse-N is the miniature sensor produced by SBG [15]. It includes three axial accelerometers. This system also embeds an industrial GNSS receiver, and runs an on-board Kalman filter able to make a data fusion of both measures. The limitation is that the model only supports a proprietary protocol. Indeed, the standard NMEA output provides only the ultimate positioning (after the data fusion). Nevertheless, several devices that can be detached from the own manufactures protocol are available on the market, and can replace the SBG sensor [16-18].

In this way, one can exploit all the features of their components, and use the raw data to check each kind of measurement acquired by the sensors, and to execute different estimation schemes.

3.1.2 Data fusion based on Kalman filter

The scientific formulation of the displacement estimation based on the Kalman filter, as provided by the Ellipse, is summarized in this section in order to clarify the sequence of steps, which have to be implemented in the software.

The aim of the proposed method is to extract the needed information to reach the best accuracy from two different measurements. The formulation to fuse acceleration and displacement is also adopted in several recent contributions [19-22].

The state-space model can be written using the definition of acceleration:

$$\dot{\boldsymbol{y}} = \begin{bmatrix} \dot{x}_1 \\ \dot{x}_2 \end{bmatrix} = \begin{bmatrix} \dot{x} \\ \ddot{x} \end{bmatrix} = \begin{bmatrix} 0 & 1 \\ 0 & 0 \end{bmatrix} \begin{bmatrix} x \\ \dot{x} \end{bmatrix} + \begin{bmatrix} 0 \\ 1 \end{bmatrix} \ddot{x}_m + \begin{bmatrix} 0 \\ 1 \end{bmatrix} \eta_a \tag{3.1}$$

$$z = x_m = [1 \quad 0] \begin{bmatrix} x \\ \dot{x} \end{bmatrix} + \eta_d$$

where $\boldsymbol{y}$ are the state variables, grouping $\ddot{x}_m$ and x_m are the measured acceleration and displacement, η_a and η_d are the associated measurement noise of acceleration and displacement. It is assumed that η_a and η_d are white noise Gaussian processes with covariance q and r, respectively. Eq. (3.1) can be written in matrix form as:

$$\dot{\boldsymbol{y}} = \boldsymbol{A}\, \boldsymbol{y} + \boldsymbol{B}\, u + \boldsymbol{w} \tag{3.2}$$

$$z = \boldsymbol{H}\, \boldsymbol{y} + \upsilon$$

where $\boldsymbol{w} \sim (0, \boldsymbol{Q})$, $\boldsymbol{Q} = \begin{bmatrix} 0 & 0 \\ 0 & q \end{bmatrix}$, $\upsilon \sim (0, R)$, and $R = r$. Moreover, let the initial state is $\boldsymbol{y}(0) \sim \left(\begin{bmatrix} 0 \\ 0 \end{bmatrix}, \boldsymbol{p_0} \right)$, and all the uncorrelatedness assumptions hold. Eq. (3.2) rigorously represents the relationships between the states, the measurements and the associated measurement noises.

Since all measured signals are discrete, a state-space model in the discrete time domain is desired. The discrete version of Eq. (3.1) is [20]:

$$\boldsymbol{y_d}(k+1) = \begin{bmatrix} x_1(k+1) \\ x_2(k+1) \end{bmatrix} = \begin{bmatrix} 1 & dt \\ 0 & 1 \end{bmatrix} \begin{bmatrix} x_1(k) \\ x_2(k) \end{bmatrix} + \begin{bmatrix} dt^2/2 \\ dt \end{bmatrix} u(k) + \begin{bmatrix} dt^2/2 \\ dt \end{bmatrix} \eta_a(k) \tag{3.3}$$

$$z(k) = [1 \quad 0] \begin{bmatrix} x_1(k) \\ x_2(k) \end{bmatrix} + \eta_d(k)$$

where dt is the sampling time. Eq. (3.3) written in compact form becomes:

$$\boldsymbol{y_d}(k+1) = \boldsymbol{A_d}\, \boldsymbol{y_d}(k) + \boldsymbol{B_d}\, u(k) + \boldsymbol{w}(k) \tag{3.4}$$

$$z(k) = \boldsymbol{H}\, \boldsymbol{y_d}(k) + \upsilon(k)$$

where $\boldsymbol{A_d} = \begin{bmatrix} 1 & dt \\ 0 & 1 \end{bmatrix}$, and $\boldsymbol{B_d} = \begin{bmatrix} dt^2/2 \\ dt \end{bmatrix}$. The noise processes have the covariance matrices defined as follow [20]:

$$\boldsymbol{Q_d} = q\begin{bmatrix} dt^3/3 & dt^2/2 \\ dt^2/2 & dt \end{bmatrix} \tag{3.5}$$

$$R_d = r/dt$$

The state-space model in Eq. (3.4) is then utilized to develop a discrete-time Kalman filter for displacement and velocity estimation. Let the initial values put to be:

$$\boldsymbol{y_d}^-(k=1) = \begin{bmatrix} 0 \\ 0 \end{bmatrix} \tag{3.6}$$

$$\boldsymbol{P}^-(k=1) = \boldsymbol{p_0}$$

$$z^-(k=1) = x_m(k=1)$$

one computes the quantities referred to as measurements updates at k by introducing the Kalman gain $\boldsymbol{K}(k)$. Subsequently, the Kalman gain is computed by the Eq. (3.7):

$$\boldsymbol{K}(k) = \boldsymbol{P}^-(k)\boldsymbol{H}^T(\boldsymbol{H}\,\boldsymbol{P}^-(k)\boldsymbol{H}^T + R_d)^{-1} \tag{3.7}$$

The measurement update is given by:

$$\hat{\boldsymbol{y}}_{\boldsymbol{d}}(k) = \hat{\boldsymbol{y}}_{\boldsymbol{d}}{}^-(k) + \boldsymbol{K}(k)[z^-(k) - \boldsymbol{H}\,\hat{\boldsymbol{y}}_{\boldsymbol{d}}{}^-(k)] \tag{3.8}$$

$$\boldsymbol{P}(k) = [\boldsymbol{I} - \boldsymbol{K}(k)\boldsymbol{H}]\boldsymbol{P}^-(k)$$

$$\hat{z}(k) = \boldsymbol{H}\,\hat{\boldsymbol{y}}_{\boldsymbol{d}}(k)$$

The measurement update is then followed by the time update:

$$\hat{\boldsymbol{y}}_{\boldsymbol{d}}{}^-(k+1) = \boldsymbol{A_d}\,\hat{\boldsymbol{y}}_{\boldsymbol{d}}(k) + \boldsymbol{B_d}\,u(k) \tag{3.9}$$

$$\boldsymbol{P}^-(k+1) = \boldsymbol{A_d}\,\boldsymbol{P}(k)\boldsymbol{A_d}{}^T + \boldsymbol{Q_d}$$

$$z^-(k+1) = x_m(k+1)$$

where $\hat{\boldsymbol{y}}_{\boldsymbol{d}}{}^-(k+1)$ and $\hat{\boldsymbol{y}}_{\boldsymbol{d}}(k)$ are the prior and the updated state estimates, respectively, while $\boldsymbol{P}^-(k+1)$ and $\boldsymbol{P}(k)$ are the prior and the updated error covariance matrices. It has to be underlined that $u(k) = \ddot{x}_m(k)$.

The procedure allows one to achieve an accurate displacement estimation in all frequency regions. As stated above, the software implementing it runs on board the inertial sensor produced by SBG. In the "proprietary free" approach pursued in this manuscript, the previous equations have to be arranged in a software to be executed at the local collection node. Its result is passed via satellite to a remote center, thus achieving a lightening of the data transmission.

3.2 Transmission mode from sending sides to a remote center

The proposed system architecture consists of a wireless network to store locally the information, and to transmit the measurements of each sensor to the Coordinator Node. After that, the information may be sent via satellite to a remote center for monitoring and maintenance purposes, as shown in Figure 3.1.

The wireless network is made of GPS devices able to receive the corrections provided by a base station located near the structure. This technique is named RTK (Real Time Kinematic) and is used to enhance the precision of the positioning systems. It measures the phase of the carrier wave of the signal, and it relies on a single reference station to provide a centimeter-level accuracy.

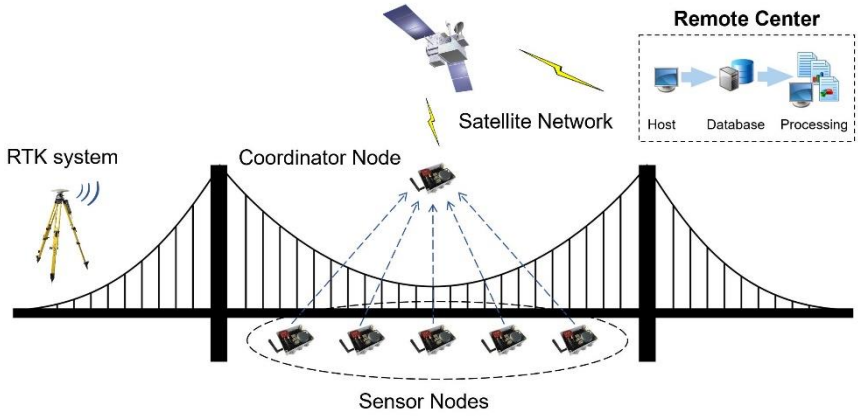

Figure 3.1 Architecture of the real-time monitoring system

The system is based on the open-access software environment of a credit card-size computer, which is used as data collector and named Raspberry Pi 2. It is run as Raspbian, a Debian-based computer operating system, and the operations are coded in Python [23]. The core activities are:

- store sensor data inside the memory of the data collector in real-time,
- create and transmit data frame to the coordinator through ZigBee,
- transfer the information with a remote center via satellite, and
- process the data with the displacement estimation method.

Each measurement point (Sensor Node) is made of a ZigBee device and a GPS receiver coupled with three axial accelerometers for real-time data collection and transmission.

At idle time, the sensor node remains in sleeping state until the power supply is not furnished to the system, which is set to be started stand-alone. To clarify its operational principle, a functional flowchart of the designed prototype is shown in Figure 3.2.

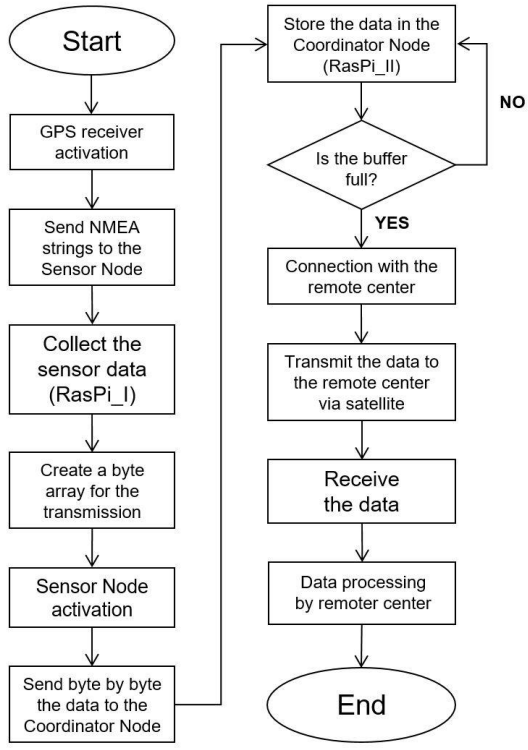

Figure 3.2 Functional flow chart of the proposed system

As soon as the power supply is furnished to the system, the sensing device produces at each time step NMEA-0183 strings, and comes with its wire ending (USB interface). The bottleneck is the power one has to provide to the data collector. Thus, low consumption surrogates of the computers are welcome and the modules of the Raspberry Pi class are the most suitable for this purpose. To minimize consumption, the conceived architecture creates a byte array (i.e., a sequence of numbers) and send the sentence by a ZigBee modulus to the Coordinator Node.

Once the buffer is full, the software stores the message inside the memory of the latter one, which can be equipped with higher power availability. From here, one can rely on internet or, to bypass any liability problem, on satellite phones to transmit the information to the remote center.

3.2.1 Wireless communication framework

This section emphasizes on the real-time data collection and on the long-range communication (when the distance is more than 100m) between the Sensor Nodes and the Router and from the Router to the Coordinator node. The process from the Sensor to the Coordinator is carried out by the ZigBee technology.

ZigBee technology offers a great trade-off in terms of power, range, data rate, and security. It organizes multi-hop network, which imposes that two devices exchange data depending on other intermediate forwarding devices. Further, the nature of this system requires that each device perform a specific networking function that determines its role within the network, as shown in Figure 3.3.

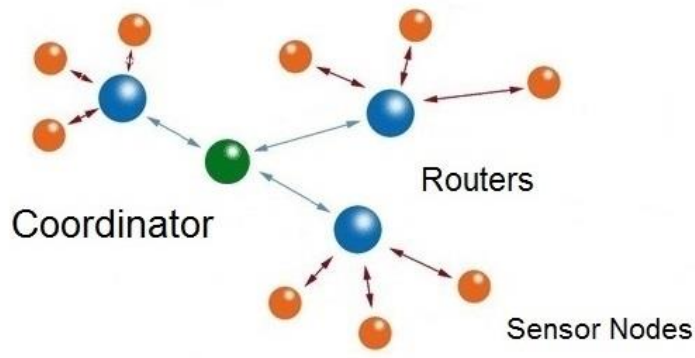

Figure 3.3 ZigBee network type for the local transmission

The developed network consists of a Coordinator, a Router and several Sensor Nodes, but the type of device does not restrict its application because it is usually determined at compile-time. The ZigBee network can be implemented by the system-on-chip (SoC) transceiver CC2530 and its corresponding protocol stack offered by Texas Instrument [24]. It integrates a radio frequency (RF) power amplifier CC2591, which allows adapting to short and medium range communication.

The hardware used for each device consists of a ZigBee to USB (Virtual RS232) adapter with a CC2530 module, a rubber antenna, an UART to USB bridge, an USB connector and a JTAG interface for downloading and debugging the firmware (Figure 3.4).

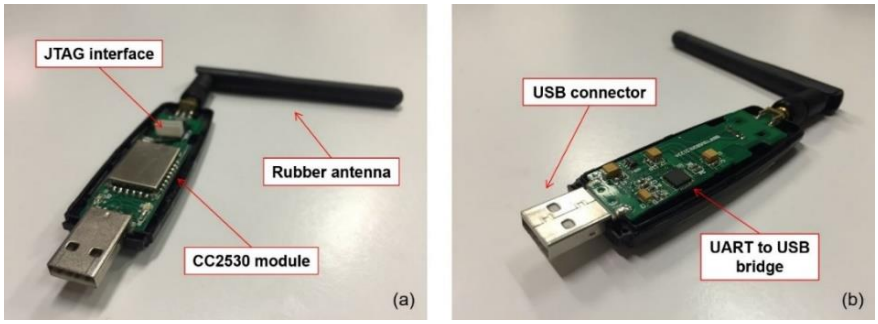

Figure 3.4 Top (a) and bottom view (b) of the ZigBee device

The CC2530 is a true SoC solution for IEEE 802.15.4 and other ZigBee applications as well. It enables to combine the excellent performance of a leading RF transceiver with an industry-standard enhanced 8051 MCU, in-system programmable flash memory of 8KB RAM. The firmware code for this kind of device is the 8051 microcontroller core integrated in the CC2530 transceiver, which is compiled using an Integrated Development Environment (IDE) software named IAR Embedded Workbench 8051. Finally, the ZigBee protocol stack (Z-Stack™) which is needed is Open Source and provided by Texas Instrument.

3.2.2 WAN architecture

The network above mentioned covers a small area, and the wireless technology represent a good solution for collecting and transmitting the monitoring data. After that, the link between the Coordinator Node and the remote site has to be carried out through a remote communication based on a terrestrial network and, if not available, via satellite (as depicted in Figure 3.5).

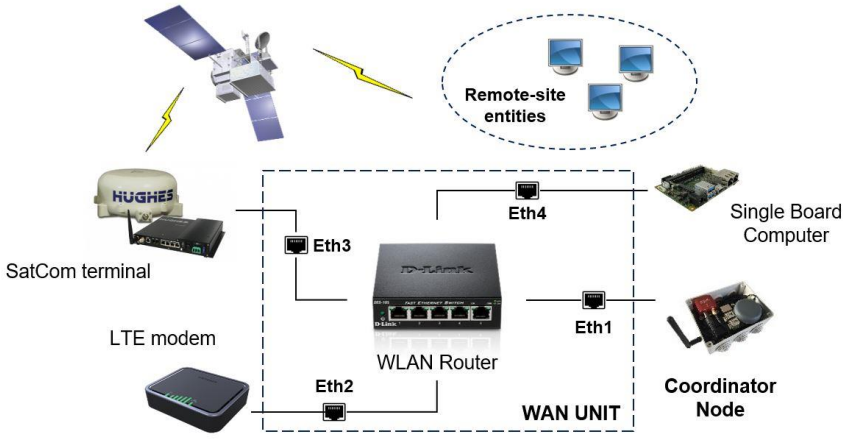

Figure 3.5 WAN architecture of the real-time SHM

This type of unit consists of several elements with the aim to connect together each of them, allowing the support of different networks. For instance, the connection to the terrestrial network is done using a Long Term Evolution (LTE) modem, which simply acts as a client in the 4th Generation (4G) network, such as a smartphone. This LTE modem is connected via Ethernet to a WLAN (Wireless Local Area Network) Router as well as the SatCom (Satellite Communication), made of satellite modem and its antenna.

The satellite connection is assigned to the Broadband Global Area Network (BGAN), which is an Inmarsat service. It offers the possibility to benefit of a bandwidth of 256kbps (upload and download) while using relatively small satellite modem and satellite antenna. In this way, the information can access the "outside world", also named the Wide Area Network (WAN), using either the satellite or terrestrial connection. The different connections and the related standards of the WAN are summarized in Table 2.1.

Table 3.1 WAN connections and their related standards

Element	Remote element	Interface	Standard
LTE modem	WLAN Router	Ethernet	IP
LTE modem	Terrestrial Network	LTE	GSM/3G/4G
BGAN modem	WLAN Router	Ethernet	IP
BGAN modem	Satellite	BGAN	Inmarsat
Single Board Computer	WLAN Router	Ethernet	IP
WLAN Router	Coordinator Node	Ethernet	IP

The satellite system for the field-testing was also proposed in the ESA 3InSat project [25]. It is from Hughes and is identified by the model 9450 [26]. It is composed of a satellite terminal (User Terminal, UT) and of an auto-pointing antenna.

To overcome the constraints of GSM/3G/4G connections, it exploits a VPN on site and connects it over the satellite link to a remote server. The information is stored by the central server into a database, and it is post-processed. In this way, the monitoring of a structure can be updated in real-time and with high precision.

3.2.2.1 Operational principle

Figure 3.6 shows the functional diagram of the communication unit for the WAN. Both 4G client and BGAN provide an interface enabling their configuration, and a specific hardware (i.e., LTE Modem and BGAN satellite terminal).

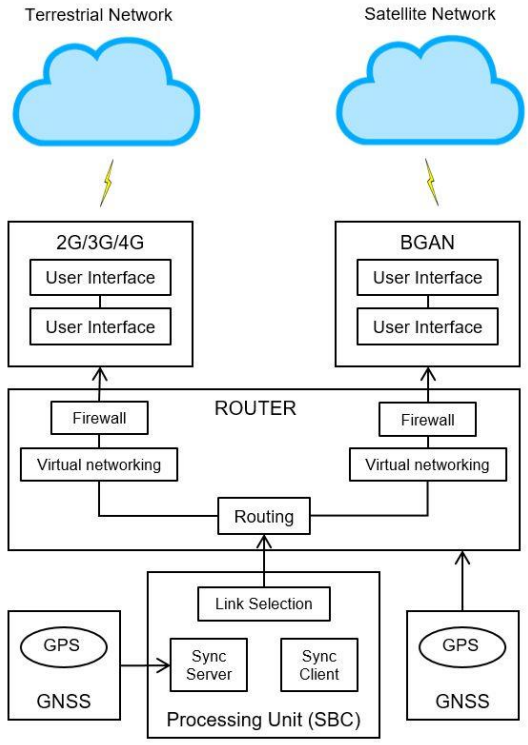

Figure 3.6 WAN functional diagram for the real-time SHM

Both elements are connected to the WLAN Router via a physical link (Ethernet), which enables a logical link between the devices (IP packets). Since both terminals enable connecting the Coordinator Node to the "outside world" (remote connection), a firewall is needed for securing the system.

The router on both interfaces provides the firewall functionality and it is also possible to further increase the security by enabling the "Virtual Networking". It consists into creating the so-called Virtual Local Area Network (VLAN) with the result that both terrestrial and satellite networks are seen as separate internal virtual networks.

Those virtual networks are generally separated from the internal Local Area Network (LAN) of the Router. Therefore, its functionalities can be summarized as follows:

- *routing* (transfer packets from one source to the right destination),
- *virtual networking* (VLAN),
- *firewall (*security), and
- support of Quality of Service (QoS).

The processing unit is connected to the Router via an external interface (Ethernet) as well. It is the Single Board Computer (SBC), which provides a timeserver for synchronizing the clock of all devices ("Sync Server" / "Sync Client") and also a "Link Selection" algorithm. This latter functionality aims to decide which link has to be selected for transmit the information to the remote site (i.e., terrestrial or satellite link). The choice is based on the availability of the two networks and on the signal quality of each one. Finally, a Global Navigation Satellite System (GNSS) module provides the synchronization of the local server with the Global Positioning System (GPS).

3.3 References

[1] Sim, S. 2016. Estimation of Flexibility Matrix of Beam Structures Using Multisensor Fusion. Journal of Structural Integrity and Maintenance, 1(2), 60-64.

[2] Lynch, J.P., & Loh, KJ. (2006). A summary review of wireless sensors and sensor networks for structural health monitoring. The Shock and Vibration Digest, 38(2), 91–128.

[3] Wang, Y., Lynch, J.P. & Law K.H. 2005. Design of a low-power wireless structural monitoring system for collaborative computational algorithms. Proceedings of SPIE 10th Annual International Symposium on NDE for Health Monitoring and Diagnostics, San Diego, USA.

[4] Rice, J.A., Mechitov, K., Sim, S-H., Nagayama, T., Jang, S., Kim, R., Spencer Jr., B.F., Agha, G. & Fujino, Y. 2010. Flexible smart sensor framework for autonomous structural health monitoring. Smart Structures and Systems, 6(5-6), 423-438.

[5] Ni, Y-Q., Xia, Y., Liao, W-Y. & Ko, J-M. 2009. Technology innovation in developing the structural health monitoring system for Guangzhou New TV Tower. Structural Control and Health Monitoring, 16(1), 73-98.

[6] Faravelli, L. & Chen Z-C. 2009. Time issues in a wireless network. Proceedings of 15th International Workshop on Dynamics and Control, CIMNE, Barcelona.

[7] Casciati, S., Faravelli, L. & Chen, Z-C. 2009. A design of multi-channel wireless sensing system for structural monitoring. Proceedings of ECCOMAS Thematic Conference on Computational Methods in Structural Dynamics and Earthquake Engineering, Rhodes, Greece.

[8] Chen, Z-C, Casciati, S. & Faravelli, L. 2015. In-Situ Validation of a Wireless Data Acquisition System by Monitoring a Pedestrian Bridge. Advances in Structural Engineering, 18(1), 97-106.

[9] Casciati, S. & Chen, Z-C. 2010. A multi-channel wireless connection system for structural health monitoring applications. Structural Control and Health Monitoring, 18(5), 588-600.

[10] Chen, Z-C. 2014. Energy efficiency strategy for a general real-time wireless sensor platform. Smart Structures and Systems, 14(4), 617-641.

[11] Chen, Z-C. & Casciati, F. 2014. A low-noise, real-time, wireless data acquisition system for structural monitoring applications. Structural Control and Health Monitoring, 21(7), 1118-1136.

[12] Casciati, S. & Chen, Z-C. 2012. An active mass damper system for structural control using real-time wireless sensors. Structural Control and Health Monitoring, 19(8), 758-767.

[13] Casciati, S., Faravelli, L. & Chen, Z-C. 2012. Energy harvesting and power management of wireless sensors for structural control applications in civil engineering. Smart Structures and Systems, 10(3), 299-312.

[14] Casciati, S. & Chen, Z-C. 2011. A multi-channel wireless connection system for structural health monitoring applications. Structural Control and Health Monitoring, 18(5), 588-600.

[15] Guinamard, A. 2014. Ellipse AHRS & INS - High Performance, Miniature Inertial Sensors User Manual, SBG Systems, France.

[16] CXL-LF Series - High Sensitivity Accelerometers. 2016. USA, Crossbow Technology Inc.

[17] Trimble 147A High Resolution Accelerometer. 2016. USA, Trimble Navigation Limited.

[18] Trimble R10 GNSS System. 2016. USA, Trimble Navigation Limited.

[19] Caron, F., Duflos, E., Pomorski, D. & Vanheeghe, P. 2006. GPS/IMU data fusion using multisensor Kalman filtering: Introduction of contextual aspects. Information Fusion, 7(2), 221-230.

[20] Smyth, A. & Wu, M. 2007. Multi-rate Kalman filtering for the data fusion of displacement and acceleration response measurements in dynamic system monitoring. Mechanical Systems and Signal Processing, 21, 706-723.

[21] Zhou, Z. 2011. GPS navigation data fusion using composed correcting Kalman filtering method. Journal of Computational Information Systems, 7(6), 2006-2012.

[22] Chatzi E-N. & Fuggini, C. 2012. Structural identification of a super-tall tower by GPS and accelerometer data fusion using a multi-rate Kalman filter. Proceedings of 3rd International Symposium on Life-Cycle Civil Engineering, IALCCE 2012, 144-151.

[23] Bradbury, A. & Everard, B. 2014. Learning Python with Raspberry Pi. Chichester (UK), John Wiley & Son Ltd, ISBN 978-1-118-71705-9.

[24] Texas Instruments. 2009. CC2530 Software Examples User's Guide. Dallas (USA), Texas Instruments Incorporated.

[25] 3InSat, Train Integrated Safety Satellite System. 2014. ESA Project: Contract 4000105788/12NL/NR.

[26] Hughes 9450-C11 BGAN Mobile Satellite Terminal. 2010. USA, Hughes Network Systems, LLC.

Chapter 4 Hardware and software integration

In general, SHM systems are used to monitor the behavior of structures during forced vibration testing or natural excitation for structural health analysis and diagnosis. It includes some sensors installed on a structure and a centralized data acquisition device. The sensors convert the structural response into electrical signal, and the data acquisition device has to sample the electrical signal output from the sensors and store the sampled data in a central data repository.

In order to ensure high quality signal sampling, structural monitoring systems employ coaxial wires as the link between sensors and the centralized data acquisition device. Coaxial wires provide a very reliable link, but their installation can be expensive and laborious. Indeed, when many sensors are required and they are far from the data acquisition device, this type of link is inconvenient.

As a promising solution to these drawbacks, wireless structural monitoring systems are emerging. A wireless structural monitoring system consists of some wireless sensors installed on a structure, and a base station receiving the data by wireless links. The power supply of the sensors are usually batteries, sometimes with an energy harvesting device.

A real-time SHM system based on wireless sensor and satellite technologies is designed in this chapter. The first part relies on previous researches [1-8], and the methodology for the components integration of the final system consists of three sections: (i) hardware know-how, (ii) functional procedures, and (iii) software implementation.

It is design through a set of practical steps for the local storage and the next data transmission from the prototype to the remote site via satellite.

4.1 Hardware know-how

Reliability, accuracy, low cost and low power are the main qualities required by a SHM system for the infrastructure monitoring [9]. The selected devices for the development of a WSN consist of an Inertial Sensor (INS) with internal GNSS receiver, a credit-card sized computer, and a GBAN ZigBee Wireless Data Transmission Device. The specific functions for each component of the tracking unit are listed in Table 4.1.

Table 4.1 Technical specifications and functions of the WSN

Hardware	Function
Ellipse-N	Exploit INS capabilities also without navigation satellites signal
GNSS antenna	Acquire GNSS positioning data with quality field (accuracy/precision)
Raspberry Pi 2	Collect positioning information to allows local storage and post-processing
GBAN ZigBee	Send information to the collecting unit using Wireless Transmission Devices

Therefore, in order to achieve a data post-processing, the local system has to be equipped with a data collector (RasPi) able to manage the storage of the information to be transmitted from the Coordinator Node to the remote control. In Figure 3.1 is shown all the hardware components for the final prototype used for the testing activity.

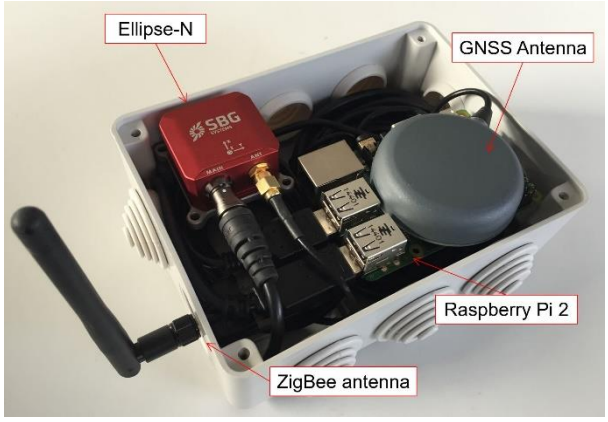

Figure 4.1 Hardware components of the local storage

Once the displacement values are correctly stored inside the memory of the data collector (Sensor Node), the information is sent by ZigBee devices to a collecting unit (Coordinator Node) placed near the infrastructure in order to be transmitted via satellite to a remote side for monitoring and maintenance purposes.

4.1.1 Micro Electro-Mechanical Systems (MEMS)

To measure the displacement of the civil infrastructures with the method described in the previous chapter, a Micro Electro-Mechanical System (MEMS) named Ellipse-N and provided by SBG System is adopted [10]. It is a miniature sensor with high-performance MEMS based Inertial System, which achieves exceptional orientation and navigation performance in an affordable package. It also includes an Inertial Measurement Unit (IMU) and runs an on-board enhanced Extended Kalman Filter (EKF).

The Ellipse series is divided in a comprehensive set of sensors and the Ellipse-N model is an Inertial Navigation System (INS), providing both orientation and navigation data. The use of positioning data by aiding equipments as an odometer can be used to provide accurate navigation data and to improve orientation accuracy.

Moreover, this model embeds an industrial GNSS receiver and supports a proprietary protocol for best performance, but also standard protocols such as NMEA for direct integration into existing applications [11]. Figure 4.2 shows a general view of the sensor.

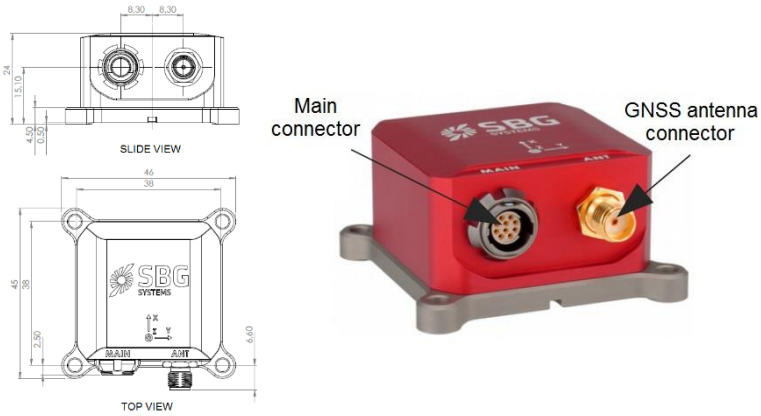

Figure 4.2 Ellipse-N model with slide and top view

In addition to the native sbgECom binary protocol, the Ellipse N implements the NMEA-0183 standard protocol for both log outputs, aiding equipments input [12]. When NMEA-0183 output is enabled, a subset of NMEA-0183 messages can be sent to external instruments and equipment connected to the receiver serial port. Figure 4.3 shows the basic organization of the sensor through a simplified block diagram.

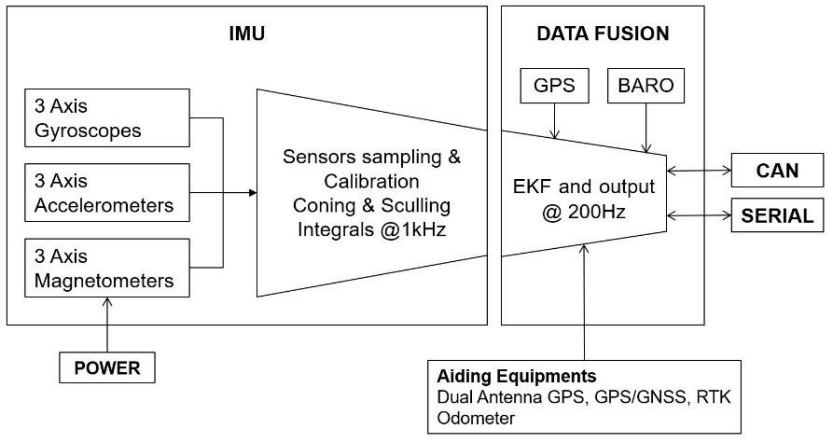

Figure 4.3 Ellipse-N block diagram

The Ellipse modular design allows to connect a wide range of aiding sensors. GNSS, odometer, and others can be connected to further enhance navigation performance. In addition, its Kalman filter is able to estimate some user entered parameters to further improve accuracy, such as GPS lever arm, odometer gain, and others.

The basic idea behind the Ellipse Kalman filter is to take the best of each sensor, without drawbacks. A high frequency prediction step (i.e., propagation) uses the inertial capabilities to precisely measure motion and navigation data. When aiding data becomes available, the Kalman filter uses it to correct the current state and prevent drift.

4.1.1.1 INS and OEM technology

With the proliferation of low cost OEM (Original Equipment Manufacturer) GPS board sets on the market today, it is difficult to judge whether any particular one may be suitable for a required application [13]. Indeed, this kind of systems offer some benefit such as cost effective, compact in size, and lower power consumption.

The main drawback is related to check the parameters setting and the compatibility with other devices in order to obtain a proper data acquisition. For this reason, it is necessary to compare the collected data with those coming from the available prototypes on the market by the manufactures.

For instance, in case of vehicle navigation systems operating in an urban environment, a few receiver capabilities stand out. The speed of a receiver to regain the satellites after a

signal blockage is investigated by some authors [14]. Indeed, since satellite constellations change, GPS position determination can be degraded and intermittent.

Continuous position and velocity are also important factors for vehicle location, and by testing the receivers in different urban scenarios, an assessment of the receiver suitability for navigation applications can be made. Two different types of GPS receivers (i.e., a geodetic-grade and an OEM type) are studied by other authors in the marine applications [15]. In this work, a kinematic test was carried out in Turkey, to assess the performance of the PPP (Precise Point Positioning) method in a dynamic environment. The PPP is a GNSS analysis technique where no observations from a reference station, as used by the conventional differential algorithms, are required.

For the case under study can be useful to describe the IG-500N OEM, which is the board level option available for the Ellipse-N and shares all characteristics and performances of the box standard with a much smaller size and weight (Figure 4.4).

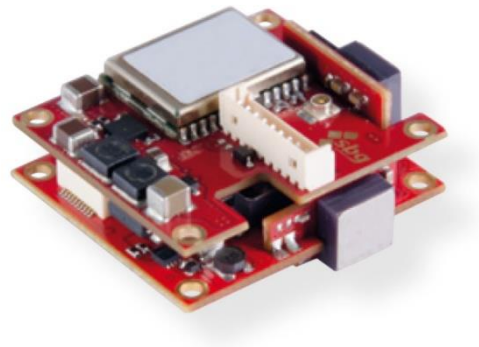

Figure 4.4 IG-500N OEM

In an incredibly small package (30x27mm) and in less than 10g, a full featured navigation that delivers consistent performance with an advanced calibration procedure and a configurable Extended Kalman filter (EKF). This model is more robust and easier to integrate than the traditional PCB (Printed Circuit Board) OEM module. The key features of the board level option and its evolution are listed in Table 4.2.

Table 4.2 Comparison of different generation of receivers

Features	IG-500N OEM	ELLIPSE-N
Dimension	27x30x14mm	46x45x24mm
Weight	10g	47g
Operating voltage	3.3 V to 30 V	5 - 36 V
Power consumption	800 mW	< 650 mW
Specified temperature	-40 to 85°C, 40 to 185°F	-40 to 85 °C, 40 to 185 °F
Roll / Pitch	0.8° RMS	0.2 °
Heading	0.5° RMS	< 0.5° GPS
Velocity	< 0.1m/s	0.1m/s
Position	< 2m	2m
Engine, update rate	50-channels, 4Hz, L1 C/A Code SBAS	72-ch, 10Hz, L1 C/A GPS, GLONASS, BEIDOU, SBAS
Output rate	100Hz	Up to 200Hz
Serial interface	RS-422, USB using an external adapter	RS-232, RS-422, USB - up to 921,600bps
Serial protocols	Binary proprietary protocol NMEA/ASCII	Binary eCom protocol NMEA, ASCII, TSS

The only way to improve the displacement accuracy of a sensor network in SHM field is exploiting the ability of some GPS devices to receive differential correction from a reference station via satellite. This method is based on RF (Radio Frequencies) and allows to achieve measurements under the centimeter level. The possibility to check the benefits for an effective case study is faced in the future direction of the present work.

4.1.2 Unconventional devices

To measure the accelerations of the bridge cables, two different devices are investigated: the 147A triaxial accelerometer and the Crossbow CXL01LF3. The first one has large dimensions and weight (it is provided by Trimble), while the second one is commercially fabricated using standard micromachining methods in a clean-room environment.

The 147A accelerometer is a force-balance accelerometer that converts acceleration signals into voltage signals to measure various low frequency and ultra-low frequency motion (Figure 4.5). It uses a force-balance feedback technique to make up for the

mechanical limitations of conventional accelerometers. This overcomes the shortcomings of nonlinear distortion and threshold of sensitivity of elastic measuring parts [16].

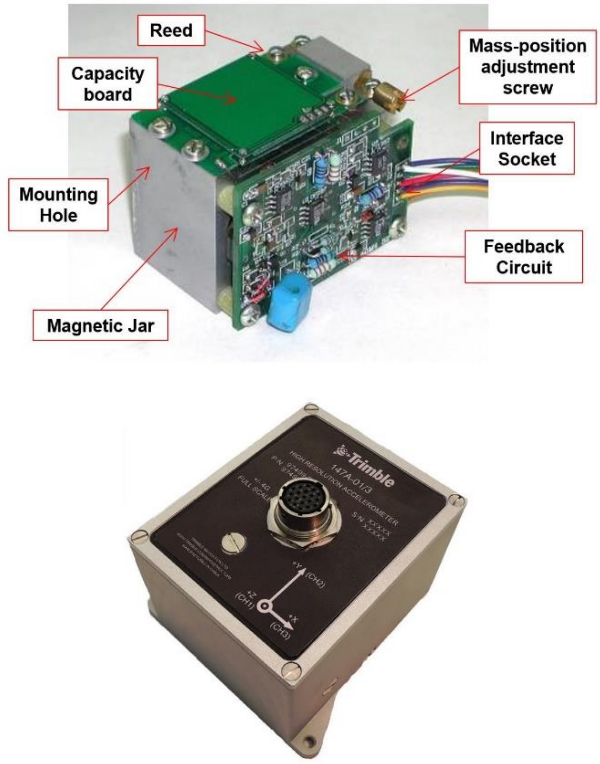

Figure 4.5 General view of the 147A triaxial accelerometer

The advanced features of the 147A accelerometer include high sensitivity, large linear range, high resolution, and high dynamic range. It is +/- 4g full scale and provides excellent dynamic range, which is useful when used with 24-bit digitizers like the 130-MC Multi-Channel Recorder and 130S Series Data loggers. In Table 4.3, the main specifications of the 147A triaxial accelerometer are summarized.

Table 4.3 147A triaxial accelerometer specifications

Features		Description
Mechanical	Dimensions	12.5x13.5x 9.8cm
	Weight	4.4lb (2Kg)
Environmental	Operating Temperature	–4°F to 140°F (–20°C to 60°C)
	Storage Temperature	–40°F to 185°F (–40°C to 85°C)
Electrical	Average Power	<0.6W
	Power Supply	+9 to +18VDC
	Full-scale Output	±10V differential, 2 VPP
	Sensitivity	2.5V/g
Performance	Full-scale Range	±4g
	Self-Noise	<1µm/s/s
	Dynamic Range	>155dB (DC to 10Hz)
	Linearity	<0.1%
	Frequency Response	DC – 150Hz (+/-3dB)

Compared to the 147A, the capacitive MEMS accelerometer is relatively inexpensive (i.e., costing about $300). The CXL02 accelerometer (Figure 4.6) has an acceleration range of ±2g, noise floor of 0.5mg, and sensitivity of 1V/g [17]. It is powered by 5V and output an Analog Voltage signal between 0 and 5V (with 2.5V corresponding to 0g).

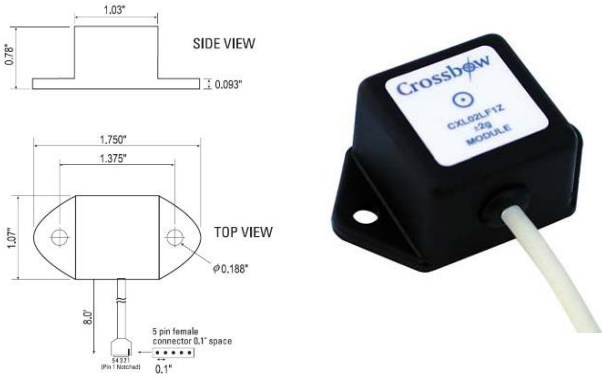

Figure 4.6 General view of the Crossbow CXL01LF3

The low noise floors associated with the MEMS accelerometers are determined to be slightly below the quantization error inherent to the 16-bit ADC. Hence, an amplification of the accelerometer outputs can drastically improve the signal-to noise ratio of the digitized acceleration signals [18-20]. Table 4.4 reports the Crossbow specifications.

Table 4.4 Crossbow CXL01LF3 specifications

Features		**Description**
Physical	Dimensions	1.98x4.45x2.72cm
	Weight	1.62oz (46gm)
Environmental	Temperature Range	-40 to +85°C
	Shock	2000g
Electrical	Supply Voltage	+5 ±0.25V
	Supply Current	4/axis mA
	Span Output	±2.0 ±0.1V
	Sensitivity	2V/g
Performance	Input Range	±1g
	Non-Linearity	±3%FS
	Noise Density	70 μg/Hz½
	Noise	0.5mg rms
	Bandwidth	DC-50Hz

At last, the GPS positioning data can be acquired by the Trimble R10 GNSS receiver shown in Figure 4.7. This type of device incorporates: (i) GNSS antenna, (ii) receiver, (iii) internal radio, and (iv) battery in a rugged lightweight unit, which is ideally suited as a RTK rover or a quick setup base station [21].

In addition, a smart lithium-ion battery inside the system delivers extended the battery life and more reliable power. A built-in LED battery status indicator allows the user to quickly check the remaining time before charging (until to 5 hours with 450-900MHz receive and transmit option at 0.5W).

Figure 4.7 General view of the Trimble R10

It also embeds some LEDs to monitor satellite tracking, radio reception, data logging status, Wi-Fi status, and power. The Bluetooth wireless technology provides cable-free communications between the receiver and controller. In Table 4.5, the main specifications of the Trimble R10 GNSS receiver are listed.

Table 4.5 Trimble R10 specifications

Features		Description
Physical	Dimensions	11.9x13.6cm
	Weight	2.49lb (1.12kg)
Environmental	Operating Temperature	–40°C to +65°C (–40°F to +149°F)
	Storage Temperature	–40°C to +75°C (–40°F to +167°F)
Electrical	Power Supply	11 to 24 VDC
	Power Consumption	5.1W
	Lithium-ion smart battery	7.4V (3.7Ah)
	Sensitivity	2V/g
Positioning Performance (RTK surveying)	Single Baseline <30 km	Horizontal: 8mm + 1ppm RMS
		Vertical: 15mm + 1ppm RMS
	Network RTK	Horizontal: 8mm + 0.5ppm RMS
		Vertical: 15mm + 0.5ppm RMS
	Start-up time	2 to 8s

Once all the needed devices are available, it is necessary to use a reliable mounting system, which is able to support their weights, ensuring the ideal horizontal position of the platform during the operations, i.e., when is fixed to the footbridge cables.

4.1.2.1 Differential GNSS with RTK system

Consolidated and available technologies for a precise location are based on Global Navigation Satellite Systems (GNSS). The navigation systems provided by engineering advances in satellite technologies were initially the NAVSTAR GPS (Navigation System with Time and Ranging - Global Positioning System) developed and maintained by the US Department of Defense and Transportation, and the Russian Global Navigation Satellite System GLONASS (Globaluaya Navigatsionnaya Sputnikovaya Sistema) [22]. Although both are national military systems, they were available for use by the international private and commercial communities [23, 24].

Recently a Chinese system (BeiDou) was completed as well as two of them designed and implemented by India, the Indian Regional Navigational Satellite System (IRNSS) and Japan, the Quasi Zenith Satellite System (QZSS), respectively [25, 26].

In Europe, concern was voiced about dependence on a foreign military system and thus plans for a civilian global navigation satellite system were put in place.

GPS employs two fundamental observables for positioning and navigation, the pseudo-ranges and the carrier-phase. The first one is a measure of the distance between the satellite at the time of transmission and the receiver when receives the signal. When used in instantaneous stand-alone mode, one obtains an accuracy of 10-20m after the removal of selective availability. The second one can be used to determine ranges with millimetric accuracy, provided the integer ambiguity problem is solved [27-29].

The system was divided in an overlay for the existing systems (GNSS-1), and a completely autonomous one with a separate space segment (GNSS-2). Further, the drop of equipment prices over the past ten years led to an enormous growth in the number of GPS users and new applications emerged such as car navigation systems, fleet management, aircraft approach, bridge deformation monitoring, and the navigation of agricultural field machinery. These multiple applications increased the necessity to improve accuracy, availability, and integrity in the systems.

Currently, Differential GNSS (DGNSS) represents a solution for these user requirements, where correctional data are emitted from a reference system placed in a known position and sent to a receiver.

In differential positioning, a minimum of two receivers, named Base Station and Rover, are involved. The Base Station occupies a known position during the session, and the

determination of the Rover related to the base represents the target of the work. Both receivers observe the same constellation of satellites at the same time, and since the base position is known, corrections may be generated in order to improve the solution at the Rover, as shown in Figure 4.8.

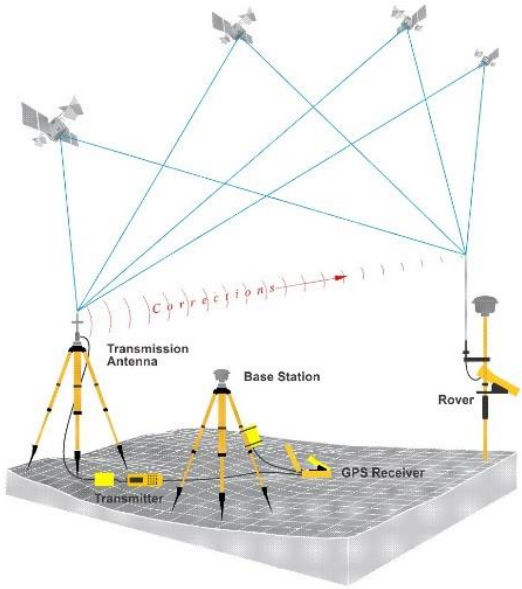

Figure 4.8 Differential GNSS with RTK positioning

The GPS signal is affected by a number of error sources including orbital and atmospheric propagation errors [30]. An improvement in the GPS performance can take the form of enhancements in the geometry of data sources (satellites), measurement quality, or both.

4.1.3 Microcontroller and RF transceivers

Regarding the wireless communication, CC2530 can be considered a good system-on-chip (SoC) solution for the ZigBee applications from Texas Instrument [31]. It allows to build robust network nodes with low material costs. The chip combines the excellent performance of a leading RF transceiver with a standard enhanced 8051 MCU, in a system programmable flash memory (i.e., 8-KB RAM) and many other powerful features.

However, many software tools have to be involved in order to develop the CC2530-based ZigBee device. First, an IDE (Integrated Development Environment) is needed to program and compile the firmware code for the 8051 microcontroller core integrated in the CC2530 transceiver, i.e., the IAR Embedded Workbench 8051. After that, a ZigBee protocol stack (Z-Stack™) is used because the developer just needs to design the application program based on it. This open source stack, with two software tools to facilitate the debug and testing of ZigBee transceiver and wireless network (i.e., SmartRF Studio 7 and Packet Sniffer), is provided by the Texas Instrument.

In addition, some hardware components are needed to make the whole development environment for the ZigBee-Serial Port adapter. The required tools include: debugger, development board, transceiver module and its adapting board, as shown in Figure 4.9.

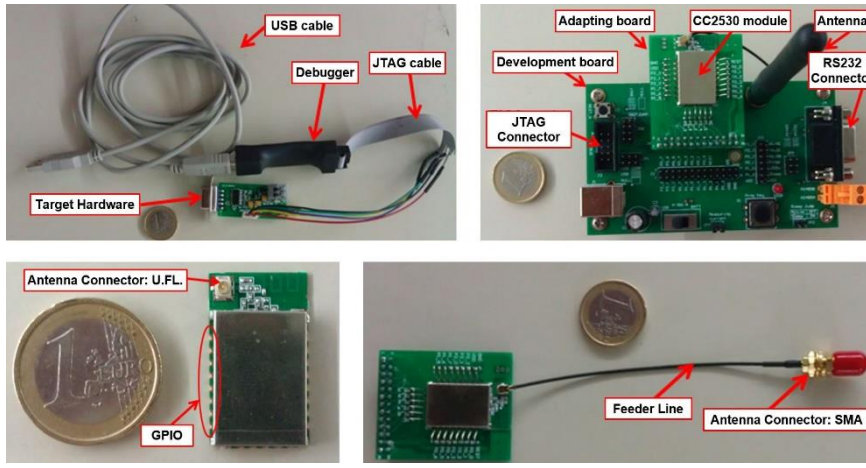

Figure 4.9 Development environment of the ZigBee Network

The debugger is used to download and debug the firmware for the CC2530 8051 microcontroller core. The development board is used to facility the access of the transceiver module resource. The latter integrates a CC2530 chip with the peripheral passive components of its GPIO (General Purpose Input and Output) and the power supply ports on a small PCB board.

Figure 4.10 shows the first prototype of the ZigBee Sensor Node, which is a ZigBee to RS232 adapter consisting of: (i) CC2530 module, (ii) antenna, (iii) UART to RS232 converter, (iv) DB9 serial port connector, (v) 5V power supply connecter, and (vi) JTAG interface for downloading and debugging the firmware.

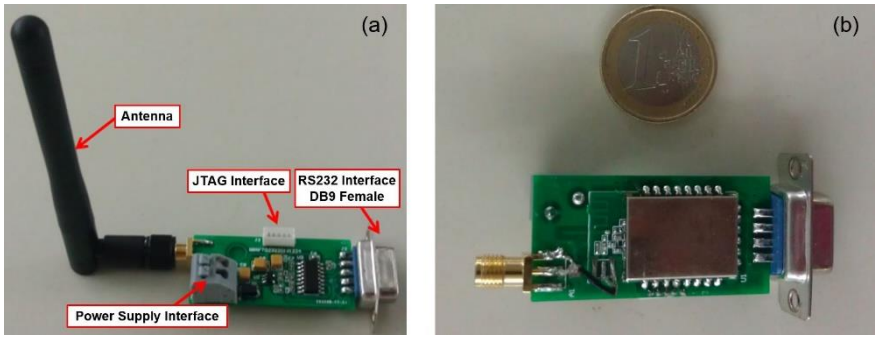

Figure 4.10 Top (a) and bottom view (b) of the Sensor Node

Otherwise, the ZigBee Coordinator Node is a ZigBee to USB (Virtual RS232) adapter made of: (i) CC2530 module, (ii) antenna, (iii) UART to USB bridge, (iv) USB connector, and (v) JTAG interface, as shown in Figure 4.11.

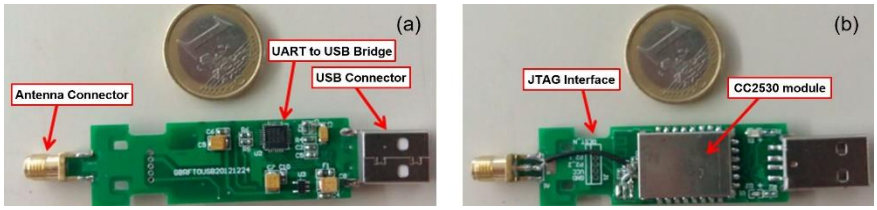

Figure 4.11 Top (a) and bottom view (b) of the Coordinator Node

It is worth notice that the first version of the ZigBee Sensor Node was design with a RS232 adapter because it was not defined in which way the transmission had to be carried out at the measurements point. After the choice to use the Raspberry Pi as data collector, it was converter in same way of the Coordinator Node. Table 4.6 summarizes all the network properties of the ZigBee modules.

Table 4.6 Network properties of the ZigBee modules

Network Properties	Description
Wireless Standard Protocol	ZigBee-Pro (High Level) IEEE802.15.4 (Low Level)
Raw Bandwidth	250kbps (raw data rate)
Frequency Band	2.4G License-free ISM From 2400-2483.5MHz
Frequency Channel	16
RF Power	1dBm to 20dBm
Network Typology	Star, Tree, or Mesh
Single Hop Range	1Km (Line of Sight)
Network Robustness	Self-organization and Self-healing Routing
Anti-RF Interference	CSMA-CA (Carrier Sensing Multiplexing Access/Collision Avoidance): avoid collision
	Acknowledge-Retransmission reliable communication: deal with temporary interference
	Frequency Agility: deal with permanent or intentional interference
Network Security	128bit AES Encryption

The firmware application of the ZigBee devices is named SerialApp and is built on the ZigBee protocol stack Z-Stack (Version ZStack-CC2530-2.5.1a), as shown in Figure 4.12. It implements a transparent data transfer between the serial port and the ZigBee stack. When a data packet is received from the air (ZigBee stack), the SerialApp passes it to the serial port. When a data stream is sent to the serial port, the SerialApp passes it to the air. Since the data over the air is based on packets and the packet length is limited, the data stream from serial port may need to be fragmented. For this reason, the SerialApp adopts a software flow control to frame the data stream from serial port into packets. Thus, the data are processed when an idle data number or time exceeds a predefined threshold.

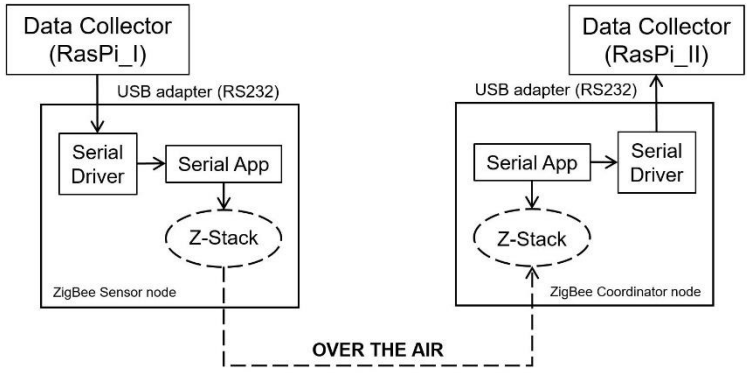

Figure 4.12 Firmware application between Sensor and Coordinator Node

To guarantee the reliability of the wireless data transfer, Z-Stack offers an end-to-end function in addition to the single-hop acknowledgement. In this way, each sending device can get always the confirmation that a data packet has been delivered to its destination.

Since many Sensor Nodes send their data to the Coordinator Node simultaneously and the data of one GPS device is long and should be divided into more than one packet, the integrity of the message may be damaged. To avoid this problem, the following method is adopted: the sentences are unpacked by character and transmitted as smaller fragments that are then reassembled by the receiving device.

4.1.4 Satellite terminal

The WAN Unit of the real-time SHM system is based on the solution provided by TriaGnoSys GmbH in the framework of the ESA project named 3InSat [32]. The 3InSat communication unit is a suitcase with the aim to record the position measurements within a train, and to forward the information over a satellite (Inmarsat BGAN) or terrestrial link (proprietary Machine-to-Machine, M2M, system provided by Vodafone).

It contains all the elements shown in Figure 4.13: (i) BGAN system composed of a terminal and of an auto-pointing antenna, (ii) Integrated Services Router for GSM/3G and connectivity between the different components, (iii) GNSS Receiver, and (iv) Laptop used as processing platform for configuration and management.

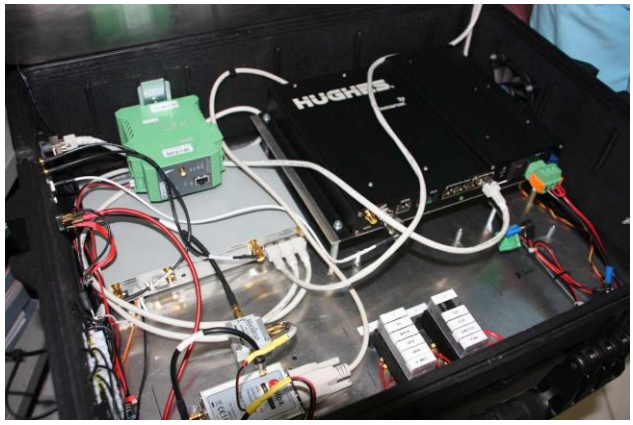

Figure 4.13 Interior of the 3InSat communication unit

From the initial configuration above described, only the satellite backhauling part was retrieved and the following subcomponents are added:

- GSM/3G/4G modem (client of terrestrial networks),
- WLAN router (Ethernet router),
- Single Board Computer (processing platform), and
- Coordinator Node (information depository).

The WLAN router aims to interconnect the subcomponents of the WAN Unit, which are connected to the central node of the network via Ethernet. Therefore, the router have a switch with four ports. Since the information relayed by the unit represents rather low volumes and is transferred with few kbps, the Ethernet rate can be at 100Mbps.

In this way, the unit can be connected at IP broadband speeds of up to 464kbps or using the BGAN terminal (Figure 4.14). The Hughes 9450-C11 terminal is fully approved for operation on Inmarsat's BGAN satellite service, and provides also high performance on the move connectivity for the most demanding environments.

Figure 4.14 Inmarsat BGAN mobile terminal

As shown in Figure 4.14, the system is from Hughes and is identified by its model number 9450. It is composed of a satellite terminal (User Terminal, UT) and of an auto-pointing antenna. Both are interconnected and operate autonomously. The UT offers in addition: four Ethernet featuring PoE (Power over Ethernet), two RJ11 ports for telephone or fax, ISDN port, and Wi-Fi. Table 4.7 reports all the terminal specification.

Table 4.7 Hughes 9450-C11 terminal specifications

Features	Description
BGAN	Up to 492 kbps.
Ethernet ports	4x RJ45 with PoE
RJ11 ports	2x: one for telephone, one for fax
ISDN port	1x
Wi-Fi	Yes, 802.11b/g, WEP security
GPS	Yes, integrated in the antenna unit
Performance	QoS selectable: 32 kbps, 64 kbps, or 128 kbps (11 simultaneous sessions)
Power supply	12V or 24V
Consumption	32W idle / 65W max (no PoE)
Dimensions / Weight	281x234x46 mm / 2.3 kg
Environment	95% relative humidity at 40°C

At last, flexible options are available for the installation on any type of vehicles. The mini-antenna may be permanently mounted for the fleet-style installation or the optional magnetic roof mount can be used for rapid installation and removal.

4.2 Functional procedures

The proposed wireless network makes use of low power consumption, small size, and fast working systems such as the Raspberry Pi (RasPi). This device is a credit card-sized single board computer developed in the UK by the Raspberry Pi Foundation with the intention of promoting the teaching of basic computer science in schools.

The Raspberry Pi 2 is based on the Broadcom BCM2835 SoC, which includes an ARM1176JZF-S 700 MHz processor, VideoCore IV GPU and is shipped with 512MB of RAM. It has a HDMI support and a Micro SD (Secure Digital) card slot for booting up due to lack of BIOS and a persistent memory [33, 34]. Figure 4.15 shows the chosen model with a view of its components.

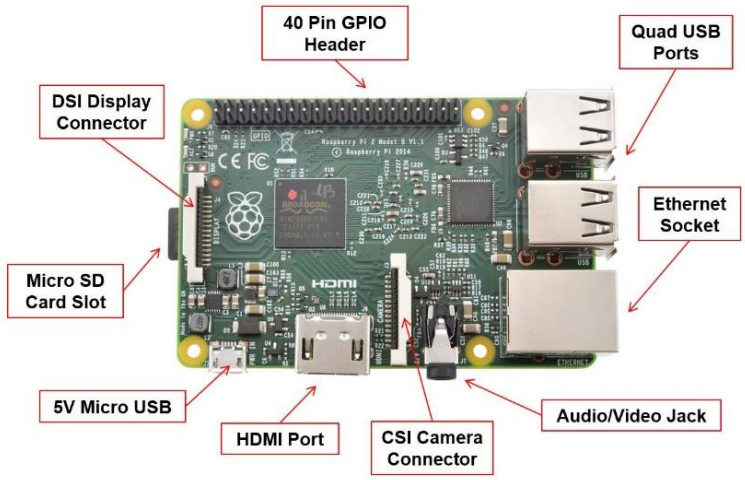

Figure 4.15 Raspberry Pi Model 2

Several tools are available for Python, which is the main programming language of the system. The Foundation provides Debian and Arch Linux ARM distributions for download, but Raspbian Wheezy has been customized to run on the Pi [35].

Raspbian is a Debian based Operating System (OS) launched on July 2012. In particular, it is an unofficial port of Debian wheezy ARMHF (ARM Hard Float), which is an ARM architecture coupled with hardware support for VFP (Vector Floating Point). This addition make fast the processes that require the use of floating point calculations, and can perform advance instructions processing contained in the ARMv6 architecture.

4.2.1 Communication protocol

The NMEA protocol is the way to transmit the information collected by the GPS receiver. The message is a string of comma-delimited text and it includes:

- an identifier to distinguish it from other messages in the data stream,
- one or more fields of data, separated by a comma, and
- a checksum preceded by an asterisk to validate the data.

All sentences in this type of format begin with a dollar signal "$", going on with talker ID code "GP" and message ID code. Data fields follow comma delimiters, although they do not contain information, and an asterisk with a checksum value follow the last one ending with a carriage return and a line feed.

The checksum is calculated from all characters in the message including commas, but not including dollar signal and asterisk delimiters. The hexadecimal result is converted to two ASCII characters (0–9, A–F) and the most significant appears first.

In the cases under study, the required strings are: (i) GGA (GPS Fix Data) that contains time and position, (ii) RMC (Recommended Minimum Specific GPS Data) to identify the SOG (Speed Over Ground), and (iii) GST (GPS PRN) for the RAIM (Receiver Autonomous Integrity Monitoring) of that position. They structure is expressed as:

$$\$GPGGA, 151924{,}3723.454444, N, 12202.269777, E, \\ 2{,}09{,}1.9{,}17.49, M, 25.67, M, 1{,}0000 * 57 \tag{4.1}$$

$$\$GPRMC, 123519, A, 4807.038, N, 01131.000, E, \\ 022.4{,}084.4{,}230394{,}003.1, W * 6A \tag{4.2}$$

$$\$GPGST, 172814.0{,}0.006{,}0.023{,}0.020{,}273.6, \\ 0.023{,}0.020{,}0.031 * 6A \tag{4.3}$$

In Table 4.8, the meaning of the GGA message fields is reported in detail.

Table 4.8 NMEA-0183 GGA message fields

Field	Meaning
0	Message ID $GPGGA
1	UTC of position fix
2	Latitude
3	Direction of latitude (N: North, S: South)
4	Longitude
5	Direction of longitude (E: East, W: West)
6	GPS Quality indicator
7	Number of SVs in use, (range 00-24+)
8	HDOP
9	Orthometric height (MSL reference)
10	Unit of measure for orthometric height (meters)
11	Geoid separation
12	Unit of measure for geoid separation (meters)
13	Age of differential GPS data record (Type 1 or 9)
14	Reference station ID (range 0000-4095)
15	The checksum data, always begins with *

After that NMEA-0183 output is enabled, a subset of these messages is sent to the data collector (RasPi) connected to the receiver serial ports. The output data transmission is provided by an USB interface, which is fully compatible with the Pi input ports.

4.3 Software implementation

The GPS device is set to provide a GGA string per sec in the NMEA-0183 format. It is connected to the first data collector (RasPi_I) by a USB link. A second USB interface host the ZigBee Sensor that transfer the data to the ZigBee Coordinator and from here to the second data collector (RasPi_II), where a text file save the strings. Any of the steps listed above requires a specific software. As RasPi_I is switched on, the following commands are executed:

```
import serial, itertools, os
from time import strftime, gmtime, sleep
```

The software imports first the libraries of the Python language. They are: (i) *os* necessary to access the File System, (ii) *itertools* to manage the counters, (iii) *serial* which drives the serial communication, and (iv) *time* to access the system clock. Some constants (baud-rate and buffer-size) are then assigned to fix a file whose name comes with date and time.

```
control = "^"
master = "/dev/master"
ellipse = "/dev/ellipse"
#master = "COM5"
#ellipse = "COM4"
baud = 38400
bufferSize = 100

def getFileNameWithTimestamp():
    return "data_" + strftime("%Y-%m-%d %H-%M-%S", gmtime()) +
".txt"
```

The next step is referred to the RasPi_II and sees as input the file name, starts the device and collects the received information in an array of suitable size:

```
def getFileName(name):
    def increment_filename(fn):
        fn, extension = os.path.splitext(name)
        n = 1
        yield fn + extension
        for n in itertools.count(start=1, step=1):
            yield '%s%d%s' % (fn, n, extension)

    for filename in increment_filename(name):
        if not os.path.exists(filename):
            return filename
```

The array elements are sent one by one to the ZigBee with a control character ending the transfer:

```
def check():
    _assertConnection()
    while 1:
        data = ser_in.read(1)
        if(data == control):
            read()
```

This method appends what it reads to a new string through the “save” function, but only if such string does not exceed the buffer’s length:

```
def read():
    _assertConnection()
    string = ""
    while 1:
        if(len(string) > length):
            check()
            break
        elif (len(string) == length):
            save(string)
            print(string)
        string += ser_in.read(1)
```

At last, it opens a file and appends a string to it. Finally the file is closed:

```
def save(string):
    file_out = open(filename, "ab")
    file_out.write(strftime("%Y-%m-%d %H-%M-%S", gmtime()) + "\t"
+ string)
    file_out.close()

filename = getFileName("data.txt")
print("Data will be written to: " + filename)
print("LISTENING: ")
check()
```

In Appendix A, a full version of sending and receiving codes is provided to show all the operations of the wireless data acquisition software implemented in Python language.

4.4 References

[1] Faravelli, L. & Chen, Z-C. 2009. Time Issues in a Wireless Network. Proceedings of 15th International Workshop on Dynamics and Control (CIMNE), Barcelona, Spain.

[2] Casciati, S., Faravelli, L. & Chen, Z-C. 2009. A design of multichannel wireless sensing system for structural monitoring. Proceedings of the ECCOMAS Thematic Conference on Computational Methods in Structural Dynamics and Earthquake Engineering. Rhodes, Greece.

[3] Casciati, S., Faravelli, L. & Chen, Z-C. 2009. Design of a Multichannel Real-time Wireless Connection System for Analog Cable Replacement Application. Proceedings of 7th International Workshop on Structural Health Monitoring, Stanford, USA.

[4] Casciati, S., Faravelli, L. & Chen, Z-C. 2010. A multi-channel wireless transmission system for structural monitoring. Proceedings of 4th International Conference on Structural Engineering, Mechanics and Computation, Cape Town, South Africa.

[5] Casciati, S., Faravelli, L. & Chen, Z-C. 2010. A Real-time Multichannel Wireless Sensing Network for Structural Monitoring Applications. Proceedings of 10th International Conference on Motion and Vibration Control, Tokyo, Japan.

[6] Casciati, S., Faravelli, L. & Chen, Z-C. 2010. A Real-time Multichannel Wireless Sensing System for Analog Cable Replacement Application. Proceedings of 5th Edition of European Workshop on Structural Health Monitoring. Sorrento, Naples, Italy, 1188-1195.

[7] Casciati, S., Faravelli, L. & Chen, Z-C. 2010. Frequency Division Multiplexing Wireless Connection. Proceedings of 6th International Conference on Wireless Communications, Networking and Mobile Computing, Chengdu, China.

[8] Chen, Z-C. 2014. Energy efficiency strategy for a general real-time wireless sensor platform. Smart Structures and Systems, 14(4), 617-641.

[9] Casciati, F., Casciati, S., Fuggini, C., Faravelli, L., Tesfai, I. & Vece, M. 2016. Framing a Satellite Based Asset Tracking (SPARTACUS) within Smart City Technology. Journal of Smart Cities, in press.

[10] Casciati, F., Casciati, S., Faravelli, L., Ramponi, A. & Vece, M. 2015. Wireless Communication: from a GPS Sensor to a Credit-Card Sized Computer.

Proceedings of SHMII 2015, 7th International Conference on Structural Health Monitoring of Intelligent Infrastructure, Turin, Italy.

[11] Guinamard, A. 2014. Ellipse AHRS & INS - High Performance, Miniature Inertial Sensors User Manual, SBG Systems, France.

[12] Trimble. 2004. NMEA-0183 Messages Guide for AgGPS Receivers. USA, Trimble Navigation Limited.

[13] Casciati, F., Casciati, S., Faravelli, L. & Vece, M. 2016. Investigating the Performance of OEM Devices for Structural Monitoring. Proceedings of EWSHM 2016, 8th European Workshop on Structural Health Monitoring, Bilbao, Spain.

[14] McLellan, J.F. & Battie, J.P. 1994. Testing and Analysis of OEM GPS Sensor Boards for AVL Applications. Pulsearch Navigation Systems Inc.

[15] Alkan, R.M. & Öcalan, T. 2013. Usability of the GPS Precise Point Positioning Technique in Marine Applications. Journal of Navigation, 66, 579-588.

[16] Trimble 147A High Resolution Accelerometer. 2016. USA, Trimble Navigation Limited.

[17] CXL-LF Series - High Sensitivity Accelerometers. 2016. USA, Crossbow Technology Inc.

[18] Lynch, J.P. 2006. A Summary Review of Wireless Sensors and Sensor Networks for Structural Health Monitoring. The Shock and Vibration Digest, 38(2), 91-128.

[19] Lynch, J.P., Wang, Y., Swartz, R.A., Lu, K.C. & Loh, C.H. 2008. Implementation of a closed-loop structural control system using wireless sensor networks. Structural Control and Health Monitoring, 15(4), 518-539.

[20] Wang, Y., Lynch, J.P. & Law, K.H. 2005. Design of a Low-Power Wireless Structural Monitoring System for Collaborative Computational Algorithms. Proceedings of SPIE 12th Annual International Symposium on Smart Structures and Materials, San Diego, CA.

[21] Trimble R10 GNSS System. 2016. USA, Trimble Navigation Limited.

[22] Lechner, W. & Baumann, S. 2000. Global navigation satellite systems. Computers and Electronics in Agriculture, 25(1), 67-85.

[23] Leick, A. 1995. GPS Satellite Surveying - Second Edition. USA, John Wiley & Sons, Inc.

[24] Parkinson, B.W., Spilker J.J. Jr, Axelrad, P. & Enge P. 1996. Global Positioning System, Volume I. USA, American Institute of Aeronautics and Astronautics, Inc.

[25] Odijk, D., Nadarajah, N., Zaminpardaz, S. & Teunissen, P.J.G. 2016. GPS, Galileo, QZSS and IRNSS differential ISBs: estimation and application. GPS solutions, ISSN 1080-5370.

[26] Quan, Y., Lau, L., Roberts, G.W. & Meng, X. 2016. Measurement Signal Quality Assessment on All Available and New Signals of Multi-GNSS (GPS, GLONASS, Galileo, BDS, and QZSS) with Real Data. Journal of Navigation, 69(2), 313-334.

[27] Vittuari, L., Gottardi, G. & Tini, M.A. 2015. Monumentations of control points for the measurement of soil vertical movements and their interactions with ground water contents. Geomatics, Natural Hazards and Risk, 6(5–7),439-453.

[28] Zanutta, A., Vittuari, L. & Gandolfi, S. 2008. Geodetic GPS-based analysis of recent crustal motions in Victoria Land (Antarctica). Global and Planetary Change, 62(1), 115–131.

[29] Abbondanza, C., Altamimi, Z., Sarti, P., Negusini, M. & Vittuari, L. 2009. Local effects of redundant terrestrial and GPS-based tie vectors in ITRF-like combinations. Journal of Geodesy, 83(1), 1031-1040.

[30] Fuggini, C. 2010. Using Satellites Systems for Structural Monitoring: Accuracy, Uncertainty and Reliability. Ph.D. Dissertation, University of Pavia, Italy.

[31] Casciati, F., Casciati, S., Chen, Z-C., Faravelli, L. & Vece, M. 2014. Development of a Reliable Wireless GNSS Sensor Network. Proceedings of EWSHM 2014, 7th European Workshop on Structural Health Monitoring, Nantes, France.

[32] 3InSat, Train Integrated Safety Satellite System. 2014. ESA Project: Contract 4000105788/12NL/NR.

[33] Schmidt, M. 2012. Raspberry Pi. A Quick Start Guide. Dallas, Texas: The Pragmatic Bookshelf.

[34] Sahani, M., Rout, S.K., Sharan, A.K. & Dutta, S. 2014. Real Time Color Image Enhancement with a high regard for restoration of skin color by using Raspberry Pi. Proceedings of International Conference on Communication and Signal Processing, 335-339.

[35] Sari, A.C., Rahayu, A. & Budiharto, W. 2015. Developing Information System of Attendance and Facebook Status for Binus University's Lecturer Using Raspberry Pi Architecture. Procedia Computer Science, 59, 178-187.

Chapter 5 Performance assessment

In this chapter, the results of three different experimental campaign are presented. The first section addresses the tests carried out in laboratory in order to validate the performance of the wireless data acquisition system. The second part took place in a train maintenance yard, and it was focused on the satellite transmission of positioning data from a railway convoy.

The data lost during the transmission and the power demand of the system are investigated. In particular, the satellite communication is checked at the railway site of Barrow Hill, near Chesterfield (UK). The specialty test-bed is exploited to evaluate the system behavior when the message has to be forwarded from the Coordinator Node to the WAN Unit, enabling the satellite broadcast to reach a remote center.

At last, all the equipment has been applied to the real monitoring scenario of the "Tesa" footbridge, located in Farra d'Alpago (Italy), where the Kalman filter-based data fusion is used to show how the GPS positioning can offer a more accurate response if coupled with the displacements achieved from a three-axial accelerometer.

5.1 Wireless data acquisition testing

Laboratory tests are here analyzed from the point of view of wireless link quality. Two aspects are worth being discussed: data packet loss, in term of PPR (Packet Reception Rate), and energy consumption. The data loss issue is addressed by a reliable communication method with a character checking mechanism. This type of approach is adopted to avoid data loss and sentence duplication as well.

After acquiring a NMEA string from the GPS sensor, the RasPi_I will send each single character of the GGA (GPS Fix Data) message to the RasPi_II within the time window of a second. If the message is checked to be correct by the character control, it is regarded as having been successfully transmitted. Otherwise, the Sensor Node will retransmit the sentence to the Coordinator Node (Figure 5.1).

Since the RasPi_I continues to acquire a new string every second from the GPS sensor, this procedure may cause a delay in the final collection of the transmitted data. To avoid this problem, the "corrupt" strings are send with a period (0.1s) less than the sampling of

the system ($\Delta t = 1s$). In this way, the next operation can be performed without changing the software behavior. Each sentence is also marked by a sequence number, which reports the date and the acquisition time.

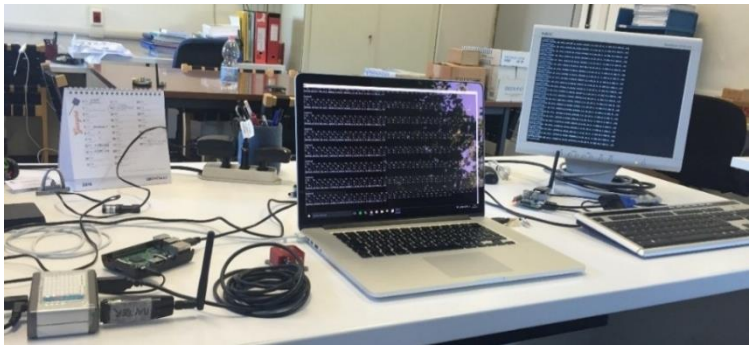

Figure 5.1 Laboratory tests to check the wireless transmission

Figure 4.1 shows the data acquisition testing carried out in the laboratory of Pavia (DICAr). After the development of the proposed data acquisition system, some tests were performed to check if the data loss is acceptable and are summarized in Table 5.1.

Table 5.1 The PRR values for the laboratory tests

Id	UTC Time (hh:mm:ss)		Length (mm:ss)	NMEA strings (n)	PPR (%)
	Start	End			
T01	12:01:09	12:09:27	08:16	499	99,80
T02	12:27:44	12:34:14	06:58	392	99,74
T03	12:35:05	12:43:22	08:17	499	99,80
T04	12:43:57	12:46:35	02:38	159	99,37
T05	12:47:00	12:55:17	08:17	499	99,80
T06	12:55:53	13:04:10	08:17	499	99,80
T07	13:05:23	13:13:40	08:17	499	99,80
T08	13:15:15	13:19:54	04:39	281	99,64
T09	13:20:17	13:28:34	08:17	499	99,80
T10	13:29:24	13:33:48	04:24	266	99,62

The PRR (Packet Reception Rate) is defined as the number of successfully received data packets divided by the number of actually transmitted data ones. In Table 5.1, its value is expressed in percentage. The three-dimensional graph of Figure 5.2 compares the percentage of NMEA strings transmitted (blue) and those received (orange) by the Coordinator Node via ZigBee.

It is worth noting that the antenna setup greatly affects the radio communication. As listed in Table 5.1, the PRR of the wireless data acquisition system is almost 100% because the antenna of the Sensor Node was elevated to the same height of the Coordinator.

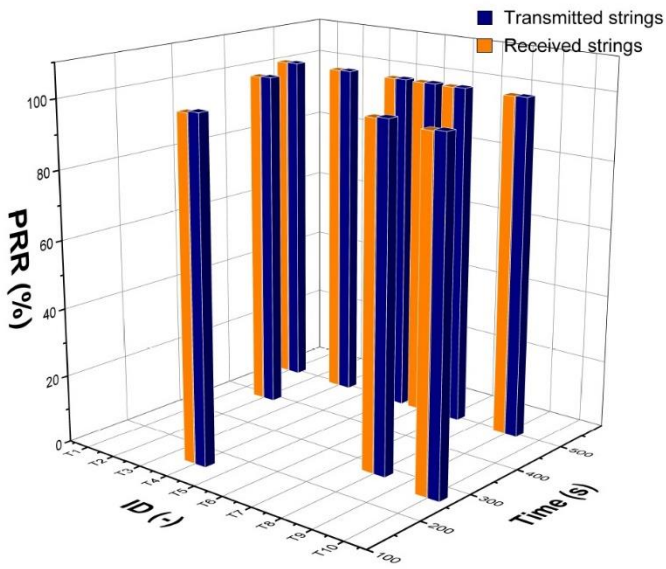

Figure 5.2 A three-dimensional graph of the NMEA string transmitted (blue) and received (orange) during the tests

The wireless data acquisition system adopts omnidirectional antennas with a high gain of 5.4dBi, but the communication range can be extended. However, a higher gain will lead to a narrower beam width and a higher directivity, since the radiation power is concentrated on the main lobe. Therefore, all the device antennas have to be set up in such as a way that their main lobes are of the same plane in order to minimize the path loss of the radio signal channel.

The RasPi is powered at 4.94V and the power consumption, when receiver and wireless device are powered on, is almost 400mA. Therefore, an external battery of 10Ah

(ROMOSS Sailing 5), which delivers 5V and 2000mA of current output, is used to provide an autonomy of 24 hours [1].

5.2 Examples of satellite communication

The FP7 European Union project named SPARTACUS (Satellite Based Asset Tracking for Supporting Emergency Management in Crisis Operation) is motivated by the ambition to provide the accurate positioning of trains, goods and people during emergencies [2]. Any kind of information has to be convoyed locally and relayed to a remote-site area in dissimilar ways, because the existing networks can be damaged, overloaded or failed.

Currently, communications based on radio interfaces are adopted for different purposes, the specific features depending on the application and the environment.

Therefore, one challenge of the project consists in identifying which mean of communication is useful to pursue the above-described target, and how they should be implemented with the other components.

The experimental activity summarized in this section is focused on the assessment of the value of academic efforts to design the tracking and collecting units. The positioning accuracy, including the correctness of the transmitted messages, is also investigated to ensure the capabilities of those units.

The proposed solution is based on satellite technologies that can be used in the tracking of critical assets as containers transporting goods. The problem is that they can be unavailable in harsh environments, such as urban locations with high density of trees or, of course, tunnels.

First, the project motivations are clarified and, after that, the governing relations of the rail transportation are detailed to explain the difference of the adopted models. Finally, the results of the functional test carried out at the Barrow Hill site are presented to emphasize the accuracy and the reliability of the entire system.

5.2.1 Overall framework

The system architecture of the proposed solution is addressed to three different application areas as described in detail by some recent papers achieved within the project SPARTACUS [3-5]. It is designed to manage every demands on-site, near emergency places and tracked entities. Moreover, the implementation includes local and remote communications that are used for the best real time display and the direct situation awareness [6].

Figure 5.3 shows a graphical representation of functionalities and technical specifications regarding positioning, data acquisition and communication units. The SPARTACUS Tracking Units (STrackUs) are connected with a low-power communication to the SColU (SPARTACUS Collecting Unit) placed into the locomotive or the front truck [7].

Finally, the SColU is linked (via Ethernet) to the SPARTACUS Communication Unit (SComU) of the locomotive. It can transmit the collected data by terrestrial or satellite networks to the control center (and to the nearest train station) for the best management of rescue operations in case of disaster.

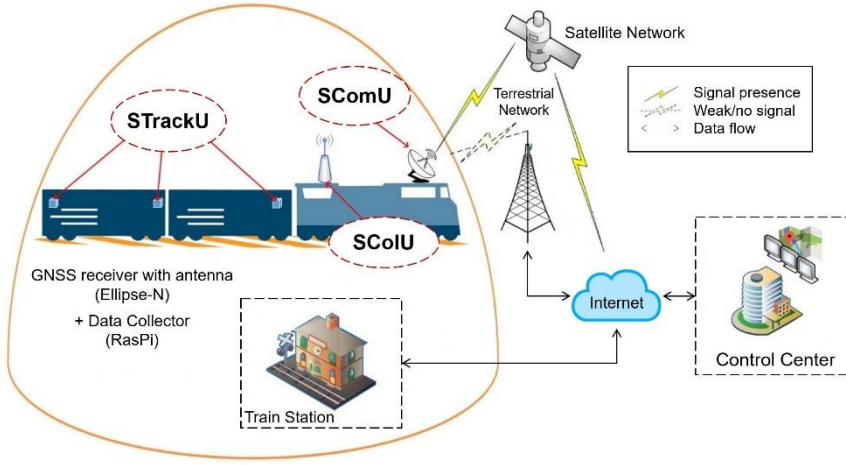

Figure 5.3 SPARTACUS architecture for the transport application (Courtesy of D'Appolonia)

Freight trains are generally made by a locomotive, some wagons and many containers. Since their owners may be different within the convoy, the STrackU is equipped with an identification code and an internal position recording for each of them. In this way, a precise positioning and timing of all components can be offered to each stakeholder in a railway ecosystem for analysis or additional verifications.

Due to the large number of required units, systems on containers and wagons need to show affordable prices, while the STrackU installed on the locomotive could be more expensive. Thus, the costs also determine the hardware and software performance: medium positioning precision with low energy consumption is assigned to containers and wagons, and high precision with high power consumption is reserved to the locomotive.

Power supplies are different for each railway component as well. A standalone device with batteries that guarantee at least 24h working time is conceived for the secondary elements and a suitable power for some hours on the train head (STrackU and SColU).

5.2.2 Governing relations

The adopted software functionalities are divided in lower and upper level functions. The lower level function uses the data coming from the low-cost sensors to estimate their medium level positioning. The upper level function integrates this information with that coming from further devices in order to provide a high accuracy position for each sensor. The adopted devices are also known as INS (Inertial Navigation Systems), and are equipped with an Extended Kalman Filter (EKF). Indeed, these receivers provide noisy measurements that can be fooled by jamming or magnetic interferences [8-10]. When data from an external odometer are available, for instance, the Kalman Filter uses them to correct the current state.

In this way, the motion measurements may be accurate, but this kind of computation suffers from drifts when the integration time becomes long [11]. For this reason, upper level algorithms are proposed to make the devices compliant with the positioning requirements.

In detail, the sequence of the units within the train chain is determined when the convoy is at rest in a station. During this phase, the positioning algorithm implemented in the SColU computes the relative distance between the locomotive and the other units. The data are received by low-power wireless connections (XBee devices) [12].

After that, the rough position of each unit is refined by the SColU and the relative position between two consecutive units is propagated from the locomotive until to the end of the train. When the train comes to another station, the upper level function re-starts from the beginning. These functionalities are designed to work when the GNSS signal is available with the aim of increasing the accuracy performance of the STrackUs.

5.2.2.1 Rail transportation

The upper level positioning algorithms are implemented in order to refine the position information of wagons and containers. They essentially process the data of each tracking units after a merge with the high-cost data of the locomotive.

It provides a better position accuracy when compared with the results achieved for wagons or containers, because the external odometer computes a precise speed measurement by sensing the angular rate of the wheels.

Moreover, the merging is performed by exploiting the geometric and kinematics constraints of the convoy. In particular, geometric constraints are given by the relative position between the vehicles and among the containers as well.

These constraints arise from empirical observations and can be used to reduce the effects of disturbances and to improve the overall positioning accuracy. The units are assumed as mass points, moving along a curve and over a plane. The radius is sufficiently large to assume that the velocity vector is aligned with the longitudinal axis of the wagons. Therefore, heading and course of a single wagon over ground may be considered the same.

The distance between the elements is constant during the trip. A maximum of three containers can be put on board for each wagon. The chained sequence of a rail convoy is shown in Figure 5.4.

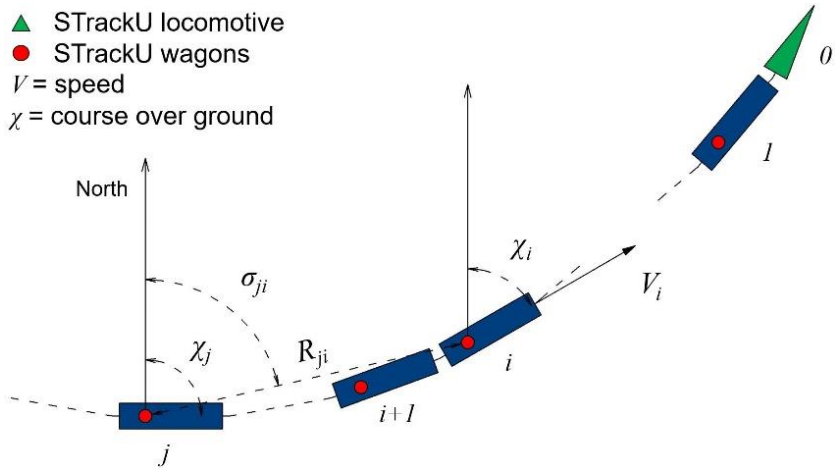

Figure 5.4 Distance (R_{ji}) and angle (σ_{ji}) between the wagons of a freight train for SPARTACUS applications (Courtesy of UNIBO)

The upper level algorithms are designed in a different way for wagons and containers. Each of them consists of two phases depending on being the train at rest or in motion. To detect the current status, the speed of the locomotive is monitored. If it is lower than the threshold of 2.78m/s, the train is assumed to be at rest.

In addition, a mathematical model describing the kinematics of the system is needed and the data merge is performed by the EKF.

Due to the similarity of the chained sequence for wagons and containers, the mathematical model is the same and the model is here proposed for the wagon chain. In Figure 5.4, i denotes the i-th STrackU (i = 0, 1…n) where n is the number of wagons and 0 (zero) is used for the locomotive. The kinematics model of the i-th vehicle is expressed by the relations:

$$\dot{N}_i = V_i \cos(\chi_i) \tag{4.1}$$

$$\dot{E}_i = V_i \sin(\chi_i)$$

$$\dot{V}_i = a_{il}$$

$$\dot{\chi}_i = \frac{a_{in}}{V_i}$$

where N_i and E_i are respectively the North and East coordinates of the position, V_i denotes the speed, χ_i is the Course Over Ground (COG), while a_{il}, a_{in} are the accelerations along and transversal to the course. The mathematical model of the kinematics of the relative motion between the *j-th* and *i-th* vehicles is:

$$\dot{R}_{ji} = V_i \cos(\chi_i - \sigma_{ji}) - V_j \cos(\chi_j - \sigma_{ji}) \tag{4.2}$$

$$\dot{\sigma}_{ji} = \frac{V_i \sin(\chi_i - \sigma_{ji}) - V_j \sin(\chi_j - \sigma_{ji})}{R_{ji}}$$

where σ_{ji} is the angle between the North direction and the Line Of Sight (LOS) direction from the j to i vehicle (j > i) and R_{ji} is the relative distance between them (Figure 5.4).

5.2.3 Specialty test-bed

The system assessment, in term of robustness and reliability of the communication links (wireless and satellite) is the goal of the tests carried out in April 2016, at the railway site of Barrow Hill. This locomotive maintenance yard is located near Chesterfield in the United Kingdom [13], and the case study was designed with the collaboration of the Centre for Railway Research (NewRail).

The experimental investigations were carried out in an area of 8.5ha with continuous track of 1200m. The site is divided in three areas due to the maximum speed allowed for each path: (i) Yard Lines at 2.2m/s, (ii) Network Rail Access at 4.4m/s, and (iii) Branch Line at 8.9m/s, as shown in Figure 5.5.

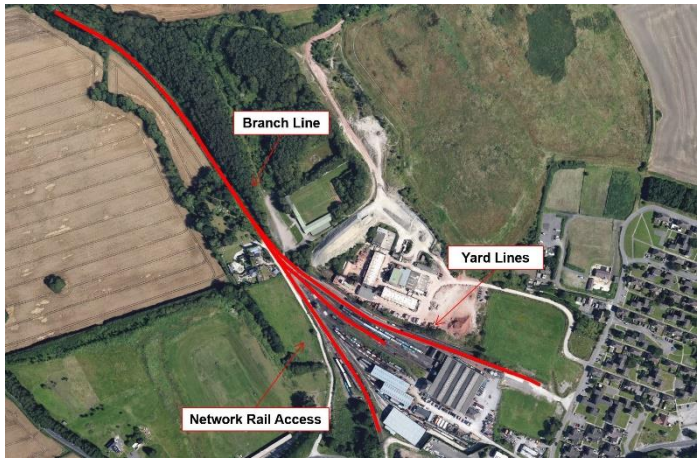

Figure 5.5 Layout of the Barrow Hill site for SPARTACUS applications (Courtesy of UNEW)

The convoy is made by a locomotive, three wagons and one container. Each wagon is equipped with a SPARTACUS Tracking Unit (STrackU), consisting of an inertial sensor (Ellipse-N), a wireless device (ZigBee), and a data collector (RasPi). The container is located on board the last wagon. The STrackUs power is supplied by portable batteries, they are set into a protective box as shown in Figure 5.6.

The desired information is recorded in NMEA format [14]. The sentences are acquired by the developed software of each STrackU, and sent via wireless to the SComU (SPARTACUS Communication Unit), which is placed inside the locomotive (Figure 5.6).

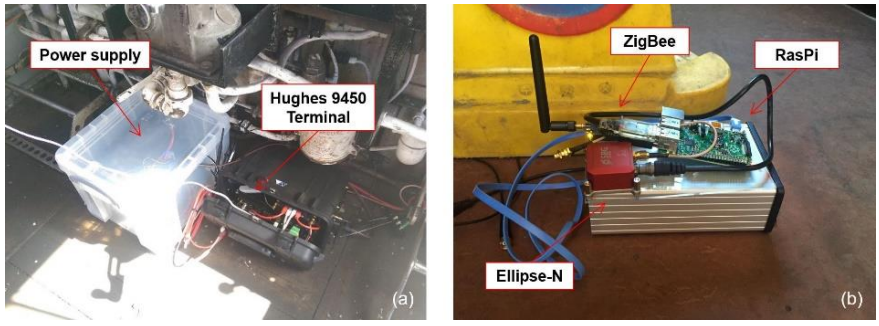

Figure 5.6 Systems on board the locomotive (a) and wagons (b)

The system on board the locomotive (SColU) is conceived to collect the positioning data of each STrackU, and to transmit via satellite the information to a remote center. For this type of application, the position accuracy of each vehicle is aim of the developed system. The case study is reported as a test of the PPR of two types of communication for a freight train in the railway site. First, the ZigBee behavior from a wagon or a container to the head train, and then the transmission, based on a VPN over satellite, of NMEA messages from the locomotive to a remote center. The results are summarized in Table 5.2.

Table 5.2 PRR values achieved during the field tests

Id	UTC Time (hh:mm:ss)		Length (mm:ss)	NMEA strings (n)	PPR (%)
	Start	End			
L1	09:15:01	09:51:05	36:04	2732	100,0
W1	09:37:49	10:37:18	59:29	372	99,46
W2	09:37:47	10:37:16	59:29	373	99,73
W3	09:38:01	10:37:21	59:20	364	98,90
C1	09:37:48	10:37:26	59:38	366	99,45

The first test (L1) is addressed to check the data transmission via satellite of the SComU, while the results labelled W1, W2, W3 and C1 are referred to the wireless communication of the message from wagons/container to the locomotive. In particular, the above listed results were elaborated from the data stored by the software in the last day of measurements. The outcome of this analysis leads to the conclusion that the system behavior is fully performed also when the message has to be forwarded from the data collector (RasPi) to the SComU, enabling the satellite broadcast.

5.3 A bridge application

The use of data fusion based on Kalman filter has become common in literature, especially for the displacement estimation of civil infrastructures [15-18]. Therefore, it is necessary to demonstrate that the result of this scientific approach can be more accurate than the single measurements carried out by accelerometers or GPS receiver.

At the same time, the behavior of existing infrastructures was investigated under wind loads or vibrations induced by people and vehicles [19-27]. It is well known that this type of problems are essential for the structural safety of long-span suspension bridges, but are

also addressed to the comfort of the pedestrians crossing a footbridge [28-36]. For these reason, the case study for the present research activities can be represented by the "Tesa" cable-stayed pedestrian bridge, which is located in Farra d'Alpago not far from Belluno (Italy). Details on this structure are provided in Appendix B, while a general view of the footbridge is shown in Figure 5.7.

Figure 5.7 General view of the "Tesa" footbridge

Overall, 16 steel cables (with a diameter of 44 and 32mm) are employed to support the two main curved GLT beams of rectangular cross-section by 123.8cm. Therefore, the aim of this experimental campaign is to measure the displacements of the footbridge cables carried out with a three-axial accelerometer (147A) and with a GPS receiver (R10), individually. After that, a data fusion between them will be made in order to prove that the proposed method offers the most reliable and accurate response.

In addition, the loads associated to the wind can be regarded as "ambient vibration" or "background noise", and long acquisitions of the cables behavior under hummer blows and "low-wind-velocity" were also collected with the Crossbow CXL01LF3 with the aim to compare the data achieved with those acquired from the Trimble 147A accelerometer.

5.3.1 Boundary conditions

Measuring the displacements of this footbridge cables is not an easy task. The main issue is due to the fact that they can have a considerable inclination, compared to an ideal (horizontal) plan where the devices have to be placed. In particular, the footbridge cables under study has been tilted about of 54° and 33°, as shown in Figure 5.8.

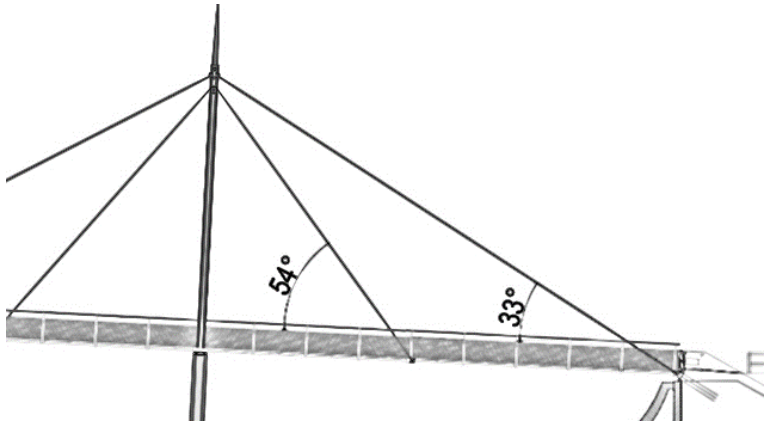

Figure 5.8 Focus on the inclination of the footbridge cables

For this reason, it was exploited a *mounting* system, which was fixed on those cables ensuring to avoid slides and rotations of two devices. The proposed solution was composed by the following components:

- a rectangular plate (thickness of 5mm),
- upper-lower parts for anchoring,
- two type of arms (230 and 340mm),
- screws and bolts for each support.

Concerning the material, it was made prevalently of steel. Since only one pair of supports is directly fastened to the plate, the system offers the possibility to regulate its configuration with two *ad-hoc* arms according to the desired inclination (Figure 5.9).

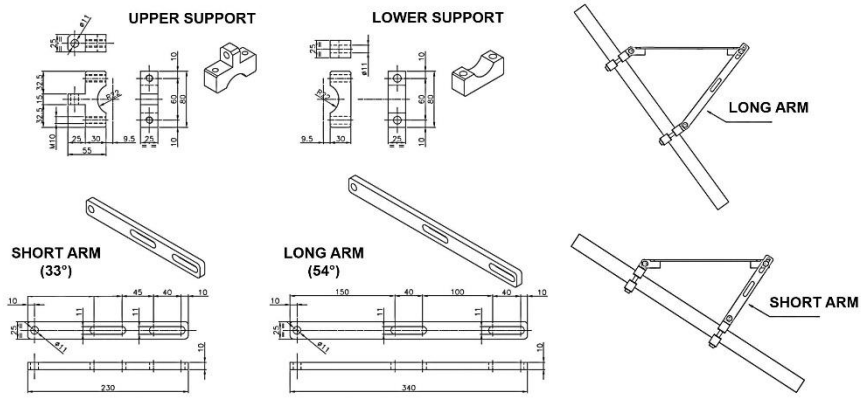

Figure 5.9 Upper-lower supports and short-long arms of the system

The plate surface is also provided with holes to fasten the devices widely described in the previous section (i.e., the 147A accelerometer and the R10 GNSS receiver), but also the potential Single Board Computers that are responsible for the wireless communication. Figure 5.10 shows in which way the final configuration of the system has been designed.

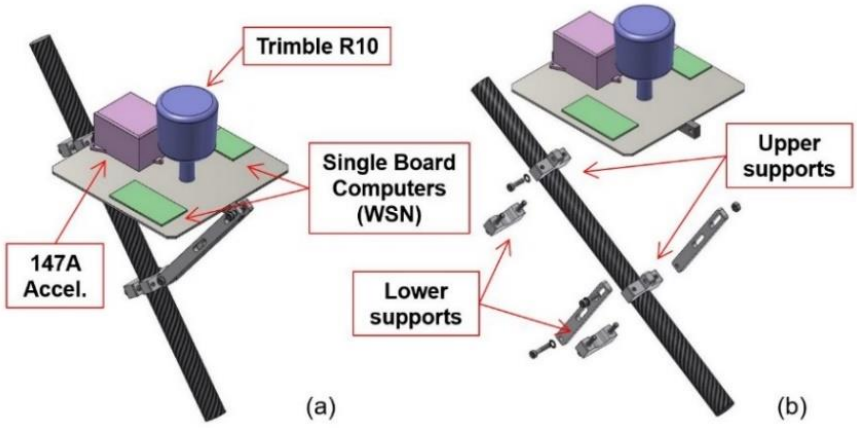

Figure 5.10 System configuration for 54° (a) and 33° solutions (b)

Once the above-described system has been subjected to some laboratory tests, the entire experimental equipment was able to be checked on the real monitoring scenario identified by the "Tesa" footbridge located in the area of Farra d'Alpago.

5.3.2 Experimental campaign

On November 11, 2016 a set of tests were carried out to acquire the cables dynamic response (i.e., the accelerations and the GPS positions of a starting point along them) under different loading conditions. The Base Station was represented by the NET R9 with its geodetic antenna, and the differential corrections were sent to the Rover (i.e., Trimble R10) by RF transmitter supplied by an external battery, as shown in Figure 5.11.

Figure 5.11 Base station with the RF transmitter

The *mounting* system was tailored to the footbridge cable that connects the antenna to the centerline of the deck, while the Crossbow was applied on the opposite cable (Figure 5.12). The 147A was equipped with a data logger, which need to be powered at 12-24V.

Figure 5.12 147A (a) and Crossbow (b) as located on the footbridge cables

The Crossbow data transmission is entrusted to wireless transceivers named WSUs (Wireless Station Units), which was placed over the deck. This technology has been developed in order to cover all the entire span length of the bridge, without the need for the intermediate storage stations. An example of this device is reported in Figure 5.13.

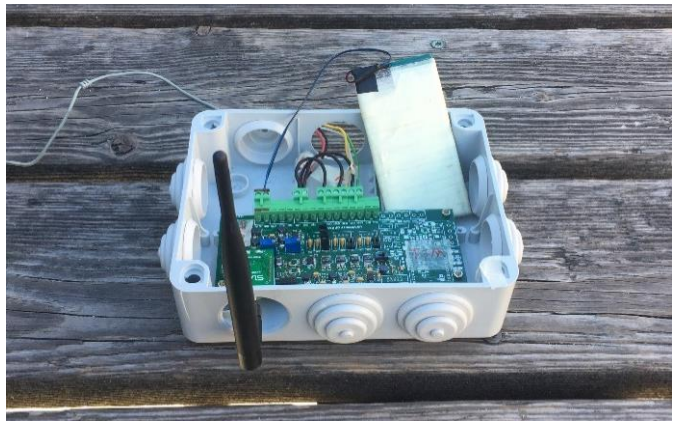

Figure 5.13 WSU employed for the Crossbow data transmission

Four groups of tests are carried out during the experimental campaign:

- "Test A", environmental loads (the bridge location is often interested by strong winds and it was used as "calibration" test for the instrumentations),
- "Test B", walking along the deck (i.e., a round trip of one person is considered),
- "Test C", hummer blows in horizontal directions (Figure 5.14), and

- "Test D", moving the cable by hand to simulate strong winds blasts.

Figure 5.14 A picture from "Test C4"

During the in situ tests, the 147A and the R10 GNSS receiver were always in the same location, while the Crossbow CXL01LF3 was deployed in the following positions:

- for the tests labelled "A" and "B", it was placed over the deck at the centerline of the footbridge, and the Wireless Station Unit was named WSU0,
- for the tests labelled "C" it was alternately anchored to the four cables opposite to the Rover position (WSU1, WSU2, WSU3, and WSU4),
- for the test labelled "D", it was anchored only to the "internal-main" cable (WSU4), as shown in Figure 5.15.

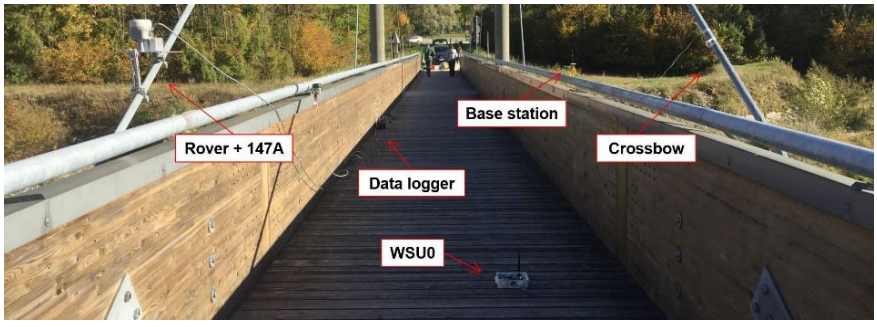

Figure 5.15 Equipment configuration during the *in situ* tests

The accelerations are acquired at 15°C and 13.3°C air temperature and with a sampling frequency of 100Hz in order to compare the data collected by the two devices. An example of the accelerations acquired by the 147A and the WSU1, along the Z-axis for the "Test D", is reported in Figure 5.16 and in Figure 5.17.

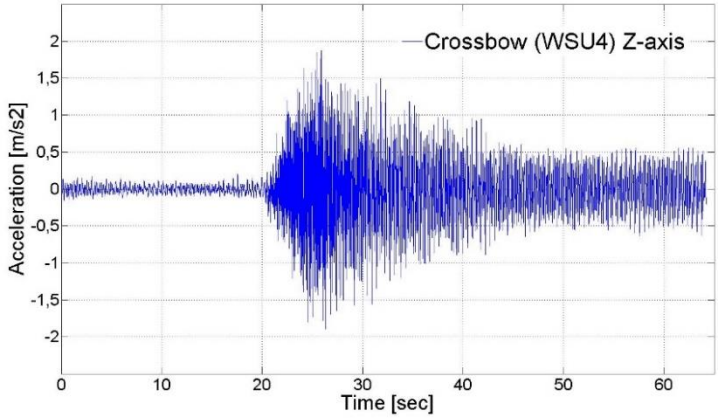

Figure 5.16 "Test D" accelerations along the Z-axis acquired by the WSU4

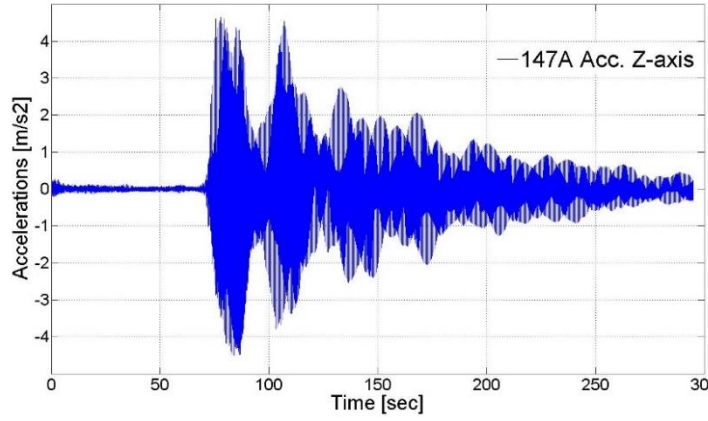

Figure 5.17 "Test D" accelerations along the Z-axis acquired by the 147A

The results has been elaborated using the standard approach proposed by the classical Fast Fourier Transformation (FFT), within the MatLAB environment [1]. The related

acceleration periodograms for the components along the Z-axis are given in Figure 5.18 and Figure 5.19.

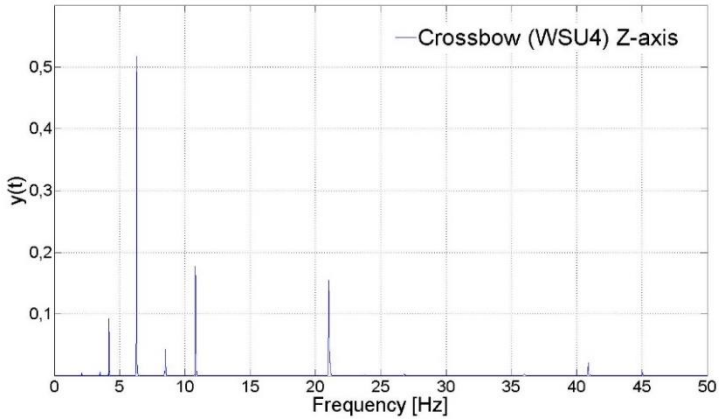

Figure 5.18 Periodograms from the signal of the WSU4: FFT along Z-axis

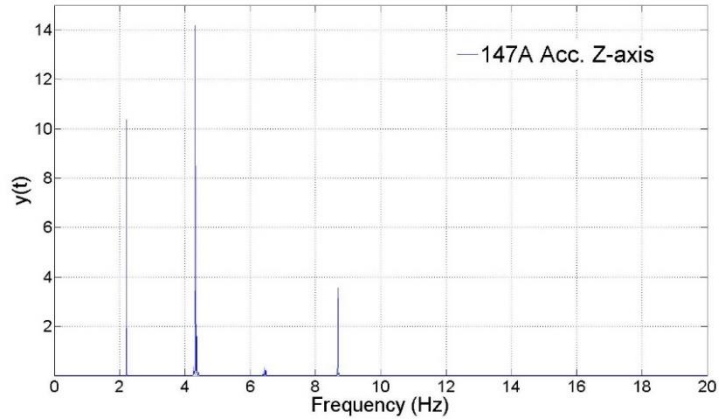

Figure 5.19 Periodograms from the signal of the 147A: FFT along Z-axis

The analysis of the acceleration periodograms shows the same ranges for the frequencies, and the experimental results confirmed the low sensitivity of the cables dynamic response to the temperature variations. The data acquired from the 147A are then integrated two times in order to achieve the displacement of the "internal-main" cable (i.e., Figure 5.20 and Figure 5.21), and it was combined with the positioning data recorded by the GPS

receiver from an ideal starting point (i.e., when the system was still). The data fusion has been made through the Kalman filter described in Chapter 3.

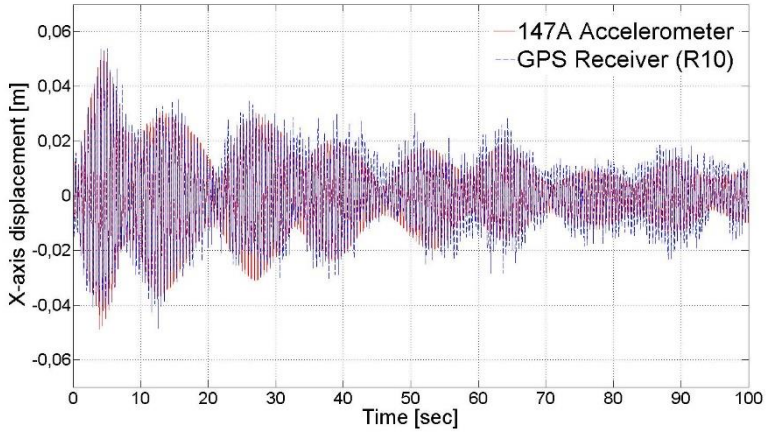

Figure 5.20 Displacement time histories along the X-axis as integrated from the signal of the 147A, and as obtained from the GPS device

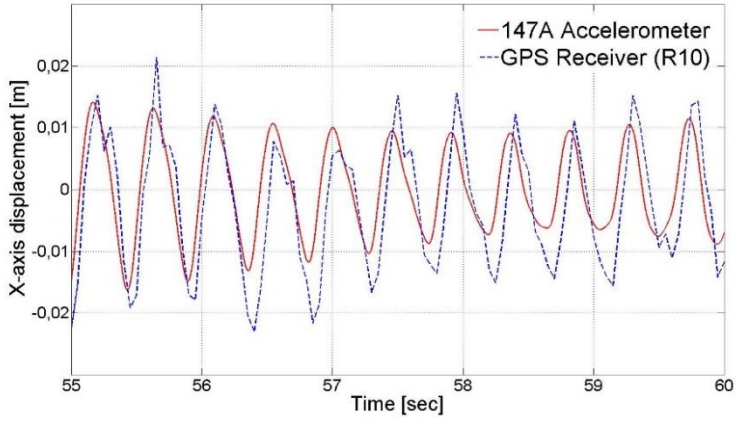

Figure 5.21 Focus on the displacement time histories as integrated from the signal of the 147A, and as obtained from the GPS device

"Test D" is here reported in order to demonstrate how the GPS data may be improved in accuracy if the measurements achieved from a three-axial accelerometer are adopted, as shown in Figure 5.22 and Figure 5.23.

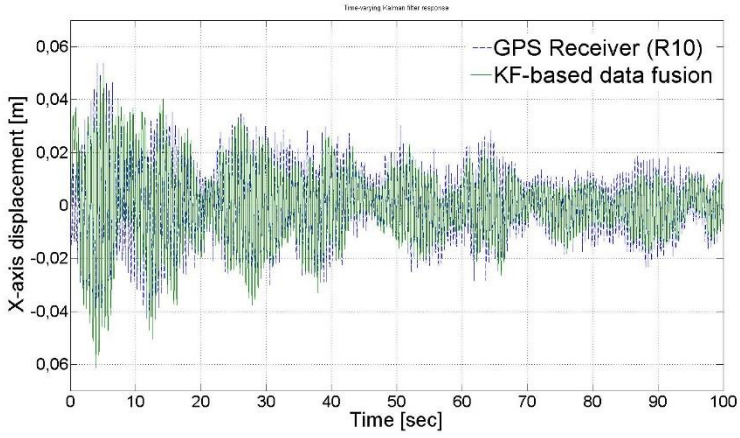

Figure 5.22 Comparison between the displacements along the X-axis recorded by the GPS device before and after the data fusion

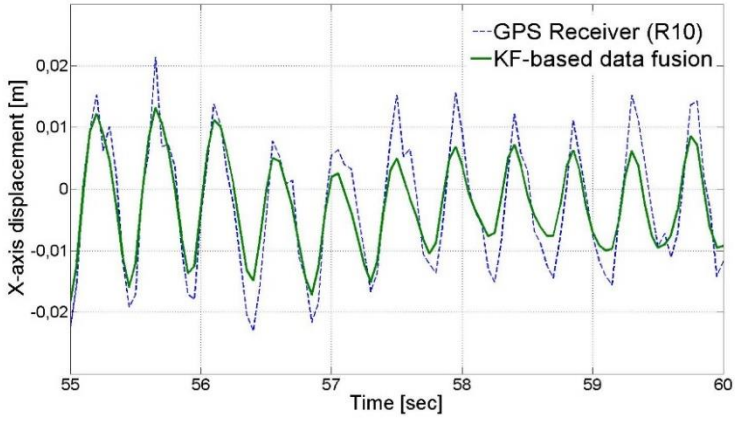

Figure 5.23 Focus on the comparison between the displacements recorded by the GPS device before and after the data fusion

5.4 References

[1] Casciati, S., Chen, Z-C., Faravelli, L. & Vece, M. 2016. Synergy of Monitoring and Security. Smart Structures and Systems, 17(5), 743-751.

[2] Spartacus Project, Satellite Based Asset Tracking for Supporting Emergency Management in Crisis Operations (SPARTACUS), ‹http://www.spartacus-project.eu/home› (2016).

[3] Fuggini, C. & Tesfai, I. 2016. SPARTACUS: Enabling Space Technologies in Security Research. Proceedings of 5th International Conference on Smart and Multifunctional Materials, Structures and Systems (CIMTEC 2016), Perugia, Italy.

[4] L. Vittuari, L., Pavkovic, B., Guinamard, A., Casciati, F., Zanzi, M., Ghetti, A., Berbakov, L. & Vece M. 2016. SPARTACUS: Positioning Units for Critical Asset Tracking and Emergency Management. Proceedings of 5th International Conference on Smart and Multifunctional Materials, Structures and Systems (CIMTEC 2016), Perugia, Italy.

[5] Ghetti, A., Vittuari, L. & Zanzi, M. 2016. Satellite and Inertial Navigation Solution in Crises Management Operation for First Responders Applications. Proceedings of 5th International Conference on Smart and Multifunctional Materials, Structures and Systems (CIMTEC 2016), Perugia, Italy.

[6] Casciati, F., Casciati, S., Faravelli, L. & Vece, M. 2016. A Satellite and Inertial Navigation Solution in Crises Management Operation for Transport and Relief Goods Application. Proceedings of 5th International Conference on Smart and Multifunctional Materials, Structures and Systems (CIMTEC 2016), Perugia, Italy.

[7] Casciati, F., Casciati, S., Chen, Z-C., Faravelli, L. & Vece, M. 2014. Development of a Reliable Wireless GNSS Sensor Network. Proceedings of 7th European Workshop on Structural Health Monitoring (EWSHM 2014), Nantes, France.

[8] Fuggini, C. 2016. Using Satellites Systems for Structural Monitoring: Accuracy, Uncertainty and Reliability. Ph.D. Dissertation, University of Pavia.

[9] Zanutta, A., Vittuari, L. & Gandolfi, S. 2008. Geodetic GPS-based analysis of recent crustal motions in Victoria Land (Antarctica). Global and Planetary Change, 62, 115-131.

[10] Abbondanza, C., Altamimi, Z., Sarti, P., Negusini, M. & Vittuari, L. 2009. Local effects of redundant terrestrial and GPS-based tie vectors in ITRF-like combinations. Journal of Geodesy, 83, 1031-1040.

[11] Guinamard, A. 2014. Ellipse AHRS & INS - High Performance, Miniature Inertial Sensors User Manual, SBG Systems, France.

[12] Texas Instruments. CC2530 Software Examples User's Guide, Texas Instruments Incorporated, Dallas, Texas, USA (2009).

[13] Casciati, F., Casciati, S., Faravelli, L. & Vece, M. 2016. Implementation of Communication, Collection and Tracking Units in Crisis Operation. Proceedings of 8th European Workshop on Structural Health Monitoring (EWSHM 2016), Bilbao, Spain.

[14] Trimble. 2004. NMEA-0183 Messages Guide for AgGPS Receivers. USA, Trimble Navigation Limited.

[15] Caron, F., Duflos, E., Pomorski, D. & Vanheeghe, P. 2006. GPS/IMU data fusion using multisensor Kalman filtering: Introduction of contextual aspects. Information Fusion, 7(2), 221-230.

[16] Smyth, A. & Wu, M. 2007. Multi-rate Kalman filtering for the data fusion of displacement and acceleration response measurements in dynamic system monitoring. Mechanical Systems and Signal Processing, 21, 706-723.

[17] Zhou, Z. 2011. GPS navigation data fusion using composed correcting Kalman filtering method. Journal of Computational Information Systems, 7(6), 2006-2012.

[18] Chatzi E-N. & Fuggini, C. 2012. Structural identification of a super-tall tower by GPS and accelerometer data fusion using a multi-rate Kalman filter. Proceedings of 3rd International Symposium on Life-Cycle Civil Engineering (IALCCE 2012), 144-151.

[19] Remennikov, A.M. & Kaewunruen, S. 2008. A review of loading conditions for railway track structures due to train and track vertical interaction. Structural Control and Health Monitoring, 15(2), 207-234.

[20] Wang, S-Q., Xia, H., Guo, W-W. & Du, X-T. 2013. Coupling vibration analysis of wind-train-bridge system considering geometric nonlinearity of bridge. Gongcheng Lixue/Engineering Mechanics, 30(4), 122-128.

[21] Reichenbach, M., Fasl, J., Samaras, V.A., Helwig, T. & Lindenberg, R. 2012. Evaluating vehicular-induced bridge vibrations for energy harvesting

applications. Proceedings of the International Society for Optical Engineering (SPIE), 8347(83472E).

[22] Cunha, A., Caetano, E., Magalhães, F. & Moutinho, C. 2013. Recent perspectives in dynamic testing and monitoring of bridges. Structural Control and Health Monitoring, 20(6), 853-877.

[23] Xing, C., Wang, H., Li, A. & Xu, Y. 2014. Study on wind-induced vibration control of a long-span cable-stayed bridge using TMD-type counterweight. Journal of Bridge Engineering. 19(1), 141-148.

[24] Li, H., Zhang, F. & Jin, Y. 2014. Real-time identification of time-varying tension in stay cables by monitoring cable transversal acceleration. Structural Control and Health Monitoring, 21(7), 1100-1117.

[25] Argentini, T., Rocchi, D. & Zasso, A. 2015. Aerodynamic interference and vortex-induced vibrations on parallel bridges: The Ewijk Bridge during different stages of refurbishment. Journal of Wind Engineering and Industrial Aerodynamics, 147, 276-282.

[26] Domaneschi, M., Martinelli, L. & Po, E. 2015. Control of wind buffeting vibrations in a suspension bridge by TMD: Hybridization and robustness issues. Computers and Structures, 155(5368), 3-17.

[27] Weber, F. & Distl, H. 2015. Amplitude and frequency independent cable damping of Sutong Bridge and Russky Bridge by magnetorheological dampers. Structural Control and Health Monitoring, 22(2), 237-254.

[28] Caetano, E. & Cunha, A. 2013. Dynamic design of slender footbridges. Proceeding of 2nd International Conference on Structures and Architecture (ICSA 2013), Guimaraes, Portugal.

[29] D. Bortoluzzi, D., Casciati, S., Elia, L. & Faravelli, L. 2013. Semi-Active Control for the Mitigation of Vibration on a Footbridge. Proceeding of 21st Congress of The Italian Association of the Theoretical and Applied Mechanics (AIMETA 2013), Torino, Italy.

[30] Casciati, S., Faravelli, L. & Bortoluzzi, D. 2013. Human induced vibrations in a pedestrian timber bridge. Proceeding of 4th ECCOMAS Thematic Conference on Computational Methods in Structural Dynamics and Earthquake Engineering (COMPDYN 2013), Kos Island, Greece.

[31] Casciati, S., Faravelli, L. & Bortoluzzi, D. 2013. Pedestrian timber bridges: experimental investigation and modelling. Proceeding of 10th International

Conference on Damage Assessment of Structures (DAMAS 2013), Dublin, Ireland.

[32] Bortoluzzi, D., Casciati, F., Casciati, S., Chen, Z-C. & Faravelli, L. 2013. Reporting the results of two experimental campaigns on a pedestrian timber bridge. Proceeding of 9th International Workshop on Structural Health Monitoring 2013 (IWSHM2013), Stanford, California, USA.

[33] Bortoluzzi, D., Casciati, F., Casciati, S. & Faravelli, L. 2013. Comparison of accelerometric response records on a timber footbridge. On the Proceeding of 2nd International Conference on Timber Bridges 2013 (ICTB2013), Las Vegas, Nevada, USA.

[34] Van Nimmen, K., Lombaert, G., De Roeck, G. & Van den Broeck, P. 2014. Vibration serviceability of footbridges: Evaluation of the current codes of practice. Engineering Structures, 59, 448-461.

[35] Bortoluzzi, D., Casciati, S. & Faravelli, L. 2014. Testing the effects of walking and running on an existing timber pedestrian bridge. Proceeding of 9th International Conference on Structural Dynamics (EURODYN 2014), Porto, Portugal.

[36] Casciati, S., Casciati, F., Faravelli, L. & Bortoluzzi, D. 2014. Modelling the human induced vibrations in a cable-stayed pedestrian timber bridge. Proceedings of 7th European Workshop on Structural Health Monitoring (EWSHM 2014), Nantes, France.

Conclusions

In this thesis, an Inertial Sensor, which also includes a GPS (Global Positioning System) receiver (i.e., Ellipse-N), is coupled with a data collector (i.e., RasPi) and wireless technologies (i.e., ZigBee) to develop a wireless data acquisition system in the SHM (Structural Health Monitoring) area. For this purpose, a Kalman filter-based approach, allowing a data fusion of the measured responses (i.e., accelerations and GPS positioning data), is proposed in view of an accurate estimation of the displacement induced on civil structures by external excitations.

The technology also exploits the ability to receive the corrections from a reference station, providing a centimeter-level accuracy with the so-called RTK (Real Time Kinematics) technique. The two receivers observe the same constellation of satellites and, since the reference station position is known, differential corrections may be generated in order to improve the results of the measurement point.

The strategy for the local collection of the message is carried out by a WSN (Wireless Sensor Network) based solution. This system is also connected to a WAN (Wide Area Network) Unit that can transmit the information to the "outside world" by terrestrial or satellite networks. The ultimate goal is to ensure the communications even if existing tools fail.

Details on the hardware components, functional procedures and software implementation are provided. A reliable method based on a character checking mechanism of the communication protocol (i.e., NMEA-0183 format) is adopted to avoid data loss issues.

The test results of three experimental campaigns are finally reported. The future extensions of the research are discussed in order to demonstrate that the entire system features a good balance for three aspects: power consumption, communication range, and link quality.

Appendix A

In this chapter, sending and receiving codes are presented to show in detail the software operations of the wireless data acquisition implemented in Python language.

The first section is addressed to the software carried out for the RasPi_I (Sensor Node), here named *master*. It has the task to acquire the NMEA message from the Ellipse-N and send the information to the RasPi_II (Coordinator Node).

The latter behavior represents the core of the second section, whose attention is focused on the so-called *slave* device.

A.1 Sending Code

```
import serial, itertools, os
from time import strftime, gmtime, sleep

print("Welcome")
'''
This script starts automatically since stored in etc/rc.local
It stops only when the host system is shut down.
'''

#GLOBALS

control = "^"
master = "/dev/master"
ellipse = "/dev/ellipse"
#master = "COM5"
#ellipse = "COM4"
baud = 38400
bufferSize = 100
try:
    print("INIT ellipse")
    ser_in = serial.Serial(ellipse,
                           baud)
except Exception, e:
```

```
    print("ERROR ellipse, ", e)

try:
    print("INIT master")
    ser_out = serial.Serial(master,
                            baud,
                            parity=serial.PARITY_NONE,
                            bytesize= serial.EIGHTBITS,
                            stopbits = serial.STOPBITS_ONE,
                            xonxoff=True)
except Exception, e:
    print("ERROR zigbee master, ", e)


#END GLOBALS

'''
This method returns a filename with a timestamp using the time
library
in a year month day hour minute seconds format.
eg: data_2015-01-01-12-55-32.txt
'''
def getFileNameWithTimestamp():
    return "data_" + strftime("%Y-%m-%d %H-%M-%S", gmtime()) +
".txt"

'''
This method returns a filename using the os and itertools
library.
It searches for filenames with the data(x).txt where (x) stands
for
an integer number between 1 and 9223372036854775807
'''

def getFileName(name):
    def increment_filename(fn):
        fn, extension = os.path.splitext(name)
        n = 1
        yield fn + extension
        for n in itertools.count(start=1, step=1):
            yield '%s%d%s' % (fn, n, extension)

    for filename in increment_filename(name):
        if not os.path.exists(filename):
            return filename
```

```
'''
This method receives as a parameter a filename using the helper
methods above,
starts a serial connection on port ttyUSB0 as long as only one
device is connected
as for the ellipse positioning device. It then cycles
indefinitely writing the data
it retrieves from the sensor in a file name with the format
data(x).txt where (x)
stands for an integer between 1 and 9223372036854775807.
'''

def readFromSensor(fileName):
    value = True
    sleep(1)
    while value:
        try:
            _assertConnection(ser_in)
            _assertConnection(ser_out)
            line = ser_in.readline()
            #if the data is not an empty line then write it to
the given fileName
            if len(line) > 0:
                write(list(line))
            #opening the file with parameters a = append and b =
bytes
                file_out = open(fileName, "ab")
            #writing the data
                file_out.write(strftime("%Y-%m-%d %H-%M-%S",
gmtime()) + "\t" + line)
            #closing the file
                file_out.close()
            #printing the data retrieved from the sensor
            print(line)
        except KeyboardInterrupt:
            _terminateConnection(ser_in)
            _terminateConnection(ser_out)
            print("Exiting")
        except Exception, msg:
            print("Error message: " , msg)
            pass


def write(string):
```

```
    _assertConnection(ser_out)
    while len(string) < bufferSize:
        string.append("x")
    try:
        for s in range(len(string)):
            ser_out.write(string[s])
            if(s == len(string) - 1):
                print("Control")
                ser_out.write(control)
        print(string)
    except Exception:
        _terminateConnection(ser_out)


def _assertConnection(ser):
    if ser.isOpen() == False:
        ser.close()
        sleep(0.1)
        ser.open()

def _terminateConnection(ser):
    ser.flushOutput()
    ser.flushInput()
    ser.close()

#starting the whole script
readFromSensor(getFileName("data.txt"))
```

A.2 Receiving Code

```
import sys, os, itertools, serial
from time import sleep, gmtime, strftime

print("Welcome")

slave = "/dev/slave"
#slave = "COM7"
baud = 38400
length = 100
control = "^"

try:
```

```
    print("INIT slave")
    ser_in = serial.Serial(slave,
                    baud,
                    parity=serial.PARITY_NONE,
                    bytesize= serial.EIGHTBITS,
                    stopbits = serial.STOPBITS_ONE,
                    xonxoff=True)
except Exception, e:
    print("ERROR slave, ", e)

def getFileName(name):
    def increment_filename(fn):
        fn, extension = os.path.splitext(name)
        n = 1
        yield fn + extension
        for n in itertools.count(start=1, step=1):
            yield '%s%d%s' % (fn, n, extension)

    for filename in increment_filename(name):
        if not os.path.exists(filename):
            return filename


def check():
    _assertConnection()
    while 1:
        data = ser_in.read(1)
        if(data == control):
            read()

def read():
    _assertConnection()
    string = ""
    while 1:
        if(len(string) > length):
            check()
            break
        elif (len(string) == length):
            save(string)
            print(string)
        string += ser_in.read(1)

def save(string):
    file_out = open(filename, "ab")
    file_out.write(strftime("%Y-%m-%d %H-%M-%S", gmtime()) + "\t"
```

```
+ string)
    file_out.close()

def _assertConnection():
    if ser_in.isOpen() == False:
        ser_in.close()
        sleep(0.1)
        ser_in.open()

filename = getFileName("data.txt")
print("Data will be written to: " + filename)
print("LISTENING: ")
check()
```

Appendix B

Some technical details concerning the Tesa footbridge [1-3], which has been used as a case study of the experimental campaign, are discussed. In particular, information on dimensions, materials, constructions techniques and stages of the footbridge is provided.

B.1 Tesa footbridge

The footbridge is located in Farra d'Alpago, an Alpine village close to the town of Belluno, as shown in Figure B.1. The bridge was built in 2005 and connects the two sides of the outlet channel from the Santa Croce Lake.

Figure B.1 Satellite (a) and lateral view (b) of the Tesa footbridge

Eco-friendly materials (i.e., steel and timber) were adopted to harmonize the structure with the surrounding environment, limiting the use of reinforced concrete to the foundations. From the geometric point of view, the span is about 110m and the double beam deck shows a width of 3.2m for the free crossing of the pedestrians (Figure B.2).

Two materials are adopted for the construction of this structure: (i) Glued Laminated Timber (GLT) element of high strength according to DIN1052 code [4], and (ii) steel elements of high strength according to UNI EN10025 code [5].

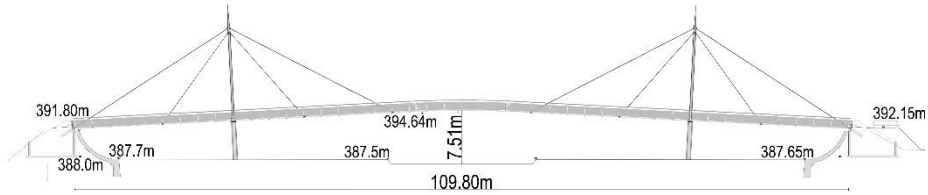

Figure B.2 Technical drawings of the footbridge

As shown in Figure B.2, the static scheme of the bridge is the classic cable stayed solution. In total, sixteen steel cables are adopted. In particular, eight internal-secondary cables of diameter 32mm, and other eight external-main cables of diameter 44mm (Figure B.3).

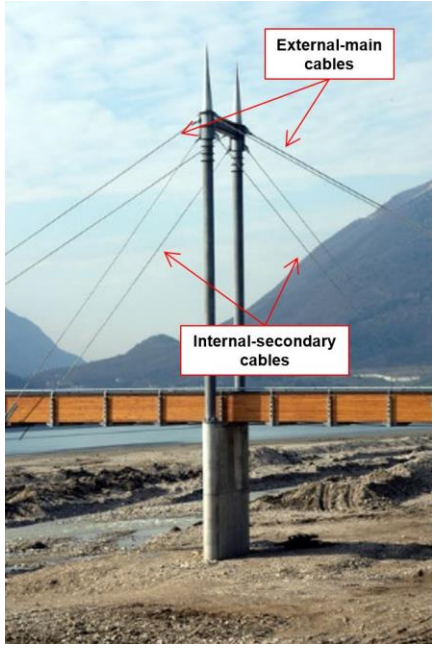

Figure B.3 Internal and external steel cables

The two antennas, located on both sides of the footbridge, are about 16m high and realized by steel tubular elements of diameter 457mm and thickness 12.5mm. Attention was paid to the design of the connection between the cables and the deck, as shown in Figure B.4.

Figure B.4 Detail of the joint connection with deck

The deck shows the classical U-shape cross section (Figure B.5). It is realized by linking two main curved GLT beams, located on the external side of the section, with transversal U-shape steel tubular elements of high strength S355J0. The vertical ones have dimension of 100x120x5mm, while the horizontal one are 100x200x5mm. Moreover, these elements are connected by steel braces of circular cross-section that provide the lateral stiffness.

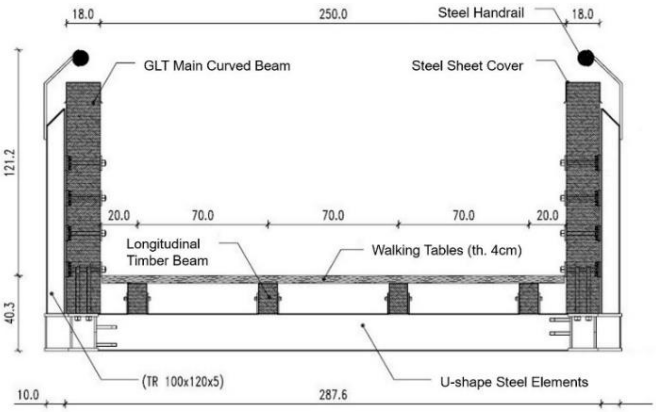

Figure B.5 Details of the deck cross-section

The structural scheme is completed mounting, on the U-shape elements, four longitudinal GLT rectangular beams with a cross section of 10x16.3cm. They are used to carry the walking deck made of larch planking with a thickness of 4cm, as shown in Figure B.6.

Figure B.6 View from the bottom of the deck

In order to allow the footbridge thermal deformation, at the ends of the two main GLT beam, a neoprene supports are posed. The span length can be subdivided into three segments. Each of them is made of curved GLT-BS14 and GLT-BS16 beams for a length of 22.5m, 65m (in the middle) and 22.5 m, respectively.

All these structural elements were realized in a factory and mounted in situ, limiting the activity on the field and making the construction process more automatized (Figure B.7).

Figure B.7 Construction stage: assembling the central section of the footbridge

Once the construction stage was finished, the static proof test required by the Italian regulation [6, 7] was carried out. In addition to the dead loads due to the structural and non-structural elements of the footbridge, loads provided by ad hoc devices was added until to reach that one provided by the regulations: $q1.e = 4.0 kN/m^2$.

Once loaded the deck, the measurement of the vertical displacement at sensitive points along the footbridge due to the above loads was carried out. The maximum vertical displacement measured in the middle of the span was 14.5cm.

B.2 References

[1] Bortoluzzi, D. 2014. Control System for the mitigation of Footbridge Vibration. PhD Thesis, University of Pavia, Italy.

[2] Casciati, S. 2016. Human induced vibration vs. cable-stay footbridge deterioration. Smart Structures and Systems, 18(1), 17-29.

[3] Casciati, F. & Casciati, S. 2016. Designing the control law on reduced-order models of large structural systems. Structural Control and Health Monitoring, 23(4), 707-718.

[4] EN 1995 Eurocode 5. DIN 1052: Design of timber structures.

[5] UNI EN 10025-2. 2005. Hot rolled products of structural steels. Part 2: Technical delivery conditions for non-alloy structural steels.

[6] D.M. 16 gennaio 1996. Norme tecniche per le costruzioni in zona sismica.

[7] D.M. 14 Gennaio 2008. Norme tecniche per le costruzioni (NTC2008).

Acknowledgements

This research activity has received funding from the European Union Seventh Framework Programme (FP7/2007-2013) under grant agreement n° [313002] SPARTACUS (Satellite Based Asset Tracking for Supporting Emergency Management in Crisis Operation), and it was supported by Athenaeum grants from the University of Pavia.

Sincere thanks to my advisor, Prof. Sara Casciati (University of Catania), gave me the invaluable opportunity to complete the present work, Prof. Lucia Faravelli (University of Pavia) for the encouragement during my academic efforts, and Prof. Vicenç Torra (Polytechnic University of Catalonia) opened my mind to the materials behavior through the numerous laboratory experiments. I was honored to have them in the timeframe of my doctoral education.

My deepest gratitude to Prof. Fabio Casciati (University of Pavia) for the academic and personal guidance that he provided through my Ph.D. studies. He taught me to face and solve relevant problems, which seemed impossible to me when moving the first steps. I am very grateful for his care over the years.

I would like to extend my acknowledgement to my family and all the people who have been part of my life because there were always, and without them, this work would not have been a possible.